Mathematical modelling of airflow during forced draft precooling operations

A thesis presented in partial fulfilment of the requirements for the degree of

Doctor of Philosophy

in

Food Technology

at Massey University, Palmerston North, New Zealand.

Nicolás Ignacio Tapia Zapata

2024

Abstract

By the year 2020, the kiwifruit industry represents approximately 37 % of the horticultural export industry sector in New Zealand. Thereof, the kiwifruit cold chain aim is to reduce losses due to poor temperature control and energy usage during refrigeration. By forced convection aided by fans in palletised kiwifruit, field heat is removed rapidly prior to storage, thus optimising shelf-life of the produce. Previous Computer Fluid Dynamics (CFD) model determined the optimal operating point for palletised kiwifruit during forced-draft cooling. However, CFD requires complex simulation, in detriment to computational efficiency and solving time. Therefore, there is an imperative to provide innovative tools that optimise package design by iterating several designs and that is applicable to the local industry sector for cold chain optimisation. In this spirit, this projects aimed to development of a simplified approach for the prediction of airflow distribution of palletised kiwifruit during forced-draft cooling, that can be coupled with an alternative heat transfer model, thus providing a fast and robust package optimisation routine that can inform cooling performance of several package design and pallet configuration.

Accordingly, an airflow model based on a resistance network approach was used as a mathematical framework. This model solved the airflow distribution problem by iterating solutions in a set of non-linear equations based on mass conservation principles, until numerical convergence criteria is reached. In this context, the subsequent airflow distribution through the formed channels of the pallet footprint were influenced by the airflow resistance through a given channel. Firstly, the influence of vent (size, location and number) and package (length, headspace and number of plates) design characteristics on the airflow resistances, indicated by the loss coefficient were studied. For a large flow regimes, large influence of vent size on the subsequent loss coefficient was observed, both empirically and aided by literature review relationships.

Additionally, vent location and number were found to not largely influence pressure drop through a vented plate, for the studied flow regimes. Lastly, little differences were found in the loss coefficient when varying length between plates, headspace dimensions and the number of plates, respectively.

Pressure distributions through different pallet design, footprints and internal packaging configurations were monitored. Minor effects of the package configurations on the local loss coefficient were observed when airflow channels are formed (empty cartons, cartons with a flat surfaced bulk). However, differences were observed when complex airflow pathways are formed (polylined and non-polylined bulk of produce). As different loss coefficient were observed at different locations within packages influenced by vent size, a literature based relationship was used to fit empirical loss coefficient at the inlet, interior and outlet of the pallet layer. These relationships were subsequently used to determine the vent loss coefficient and thus the airflow resistance for a given system. A geometric model to characterise pallet footprint given by package design was developed, where the effective venthole areas were calculated, prior to characterise the airflow resistances. Subsequently, by using an Graph Theory based algorithm, a set of node and loops equations were obtained for a given pallet footprint, thus obtaining network structure for all airflow pathways within the pallet layer. The model solver consists in an iterative approach were the non-linear equations were linearized by an iterative solving algorithm was used to predict the consequent airflow distribution in approximately 4 seconds. This model was verified and validated against empirical data of pressure distribution. The model successfully predicted the status-quo pallet footprint airflow distribution and an alternative package design. However, the model failed to predict the airflow distribution where vent size varies within the pallet footprint, caused by vent obstructions. Although a robust mathematical framework for the prediction of airflow in palletised product was provided, further work on airflow resistance is needed.

Acknowledgments

Firstly, I would like to thank my supervisory team Dr. Richard Love (chief supervisor), Prof. Andrew East (co-supervisor) and Dr. Emilia Nowak (co-supervisor), for their immense support, patience and influence in my development as a young researcher. Thank you for giving me the opportunity to do what I like: learning natural sciences. Additionally, thanks to the team at the postharvest technologies office at Massey University, for their kindness and good moments during my period in New Zealand. Special thanks to Sebastian, in who I found a brother, and uncountable adventures in *Aotearoa*.

Thanks to OJI Fibre Solutions and Zespri International who provided direct support this project, as part of the Fibreboard Packaging Design Project (MAUX1302), in alliance with the New Zealand Ministry of Business, Innovation and Employment.

Thanks to my undergraduate thesis supervisor, Prof. Juan Antonio Cañumir, for encouraging me to pursue a PhD program, and to direct me to New Zealand, a place that became an important place in my life.

Thanks to my parents and my beloved brother, for their kindness, support, and enormous sacrifice during my young life, for trusting me when I decided to leave Chile. Without their advice, none of this would have been possible.

This work is dedicated to Leonardo, for his patience and emotional contention.

Table of Contents

List of Tables

List of Figures

1. Introduction

1.1. Postharvest industry and the cold chain in New Zealand

By the time of June 2020, the value of the horticultural export sector in New Zealand reached NZ $ 6.7 B, from which approximately 37 % corresponds to exports of fresh kiwifruit (Fresh Facts, 2020). Despite the remote geographical location of New Zealand in comparison to the major markets in the northern hemisphere, the high quality of New Zealand's fresh produce at the destination markets is one of its many attributes. This accomplishment was forged by constant research in refrigeration technologies and attempts to design efficient packages to extend produce shelf life (Carson and East 2018).

The catenation of all individual unit operations, from the produce harvest to the consumer is referred as the 'Supply chain', with focus on reducing food losses and energy usage during the whole chain process (Fahimnia et al. 2015). More specifically, all the postharvest operations that require the produce to be refrigerated are denominated as 'Cold chain', which is a major part in case of perishable produce. A flux diagram of the supply and cold chain of kiwifruit are indicated in the diagram of Figure 1.1.

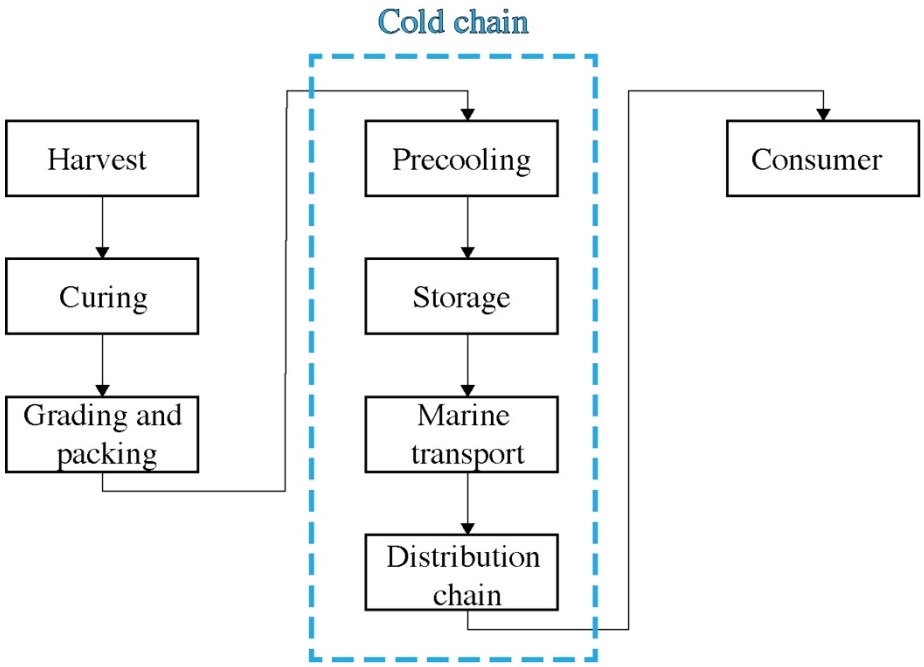

Figure 1.1. *Supply chain diagram of fresh kiwifruit. Cold chain operations are depicted by a blue rectangle.*

After harvesting, the produce is stored in wooden bins at ambient temperature – a process commonly known as curing. Here, the fruit is acclimatised prior to entering the packhouse, reducing loss of quality attributes. In this matter, appropriate humidity and temperature control during curing of kiwifruit can have an impact in reducing the risk of subsequent development of botrytis cinerea, rot incidence, and chilling injury, among other quality disorders (East et al. 2018). Prior to the packaging, the produce in graded by size by means of automated sorting technologies.

1.2. The roll of package design in the kiwifruit cold chain

The packaging system of kiwifruit consist in a bulk of produce – loose bulk or individual trays – wrapped in a polyliner bag that preserves moisture content of the produce during subsequent storage. Once the produce is packaged in large, rigid structures denominated palletised produce, the temperature of the pallets are drastically lowered from field to storage temperature, from 20 – 30 to 0 – 2 °C, respectively (*ASHRAE handbook* 1994), by forcing high speed refrigerated air blasts through the package ventholes in a batch operation called precooling (Thompson 2014). This drop of temperature reduces respiration rate of the produce, thus retarding senescence and ethylene production, which can influence kiwifruit softening (Zhao 2017).

Rapid cooling the produce after packaging extends shelf life, minimising the loss of quality attributes, ensuring availability and flux of produce to the destination markets, minimising food waste during the supply chain. Additionally, the removal of field heat from refrigerated storage rooms or marine transport requires large refrigeration units and is energetically ineffective for large amounts of produce. Hence, the design and optimisation of a precooling operation is a key cost function for an optimal cold chain assessment, extending shelf life of the produce and avoiding subsequent losses in energy and operational resources. To optimising the cooling performance of a given produce aided by package design, a thermodynamics overview of the operation is therefore fundamental (Olatunji 2018; O'Sullivan 2016; Tanner 1998).

1.3. Modelling in postharvest cooling operations

Extended research had been conducted on modelling the forced-draft cooling, subsequent storage and transport of horticultural produce (Defraeye et al. 2015). Additionally, the capacity of decoupling the momentum an energy balance gives flexibility to incorporate different modelling approach despite their complexity (Ferrua and Singh 2009d). Tanner (1998) developed and validated a heat and mass transfer model based on discretising the system in zones, where volumes of different components are interacting within and between adjacent zones, describing the flux of mass and energy during cooling of apples. Here, the heat (or mass) transfer model is decoupled from the momentum of the refrigerated air, however, these were estimated empirically as a model input. Subsequently, Smale (2004) developed a simplified airflow modelling approach to predict airflow distribution in reefer containers, which were subsequently coupled with the zonal heat transfer model developed in Tanner et al. (2002).

Recently, with more available computational resources, an insightful numerical model of palletised kiwifruit was developed and validated by O'Sullivan (2016), which stated the thermodynamic overview of the current kiwifruit packaging system and its cooling performance. In parallel, recent advances in optimization algorithms open a reasonable question, whether a fast simplified modelling framework can be transformed in a useful tool for process optimisation and package design, where multiple parameters and several packages can be simulated simultaneously (Martinez-Hermosilla et al. 2018; East and Smale 2008). In addition, Olatunji (2018) developed a simplified zonal heat transfer model to predict cooling performance of single kiwifruit package. More specifically, geometrical procedures for representing a packaging system geometry were developed (Olatunji et al. 2020). Under this context is that the applicability of an integrated modelling framework for optimising cooling operations based on package design becomes relevant and opens a window for the exploration of airflow characteristics of palletised kiwifruit for modelling purposes.

1.4. Project purpose

This project aims to provide a mathematical framework for the prediction of airflow distribution inside palletised polylined horticultural produce. This approach can subsequently be implemented in future optimisation routines, by coupling an airflow model with a simplified heat transfer model, such as zonal approach. Consequently, the mechanical airflow characteristics of a kiwifruit packaging system must be accounted for. More specifically, the airflow channels formed at the headspace of the polyliner must be somewhat quantified, enabling ease and fast prediction of airflow distribution in palletised kiwifruit for a given package design. Currently, there is little to no data on experimental airflow related data of palletised produce during precooling, nor their effect on the resulting aerodynamic performance given by package design. Therefore, a set of data must be obtained to primarily characterise the airflow phenomena during forced-draft cooling operations.

2. Literature review

2.1. Precooling operations

Precooling is one of the most used postharvest operation that extends shelf life of horticultural produce. This operation aims to remove field heat from horticultural produce, thus slowing down its metabolism, minimising its quality loss prior to storage and subsequent transport (Brosnan and Sun 2001). Consequently, metabolism activity, respiration rate and ethylene production of the produce are also minimised. Additionally, the heat removal of the produce depends majorly on the ability of a given cooling operation to remove heat load from the produce by its capacity to reach all fruit inside a stack with relative high local velocity of the cooling medium (Thompson 2014). Different refrigeration methods can be used as a precooling process, and their applicability will depend majorly on the produce physiological characteristics. As cooling media can vary from air to water, adding vacuum can also be used as means to achieve optimal produce storage temperature. However, let us focus on the air-based precooling methods which aid rapid cooling of palletised kiwifruit.

2.1.1. Room cooling

One of the most straight forward and easy to implement precooling technique is room cooling. This convective operation cools down a refrigerated chamber filled with palletised horticultural produce using the evaporator fans of the room. The pallets are distributed in the room more or less symmetrically respect to the fans within the chamber, as depicted in Figure 2.1. Despite the

relatively easy implementation of this process in an industrial framework, it requires a considerable amount of refrigeration capacity and long cooling times, making it the slowest cooling method (Boyette, Wilson, and Estes 1989). The use of room cooling is therefore more suitable to maintain low temperature of palletised produce through storage rather than precooling large amounts of produce from field temperature. However, it implies a considerable amount of loss of mechanical work, in detriment of convective energy available to force rapid cooling, thus creating potential warm spots due to poor delivery or airflow local velocity (Verboven, Hoang, and Nicolaï 2003).

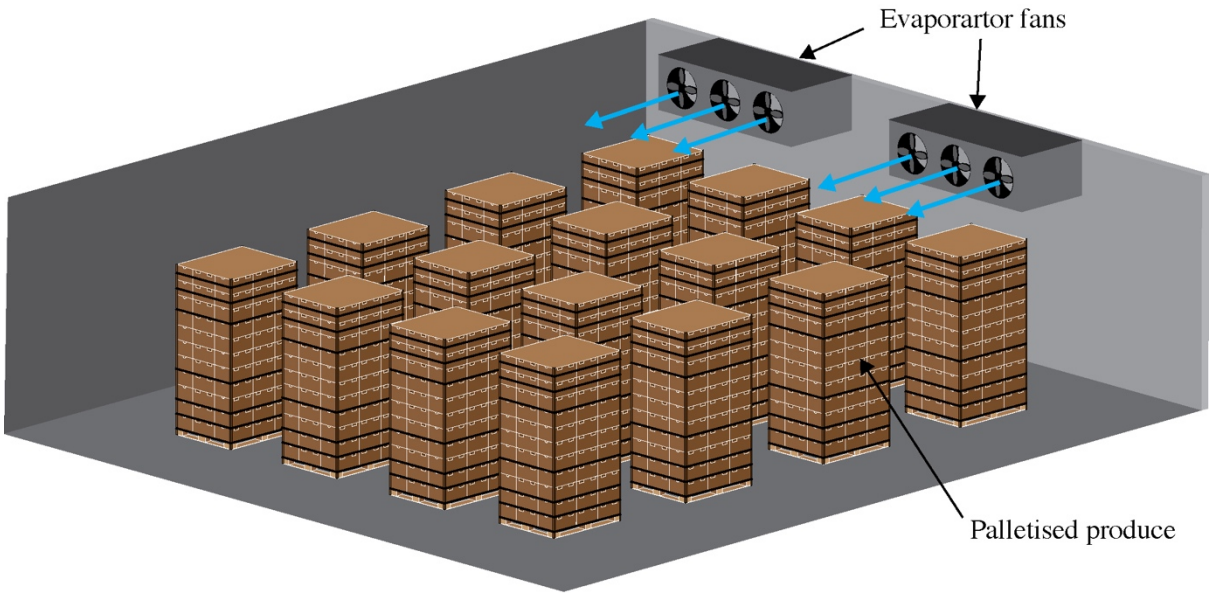

Figure 2.1. *Diagram of a typical room cooling operation filled with palletised horticultural produce.*

2.1.2. Forced-air cooling

Forced-air cooling – or also called forced-draft cooling – is the most energetically effective and widely used precooling operation (Brosnan and Sun 2001). Aided by a fan, air is pulled through the palletised system, thus cooling the produce by forced convection, as showed in Figure 2.2 for palletised kiwifruit. By maximizing the available potential mechanical work of the refrigerated air, the forced convection for heat removal from the produce is thus enhanced. Providing directed high currents of airflow through the palletised stacks, cooling performance of palletised produce can be thus optimized prior to storage. In this context, diverse studies – both empirical and numerical – have been performed in order to enhance air circulation within packages of produce, and consequently, optimize its cooling performance. Experimental work of palletised cooling performance by Mercier, Brecht, and Uysal (2019) explored the temperature uncertainty of palletised strawberry during an industrial forced-draft cooling operation. Additionally, large experimental trials and subsequent numerical simulation had been carried to characterize cooling kinetics of kiwifruit, apples, and citrus fruit (Tanner 1998; O'Sullivan 2016; Wu et al. 2018; Ferrua and Singh 2009a).

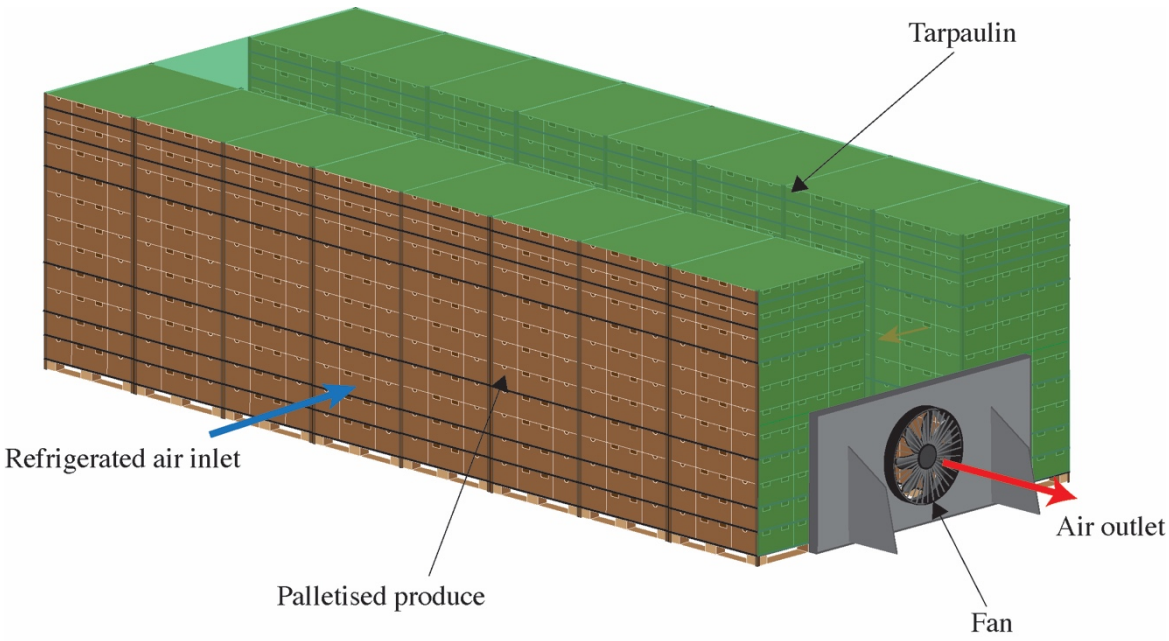

Figure 2.2. *Diagram of an ideal forced-draft cooling of palletised produce.*

2.2. Packaging design

The main constrain to keep in mind when designing a package is to bear big loads of produce (i.e. when forming large palletised structures). Additionally, the cooling performance of a produce is determined by an appropriate vent design that allows air ventilation inside the package, thus removing sufficient field heat from the produce. Therefore, an optimal package design must be somewhat a trade-off between mechanical and cooling performance. Typically, the produce is packed inside ventilated cartons, typically made of corrugated cardboard or plastic, and the packaging configuration can be multiple: loose bulks, polylined produce, perforated linen or secondary packed units – such as clamshells (Pathare et al. 2012).

In the case of kiwifruit, a polyliner bag is used to help to preserve the produce moisture content and thus prevent shivering injury throughout the cold chain. One the most used packaging system is the Modular Bulk Package (MBP) design. This design consists in a typical cardboard box with a lid folded at the top, leaving a gap in the headspace of the bulk (Figure 2.3). A typical kiwifruit package design also contains hand holes for easy handling and to allow refrigerated airflow through the headspace, thus acting as an airflow channel that cools down the kiwifruit bulk from the top towards the interior of the bulk.

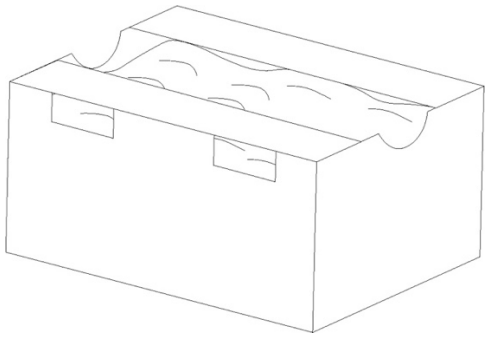

Figure 2.3. *Draw of a kiwifruit Modular Bulk Package (MBP) design with a polylined bag filled with produce.*

By placing a number of ventholes in key locations within the package faces, rapid and homogenous cooling can be achieved. While venthole size allows more refrigerated air per unit time into the horticultural bulk, this ventholes must be distributed and located optimally, ensuring cooling uniformity without compromising the mechanical performance of the package (Defraeye et al. 2015). Maximum venthole total open area (TOA) of 14 % had been reported for optimal cooling rate (de Castro, Vigneault, and Cortez 2004). However, this limit was performed on loosely packed spherical produce without taking in account mechanical stability of the package.

2.2.1. Cooling performance

Cooling performance of a given packaging system is measured by two fundamental metrics: its cooling time, and the cooling uniformity among the produce during the precooling process. Cooling measurements may be conducted at different locations over the entire cooling process, with different initial temperature, or simply comparing two different packaging systems. Typically, a dimensionless fractional value respect to the initial temperature of the produce is introduced; the so called Fractional Unaccomplished Temperature Change (FUTC) (Brosnan and Sun 2001; Dincer 1995). All measured fruit or averaged package initial FUTC value is referred to 1 as initial value, decreasing towards 0. The formula of this metric value is defined as:

$$Y = \frac{T_i - T_{ref}}{T_{i(0)} - T_{ref}} \qquad 2.1$$

Where,

T_i: Temperature of the produce at time i (° C).

$T_{i(0)}$: Temperature of the produce at time $i = 0$ (initial temperature) (° C).

T_{ref}: Temperature of reference, in this case, refrigerated air (° C).

Additionally, the optimal cooling time was defined as when the value of the Y reaches a value of 0.125: the seventh eight cooling time (SECT). Similarly, the half cooling time (HCT) is defined as the time when the FUTC values reaches 0.5. This information allows to quantify cooling performance per unit of produce, allowing the comparison of cooling performance for different packaging system during precooling (Defraeye et al. 2015).

Another important metric to account for is the heterogeneity of the cooling process. Due to the ventholes, complex airflow patterns are formed inside the package, hindering the uniformity of the process, resulting in spatially allocated warm spots throughout the cold chain (Alvarez and Flick 1999). The Heterogeneity Index (HI) accounts for the spatial variability within a package system with horticultural produce (Dehghannya et al., 2011), and it is defined as:

$$HI = \frac{\sqrt{(T_i - \bar{T}_i)^2}}{\bar{T}_i} \times 100 \qquad 2.2$$

Where,

T_i: Temperature of the produce or location at time i (° C).

$\bar{T}_i$: Average temperature of all measured produce at time i (° C).

This metric indicates the relative standard deviation of a given measurement respect to all the measured individual fruit at a given time. However, this value does not account for the cooling profile along the cooling period, making it challenging to characterize cooling performance during the whole precooling operation. Olatunji et al. (2017) addressed this problem by introducing a

new metric, the Overall Heterogeneity Index (OHI). This indicates the temperature relative deviation from the mean of the measured population during the whole cooling process. OHI is thus defined as:

$$OHI = \int_{0}^{1} \int_{\bar{Y}_{end}}^{\bar{Y}_{start}} |\Delta Y| dF(\Delta Y) d\bar{Y} \qquad 2.3$$

Where,

ΔY: Dimensionless temperature difference for all measured locations during cooling.

$\bar{Y}$: Averaged unaccomplished temperature change over the cooling process.

$F(\Delta Y)$: Cumulative distribution of ΔY during the cooling process.

In a typical cooling experiment, values of $\bar{Y}$ range from 1 to 0.125 (SECT), as $\bar{Y}_{start}$ and $\bar{Y}_{end}$, respectively. Thus, this defined integral delivers an indicator of heterogeneity over the cooling process, accounting for fruit cooling heterogeneity over time respect to the entire measured population. Finally, a new cost function of minimizing the OHI must be considered for evaluating cooling performance of horticultural produce, altogether with the cooling time metrics of HCT or SECT.

2.2.2. Airflow resistance

During forced convective cooling, a fan forces refrigerated air through the ventholes of the packaging system, hence cooling the product (Figure 2.4). The air that contracts and expands through the system forms complex airflow patterns, resulting in a pressure difference through the system. The geometry of the packaging system varies for different produce, packaging elements

and venthole design of the package, thus influencing the total pressure gradient and the energy required to accomplish adequate cooling.

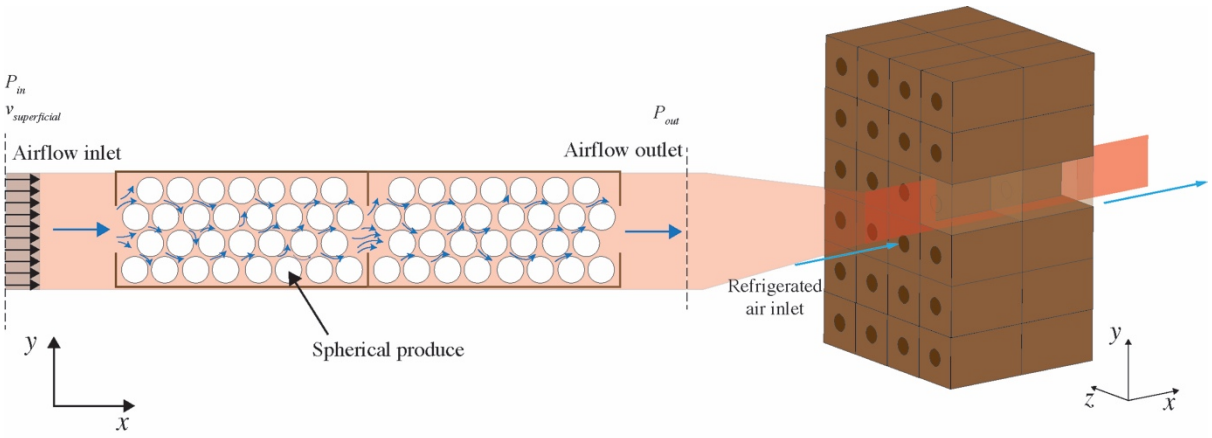

Figure 2.4. *Cooling diagram of spherical produce in ventilated cartons.*

By using Bernoulli's formula to establish the mechanical energy balance of the system, the following equation is obtained:

$$z_1 g + \frac{p_1}{\rho} + \frac{v_1^2}{2} = z_2 g + \frac{p_2}{\rho} + \frac{v_2^2}{2} + \Delta H_m + \Delta H_f \qquad 2.4$$

Where

z: Height of reference point (m).

p: Gauge pressure at reference point (Pa).

ρ: Air density (kg/m^3).

g: Gravitational acceleration (m/s^2).

v: Mean duct velocity at reference point (m/s).

ΔH_m: Head loss due to minor losses (m).

ΔH_f: Head loss due to friction (m).

As deducted from the diagram in Figure 2.4, potential energy terms are neglected as there is no relative difference in height between inlet and outlet of the airflow. Additionally, the head loss can be summed, including head loss dues to friction and due to any component. Thus, the simplified formula is established as:

$$\Delta p = \rho_{air} k \frac{v^2}{2} \qquad 2.5$$

Where

Δp: Pressure drop between the two reference points (Pa).

k: Loss coefficient of the packaging system (-).

v: Superficial velocity at airflow inlet (m/s).

This is a more or less straight forward method to introduce a metric of the relative airflow resistance of a given stack. Alternatively, diverse approaches have been developed for different cooling and packaging scenarios. Generally, the pressure drop through a package system had been expressed using Ramsin's equation (V. Chau et al., 1985; Smale, 2004), which also associates the pressure decay to a coefficient related to the relative airflow resistance, for a wide range of flow regimens and packaging configurations. This relationship is described by:

$$\Delta P = a v^n \qquad 2.6$$

Where

v: Superficial velocity of airflow through the packaging system (m/s).

a: Ramsin coefficient dependent on the systems geometry (kg·s/m).

n: Ramsin exponential coefficient dependent on the system geometry and flow regime (-).

This approach is had been used to characterize airflow resistance of a given packaging system during forced air cooling (Vigneault et al. 2004; Ngcobo et al. 2012), and additionally for storage and transport of horticultural produce (Getahun et al. 2017; Smale 2004).

2.2.3. Vent size

Produce cooling by forced convection is largely influenced by the size of the ventholes contained in the package. The size of the venthole determines the amount of refrigerated air per unit area that enters the produce bulk, thus enhancing the convective heat transfer coefficient at the produce-air boundary layer (Kondjoyan, 2006). Besides the roughness of the flow channel, the presence of an orifice in a pipe – or a venthole in a package – results in a loss of pressure due to the component acting as a resistance to the flow motion. The resistance of a venthole is thus inversely proportional to its size (the bigger the venthole, the lower its resistance) and consequently, lower pressure drop (de Castro et al., 2004; Vigneault and Goyette, 2002; Vigneault et al., 2004). The opening ratio of a package is typically referred by a Total Open Area (TOA) (Defraeye et al. 2015). This ratio of the opening size respect to the relative size of the airflow channel is defined as:

$$TOA = \frac{A_1}{A_0} \qquad 2.7$$

Where,

A_1: Total cross sectional area of the venthole (m^2).

A_0: Cross sectional area of the package panel (m^2).

By using the notation indicated in Equation 2.5, the loss coefficient (k) is the main variable that relates to the apparent airflow resistance, and it is specific for a given geometrical configuration. Typically, the loss coefficient for an orifice inside a duct of a given size is found in literature as an empirical indicator, with known values of pressure drop and superficial airflow velocity (*ASHRAE,* 1985). Alternatively, Idelchik and Steinberg (1994) ventured the following analytical formula for a sharp edged orifice of a given TOA:

$$k = \left[k_D + k_C \cdot \left(1 + 0.707 \cdot \sqrt{(1 - TOA)} - TOA\right)^2\right] \cdot TOA^{-2} \qquad 2.8$$

Where

k_D: Loss coefficient at the discharge of the orifice (-).

k_C: Loss coefficient of the stream jet contraction of the orifice (-).

TOA: Total open area. Ratio of the area of the orifice respect to the cross sectional area of the air duct (-).

Although the venthole size is important to the cooling performance, parameters such as mechanical stability throughout the cold chain plays a key role in the overall package performance (Berry et al., 2019). When an optimal TOA had been reached, the cooling time also reaches its optimum. de Castro et al. (2004) stated an optimal value of 14 % TOA for an orifice filled with spherical cooling simulators. Ferrua and Singh (2009c) concluded that at higher airflow rates, most of the refrigerated airflow bypasses the produce, in detriment of additional the heat removal from the produce. Case-sensitive analysis of cooling optimization affected by venthole size, constrained to the number and location of vents must be performed accordingly, considering the internal package configuration and produce characteristics (i.e. produce geometry, presence of polyliner bags and plastic container units).

2.2.4. Vent number and location

The main premise for placing a certain the amount of ventholes in a package, is mainly to effectively distribute the refrigerated airflow that enters the packaging system, so cooling performance is homogeneous among all produce, minimizing the airflow bypass. Thus, a given Total Open Area (TOA) is distributed across different locations of the panel of the package. By incrementing the number of vents, better cooling time and uniformity is achieved (Dehghannya et al., 2011). Additionally, de Castro et al., (2004) investigated the effect of the vent number and location for cooling spherical produce bulk, concluding the benefits of having peripheral openings spread on the longitudinal axis, improving the overall cooling performance of the produce.

2.2.5. Pallet footprint

The allocation of different packages into a larger structure – namely pallets – results in complex airflow networks that influences the cooling performance of the different packages within the pallet layer. The amount of refrigerated air that enters each package must be evenly distributed, allowing airflow bypass towards the back of the pallet, or minimizing the airflow short-circuiting affected by venthole obstruction or blockage – often caused by package rotation within the footprint. As a consequence of forcing airflow through the stack, a pressure loss is imposed over the system (Defraeye et al., 2015). The rate of pressure drop is thus influenced by the losses of mechanical work of the fluid: the losses attributed to friction (roughness of the packaging material), but most importantly, of the resistance to flow motion imposed by the produce bulk and the package ventholes. Therefore, all the efforts of modelling the airflow characteristics of a palletised system must prioritize these airflow resistances as a function of internal packaging of the produce and the airflow network formed by the palletised structure. Defraeye et al. (2013) and

Defraeye et al. (2014) simulated the cooling kinetics of palletised oranges for package design, concluding that minimizing short circuiting and the resistance to airflow of the packages can achieve more airflow at the same energy consumption, thus enhancing the cooling performance of the produce. Similarly, Ambaw et al. (2017) simulated and validated the cooling kinetics of two package designs with different pallet footprints of palletised pomegranates, obtaining different airflow patterns – and consequently different pressure drop – through the pallet footprint during precooling. More specifically, the presence of plastic liner bags increased the relative airflow resistance of the system due to airflow short circuiting. Additionally, O'Sullivan (2016) characterized the cooling performance of palletised kiwifruit for the Modular Bulk Pack (MBP) design (Figure 2.3). Primarily, the pallet orientation had an effect on the overall airflow resistance, decreasing the pressure drop when the airflow enters on the 1.2 m face of the palletised structure at different fan speeds. Additionally, O'Sullivan et al. (2017) ventured to simulate the cooling kinetics of a novel package design for an MBP design that allows airflow bypassing towards the back of the pallet. More specifically, the pressure drop and the energy required to achieve the half cooling time (HCT) were reduced by 24%, and cooling uniformity was further improved at constant pressure drop.

The best approach when establishing a comparison point when studying the cooling performance of two or more packaging configurations is to employ the same fan energy during the cooling process. More specifically, at the same energy employed by the fan, the rate of turbulent dissipation of the air kinetic energy, expressed in pressure loss can be thus minimised. Thus, a given packaging configuration (internal packaging elements, pallet footprint and orientation) results in an airflow resistance network. The optimization of this variables can enhance the superficial velocity through the pallet, potentially enhancing the cooling performance of the produce.

2.3. Modelling approaches in forced air operation

Altogether with experimental exploration of cooling performance of packed horticultural produce, mathematical models have been developed accordingly with the recent advances of computational power (Pathare et al., 2012). However, the complexity of such mathematical models often consume a vast amount of computational resources, making this methodology computationally too expensive, and hence unsuitable for the construction of optimization algorithms (Martinez-Hermosilla et al., 2018). Alternatively, different interpretation of models has been developed, with diverse degrees of simplification, which can predict the cooling performance of a packaging system with sufficient accuracy and optimal simulation time.

2.3.1. Direct numerical simulation (DNS)

This approach is known by its high resolution, based on the mathematical scheme of finite element approach (Chow, 1979). Here, the geometry of the system is discretized into a finite number of elements forming a mesh of elements based on the model geometry, and subsequently, the energy, momentum and mass balances are performed for each finite element over the time of the operation (Dehghannya et al., 2010). More specifically, these balances are expressed in the form of partial differential equations, which are complex to solve without a specific Computer Fluid Dynamics (CFD) interface package. The momentum balance of a fluid over a given system is described by Newton's first law of mass conservation and the Navier-Stokes equation, respectively, as follows:

$$\nabla \cdot \vec{\boldsymbol{v}} = 0 \tag{2.9}$$

$$\rho\left(\frac{\partial \vec{v}}{\partial t} + \vec{v} \cdot \nabla \vec{v}\right) = -\nabla p + \nabla \cdot \bar{\tau} + \rho g \tag{2.10}$$

Where,

$\nabla \cdot \vec{\boldsymbol{v}}$: Field of local velocities over the cartesian space (m/s).

∇p: Local pressure of the fluid over the cartesian space (Pa).

$\nabla \cdot \bar{\tau}$: Field of sheer stress tensor (local changes in viscosity) in the cartesian space (N/m^2).

$\frac{\partial \vec{v}}{\partial t}$: Fluid acceleration over time (m/s^2).

$\vec{v}$: Local velocity of the fluid (m/s).

ρ: Fluid density (kg/m^3).

g: Gravitational acceleration (m/s^2).

This relationship computes the approximated solutions of local pressure and velocity of the fluid within the system. When describing airflow motion in highly turbulent systems, the relationship in Equation 2.10 is commonly presented as the Reynolds-Averaged Navier-Stokes equation (RANS), which is a re-arranged version of the Navier-Stokes model that incorporates the fluid oscillations around the mean values of the physical properties of the fluid (velocity, density, viscosity). Additionally, a magnitude of the turbulent viscosity is represented as Reynolds stresses (Chow, 1979). To describe these stresses, different turbulence models had been developed to estimate turbulent dissipation rate, among the most used ones are the k-ε and k-ω models, particularly used to model airflow during forced-air cooling of horticultural produce (Han et al., 2015; O'Sullivan et al., 2016; Defraeye et al., 2014). Additionally, Han et al. (2019) studied the

accuracy and applicability of different turbulence models, and estimated their sensitivity when predicting cooling performance of apples during storage.

The evident benefits of this approach has allowed the evaluation of diverse scenarios during the cold chain, more specifically, Wu et al., (2018) used a DNS approach to evaluate cooling performance during multiple operations in a virtual cold chain. Additionally, Ferrua and Singh (2009b) and Ambaw et al. (2017) developed a numerical modelling routine based on DNS to simulate the cooling performance of strawberries and grapefruit, respectively. More specifically, O'Sullivan (2016) successfully developed a DNS model to predict the cooling performance of palletised kiwifruit. Although this approach stands out by its resolution and precision, their computer power and the solving time needed by the DNS obscures the spirit of the project, which is to develop an airflow model that preserves sufficient output accuracy, minimizing the computational resources for subsequent development of optimization routines.

2.3.2. Porous Media

When a solid matrix – namely produce – is interconnected by a network of air voids or pores, is commonly referred as a porous media. This approach is widely used in the field of food engineering; more specifically in fluid mechanics, absorption, drying, cooling, and cooking of food materials (Dehghannya et al., 2010). By volume averaging the Navier-Stokes equations for a porous, confined bed, the following proposed Darcy-Forchheimer relationship was presented by Whitaker (1996). Generally, the relationship between pressure drop and superficial velocity is represented by:

$$-\Delta p = \frac{\mu_{air}}{\kappa} u + \beta \rho_{air} u|u| - \mu_{eff} \nabla^2 u \qquad 2.11$$

Where,

Δp: Pressure drop through the confined packed bed (Pa).

μ_{air}: Air dynamic viscosity (Pa · s).

κ: Permeability of the porous bed (m^2).

u: Airflow superficial velocity (m/s).

β: Forchheimer coefficient – depends on the geometry of the produce (kg/m^2).

ρ_{air}: Air density (kg/m^3).

μ_{eff}: Effective airflow dynamic viscosity at the boundary wall of the packaged bed (Pa · s).

The permeability of the porous bed is a function of the porosity of the packed bed. Additionally, The Forchheimer coefficient is assumed to be for spherically shaped produce, and has been estimated by the Ergun relationship, which relates to the relative airflow resistance imposed by the produce (Dehghannya et al., 2010).

Normally, the range of fluid flow – namely in terms of Reynolds number – where this relationship stands is limited and not well understood during turbulent regimes. However, Van der Sman (2002) explored the pressure decay in a confined packed bed of produce with an orifice plate of different sizes, assessing the applicability of the Ergun relationships for potatoes and oranges, and the Darcy-Forchheimer-Brinkmann for turbulent airflow rates, and additionally, stated the relationship between pressure drop and orifice open areas for mandarins and potatoes. In addition, Verboven et al. (2004) implemented a CFD approach, estimating the resistance contributed by

the produce and the contribution of the Brinkmann term of Equation 2.11, attributed to airflow near the walls. Finally, for modelling purposes, Verboven et al. (2006) recommends the use of direct numerical simulation through CFD as a better alternative for airflow through vented packages. Although his approach is not accountable to predict airflow in polylined produce, it gives another perspective where airflow resistances are somewhat estimated as a function of the geometry of the bulk of produce and vent design.

2.3.3. Resistance Network Modelling

The resistance network approach for fluid flow distribution modelling had been primary used in the field of hydraulics (Wood and Charles 1972), and is based on a second interpretation of an electric circuit framework (McIlroy 1950). Here, a given amount of fluid is distributed in a network, that by observing the mass conservation at nodes and loops, results in a set of non-linear equations, which are solved iteratively (Ellis 1996), thus estimating fluid distribution in a given fluid network.

In postharvest applications, Smale (2004) developed a simplified network model framework to estimate airflow distribution in shipping containers with palletised produce. One of the shortcomings of this approach lays on the low resolution on such model, which makes difficult to estimate accurately the local air velocity at the surface of the whole bulk (Smale et al., 2006). For forced-draft cooling applications, such simplifications can potentially give an acceptable estimation of the convective airflow performance at the top of a polylined bulk, as referred in the standard kiwifruit packaging systems (Olatunji, 2018). Additionally, this approach distinguishes itself by its simple computational implementation and fast solving time, approaching fast convergence for simple networks (Ellis, 1996). The study of networks at its pure mathematical

form – also known as Graph Theory – is a discipline of mathematics that studies spatial networks in matrix form (Tarjan, 1971), thus aiding to incorporate the conformation of networks for airflow distribution, for a defined pallet footprint.

2.3.4. Lattice-Boltzmann Method

Another interpretation of the Navier-Stokes equations to estimate fluid kinetics is the Lattice-Boltzmann Method (LBM). This approach is a finite difference scheme, where the fluid is modelled as a finite amount of particles in a network of lattice gas particles at a mesoscopic scale (Figure 2.5). Thus, the exchange of momentum is a result of the interaction of this particles in streaming and collision steps over time. The Boltzmann transport equations is defined as:

$$\frac{\partial f}{\partial t} + \vec{u} \cdot \nabla f = \Omega \qquad 2.12$$

Where,

f: Particle distribution function $f(\vec{x}, t)$ at each lattice node.

$\vec{u}$: Particle velocity (m/s)

Ω: Collision operator.

t: Simulation time

In each two dimensional Lattice node, a particle can adopt 9 different directions – or 27 in the case of a three dimensional grid. Additionally, the velocity of a particle is estimated by a probability function $f_i(\vec{x}, t)$, that represents the particle distribution function in the i direction of each node (i= 1…9), as indicated in Figure 2.5a. The particle streaming and collision process are hence numerically estimated for single phase fluids (such as refrigerated airflow) by the Bhatnagar-Gross-Krook (BGK) collision model (Nourgaliev et al., 2003). Alternatively, different approaches such as Large Eddy Simulation (LES) and Multi Relaxation Time (MRT) had been proposed for more turbulent and complex flows (Yasduda et al., 2013; Park, 2015). The boundary conditions at the no-slip wall at the boundary of the flow domain are typically described by the Bounce-back approach, while the pressure and velocity boundary conditions are described by the Zou-He Boundary condition (Zou and He, 1997).

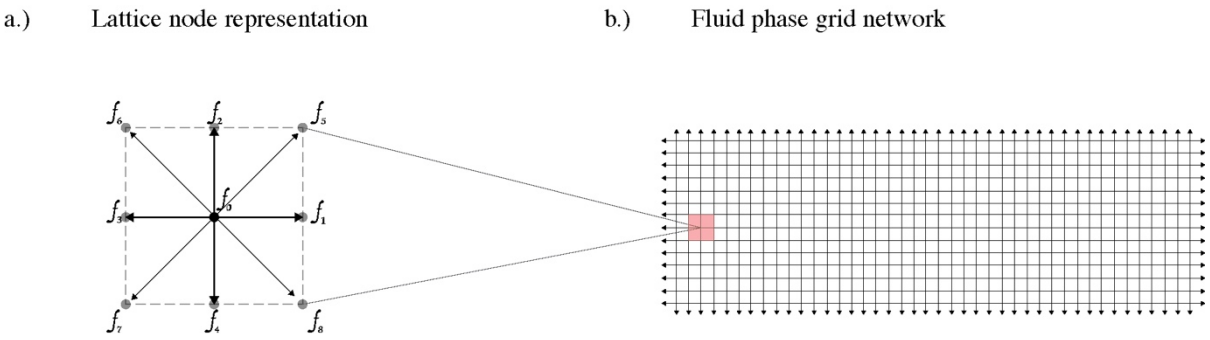

Figure 2.5. *Diagram of a grid in a Lattice-Boltzmann scheme: a.) Diagram of a Lattice node and b.) Geometrical domain of a LBM grid.*

van der Sman et al. (2000) developed a one dimensional Lattice-Boltzmann model to estimate cooling performance of cut flowers, obtaining a good prediction of temperature and mass transport in the produce during the cooling process. Despite the simplicity and effectivity of this approach for cooling operations, an implementation of a two – or three – dimensional model in complex packaging systems, in addition to the implementation of a suitable turbulence model is computationally and time expensive.

2.4. Empirical methods to investigate airflow in forced-air cooling operations.

To primarily characterise the cooling performance of any palletised produce, variables such as temperature, pressure drop and velocity must be considered, allowing to put a metric that measures cooling efficiency in terms of cooling capacity per used energy (Defraeye et al., 2015). Typically, a direct measurement monitors specific variables at specific locations in the packaging space. Thus, pressure drop through the pallet layer can be measured at the inlet and outlet of the pallet, while velocities are arbitrary measured at different points of interest (i.e. near the ventholes, inside the produce bulk, package headspace). With the flourishing progress in computer capacity and technology, indirect measuring methods had been developed, allowing for a more resolute estimation of a velocity field across the system.

In the spirit of creating a simplified airflow model, a characterisation of airflow related variables must be measured and incorporated into the model boundary conditions, and subsequently validated against empirical data of the same system, measuring the model sensibility and potential errors (O'Sullivan et al., 2014).

2.4.1. Gas tracer particles

The use of tracer gas particles as a marker to monitor airflow motion at specific location had been used to estimate airflow distribution in cooling applications (O'Sullivan et al., 2014). This methodology measures gas concentration at specific location in a packaging system. Smale (2004) studied the airflow distribution in packaging systems using carbon monoxide as a tracer. Additionally, airflow through cartons in apple cooling operations was monitored by Tanner et al.

(2002). However, the injection of an external gas to a real precooling process makes this technique ineffective for an industry scale precooling process, not to mention the amount of gas needed to ensure constant monitoring during the whole operation for high fan speed.

2.4.2. Laser Doppler Anemometry (LDA)

By using tracer particles, a laser sheet at a given frequency is projected in the airflow domain. Thus, the fluid relative velocity is therefore estimated by changes on frequency of the scattered light produced by the movements of the tracing particles. Therefore, by observing the changes on the frequency due to flow motion, a magnitude of the particle speed can be thus estimated. This method is typically used for a wide range of fluid velocities (from 10^{-4} to 10^{3} m/s), and provides measurements of velocity at specific locations at a given time. Early experimental work by Alvarez et al. (2003) assessed the airflow characterization at the headspace of a porous bed, simulating a bulk of horticultural produce in a package. Additionally, Merai et al. (2018) assessed the characterization of airflow in a transport container filled with carcasses using a LDA method. Likewise, Pham et al. (2021) monitored airflow through a pallet of a heat generating produce such as cheese during cooling.

This approach presents various advantages compared to other airflow measurements mechanisms, its accessibility to certain locations within the domain, without physically obstructing the system with sensor placements. However, there is no higher benefit on incrementing the airflow estimation resolution, as this approach assess point velocity measurements at given locations.

2.4.3. Particle Image Velocimetry (PIV)

This indirect airflow method estimates the airflow field at a defined plane, aided by a laser sheet at a given time step period by using tracer particles. These time step periods are captured by a high resolution camera, subsequently, estimating a vector field where local particle velocities are estimated, based on particle displacement at each time interval (Gao et al., 2013). The applicability of this method reside in the accessibility of a laser pulse through all potential airflow voids within the system. Hence, typical transparent packaging systems such as silica are commonly used.

Ferrua and Singh (2009c) Monitored the airflow field through a package system using PIV measurements, good agreement was found when comparing the apparent velocity vector field with a an airflow model using Direct Numerical Simulation (DNS). Additionally, Chaomuang et al. (2020) implemented a PIV system to obtain airflow 2-D airflow fields inside refrigerated cabinets, and subsequently, finding good agreement between experimental and a CFD 2-D airflow model.

Despite the great resolution and feasibility of this method, it is limited to a laboratory to pilot scale experiments, for which a palletised system must be simplified according to potential airflow symmetry conditions within the geometrical domain (Ferrua and Singh 2009a).

2.4.4. Anemometry

Local velocity at specific locations is typically measured by anemometry. Their robustness, easy implementation and relative low cost makes this approach practical to estimate airflow render in cool stores. Most used anemometers are thermal and vane anemometers, and their use will depend on the flow speed range and location. Thermal anemometry consists in an electrical resistance that acts as a sensitive instrument, where convective cooling upon this sensor influences a change on its resistance. Consequently, a voltage drop is thus correlated with flow speed characteristics. The use of thermal anemometers to measure point velocity in packaging systems had been explored by Alvarez and Flick (1999) for aerodynamic studies of airflow through bins stacked with spherical produce. Additionally, monitoring of point velocity for the validation of DNS models had been developed for single packages and pallets of apple (Han et al. 2018; Han et al. 2015). Alternatively, vane anemometry uses a rotating vane, where the rotation rate of the vane is proportional to the airflow speed in a one dimensional orientation according to the vane placement respect to the airflow direction. This method is best suitable in larger spaces rather than measuring airflow in small voids, such as beds of produce.

2.4.5. Barometry

The pressure differential between two specific points within a packaging systems can be measured by using a barometer. The most used instrument to achieve this is a pressure transducer, which measures a difference in pressure between two locations using a piezoelectric sensor, relating pressure to a sensor displacement, and consequently a voltage decay is observed, which is linearly correlated to a differential in pressure between the two locations (O'Sullivan et al., 2014). These sensors are typically best suited to high flowrates – such as forced-draft cooling—where a

significant water column displacement can be detected. Notable experimental work been performed to monitor pressure differential through the system to obtains aerodynamic characterization of a given system (Ngcobo et al. 2013; O'Sullivan 2016; Han et al. 2018). Additionally, this method had been used to monitor pressure drop in commercial cold stores in apples and kiwifruit precoolers (Shim et al., 2016).

2.5. Literature review conclusions and thesis general objectives

The importance and benefit of optimising the cold chain process of exported kiwifruit lays in a proper assessment of cooling performance of palletised produce during forced-draft cooling, as indicated in section 2.1. Additionally, package design is the main feature that enhances airflow distribution in a pallet arrangement (section 2.3). However, the influence of venthole design variables (size, location, number) on the apparent airflow resistance, and more specifically the loss coefficient it is still unclear. Hence, characterisation of airflow resistances during forced-air scenarios opens the question towards the relevant variables and boundary conditions of the model. Additionally, the extrapolation of these insights on airflow resistance to a pallet scale scenario is fundamental for characterising airflow resistances in palletised systems, and most importantly, to estimate the venthole loss coefficient within a palletised stack based on analytical correlations.

Different modelling schemes were described and contextualised in section 2.4 with previous research in postharvest applications. Although the DNS approach is the most detailed modelling framework, it is computationally expensive and long solving times makes this approach disadvantageous for optimisation algorithms for forced-air cooling. Similarly, the turbulence modelling implementation in the Lattice-Boltzmann method (LBM) is computationally expensive for prediction of 2-D airflow field during precooling of pelletised kiwifruit and their solving times

can vary from 40 min up to an hour, which is contrary to the prerogative of developing a robust and fast methodology to predict airflow distribution. Alternatively, the resistance network model approach described in section 2.4.3 provides a robust alternative to the common numerical methods based on a finite difference scheme.

Finally, the complexity of implementing an indirect airflow measuring technique is out of the time and spirit of this project. Instead, variables such as point velocity and pressure can be directly measured by anemometry and pressure transducers, respectively. Therefore, this thesis sets the grounds to give answer to the following general objectives:

I. Investigate the effect of venthole design parameters such as size, location, and number on the apparent airflow resistance of a packaging system.
II. Investigate possible correlation between venthole design and airflow resistance in palletised systems.
III. Develop and validate a fast, flexible, and robust airflow model approach to predict airflow distribution palletised kiwifruit.

The development of the subsequent chapters of this manuscript shall give form and answer to each of these objectives.

3. Characterising airflow resistances for different vent hole designs

3.1. Introduction

As discussed in the previous review chapter, box design can change the cooling performance of a given horticultural produce, so there may be an optimal design. A key package design feature that influences cooling performance is the vent hole design. The size, number and location of the vents on the face of a package can enhance or diminish the amount of airflow and its distribution, thus improving or inhibiting both cooling rate and uniformity within a palletised system. The network of vents formed when multiple packages are palletised also influences airflow and distribution, and so may also be a critical package design feature.

The current kiwifruit package design is different from the commonly investigated in literature. Unusually for horticultural produce, kiwifruit are enclosed in a polyliner bag within the package. The intent of the polyliner bag is to prevent significant water loss during the cold chain operation. The presence of the polyliner prevents airflow, thus vent holes in kiwifruit boxes are placed at the top of the panel, allowing an airflow pathway throughout the headspace of the package above the fruit and polyliner.

This chapter intends to determine the apparent significance of vent hole design parameters to the overall airflow resistance of a given package design, and to compare the measured impact with predictions based on literature. The purpose of this is twofold: identifying factors which appear to have a measurable impact are factors that need to be accounted for in an airflow modelling

scheme, and also to determine whether the literature based predictions are accurate enough for this predictions in this cooling application.

In particular, the factors to be considered are:

- Vent hole design factors: vent size, number, and location within a box panel.

- Package design parameters: distance between consecutive box panels (i.e. the length of the box in the airflow direction), headspace cross sectional area (available volume of the airflow pathway) between panels, and number of panels (where the existence of an additional panel due to a subsequent package is included).

3.2. Materials and methods

3.2.1. Wind tunnel

A temperature controlled wind tunnel was used to test the effect of different vent design parameters and monitor pressure across multiple panels on the airflow direction, similar to a real scale horticultural package. Figure 3.1 shows the longitudinal section of the wind tunnel, located in the Bio Process Laboratory at Massey University, Palmerston North, New Zealand. A flow straightener section followed by a grid inside the tunnel is used to achieve uniform airflow distribution inside the test section. The tunnel has a square cross section with an internal side length of 27.8 cm and a variable speed drive fan for airflow speed control is also integrated.

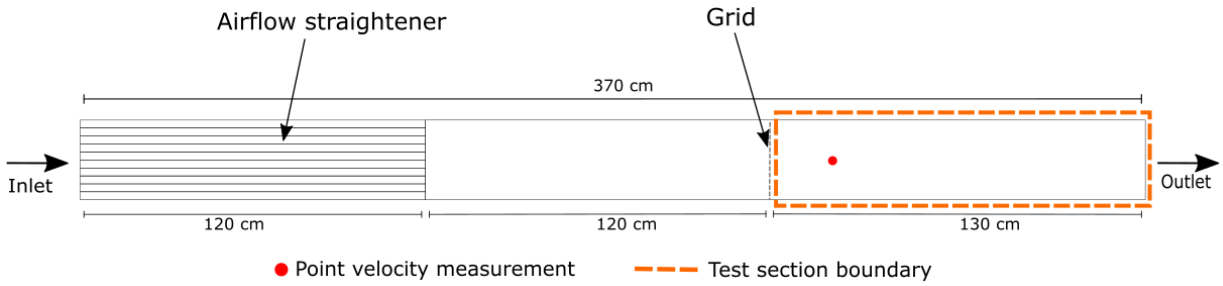

Figure 3.1. *Longitudinal drawing of the variable speed fan wind tunnel and test section.*

The velocity distribution over the duct cross section is practically never uniform (Figure 3.2b). Therefore, the mean duct velocity is used to describe the airflow motion during the experiment. Point velocity was measured at multiple points across the area of the duct, according to Figure 3.2a. It is more convenient for experimental work to be able to make a single point velocity measurement in the duct and extrapolate the average duct velocity. Thus, a calibration curve that relates the mean cross sectional velocity in the tunnel to a measured local point velocity is depicted in Figure 2c. The measured locations are described in Figure 3.2a. Finally, point velocity was measured with a hot wire anemometer with a ± 2 % accuracy (9545 Velocicalc Air velocity meter, TSI, USA).

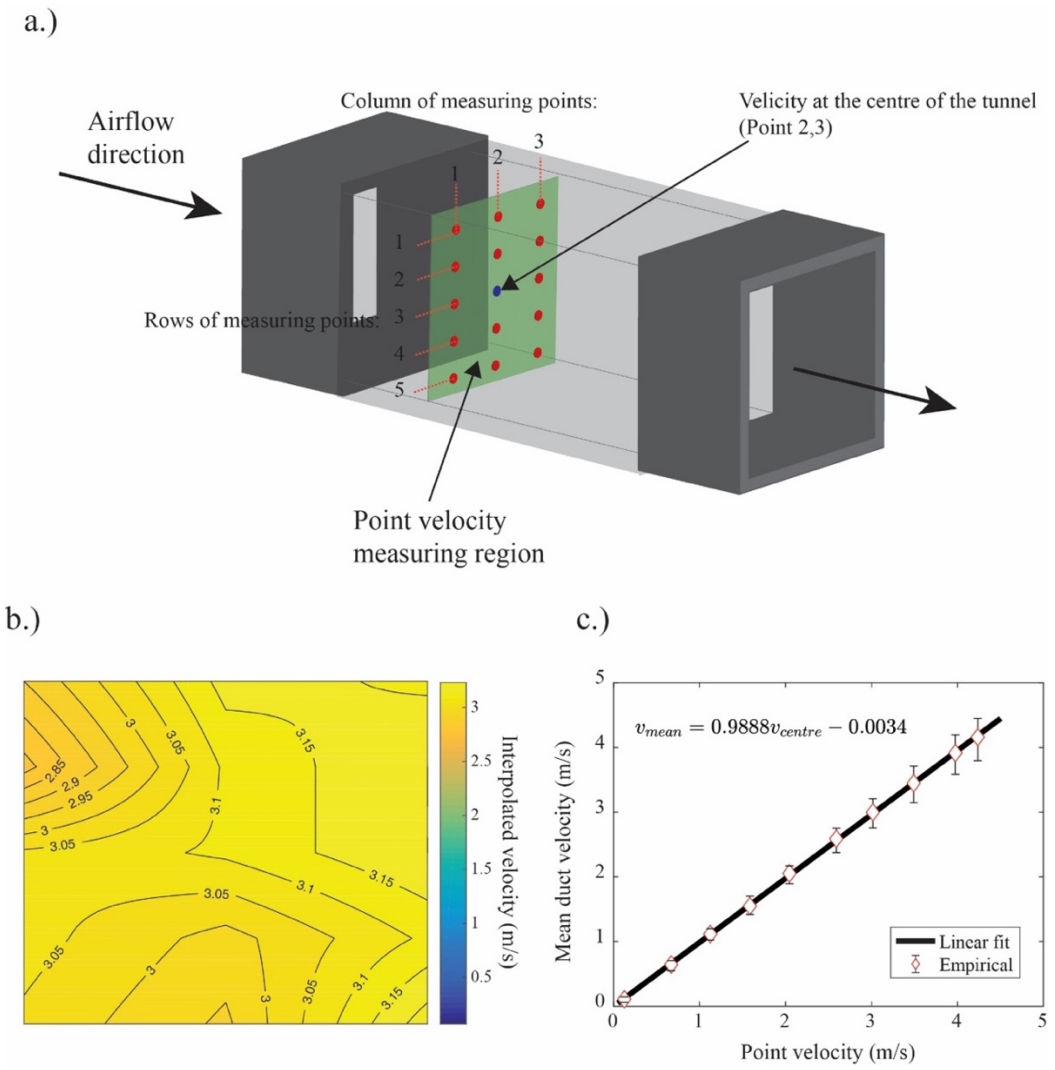

Figure 3.2. *Mean duct velocity correlation diagram. a.) experimental set-up of point velocity measurements, b.) linearly interpolated contour plot of velocity distribution in the measured cross section region, and c.) correlation of point velocity at the center of the duct and the corresponding mean duct velocity from all measured points.*

3.2.2. Vent designs

Three vent design parameters were investigated to measure the incidence of the vent hole design on the apparent airflow resistance; vent size, location and number, as depicted in Figure 3.3. Each plate was made of medium density fibre (MDF) of 5 mm thickness, cut with a laser cutter (Fusion M2 Epilog Laser, Epilog, USA), mimicking the average box panel used in package design for the

horticultural industry. Box panels are in fact made of corrugated card with an outer face on either side separated by a corrugated flute. The typical thickness of the corrugated card used in kiwifruit boxes ranges between 4 and 11 mm – in cases where the package is folded in two layers of flute. In this case, MDF plates were used instead of corrugated card as the more hardy MDF would not easily deform. This allowed many measurements to be made with the test plates without uncontrolled changes in geometry due to deformation and damage from handling in previous experiments.

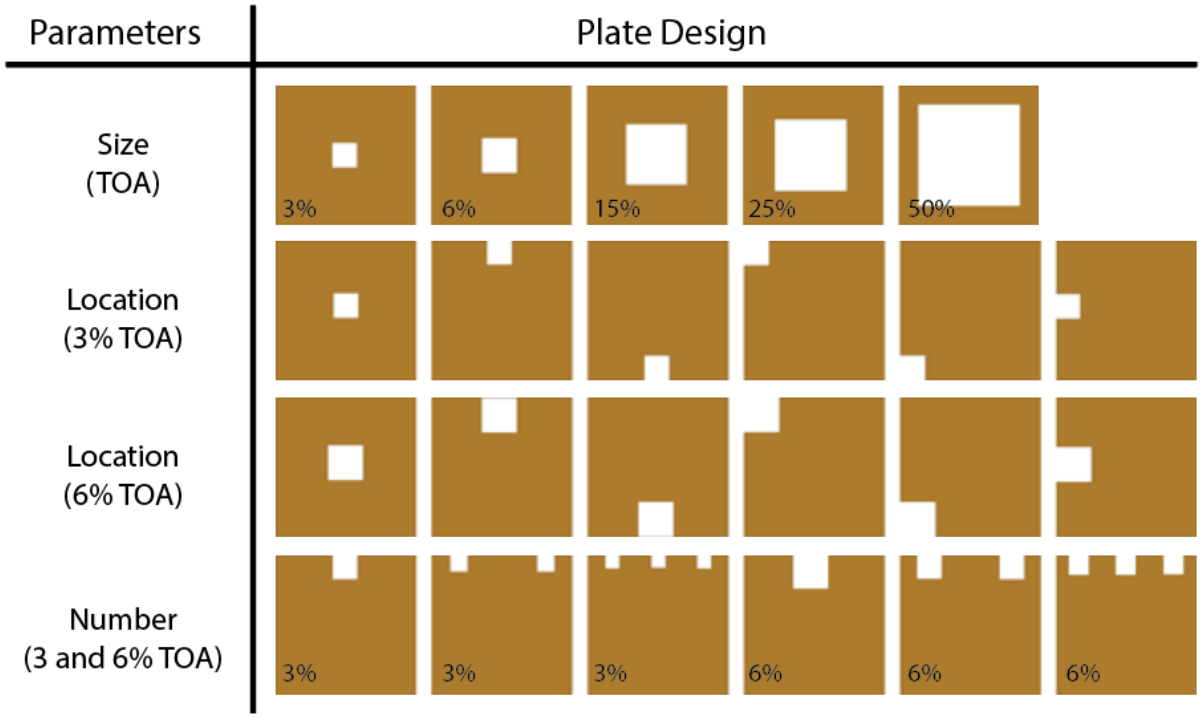

Figure 3.3. *Diagram of all the studied plate designs. Each plate has a 27.8 cm diameter.*

3.2.3. Pressure measurements

Two different sets of piezoelectric sensors probes were used to measure pressure in the wind tunnel. The specifics of each set and their logging interface are detailed as follows:

1) One ±1 H_2O inch (± 248 Pa), and one ± 2 H_2O inch (± 496 Pa) sensor (SSCSNBN002NDAA5, Honeywell, Morris Plains, USA) with 2% accuracy. Data was logged directly into the operating system using a data logger interface (Picolog1216, Pico Technologies, UK).
2) Ten ±1 H_2O inch (± 248 Pa) sensors (P992-1B-A, Sensata-Kavlico, MA, USA) with 2 % accuracy. Data was stored using a Squirrel data logger interface (2040 Series Squirrel Meter/Logger, Eltek Ltd., Cambridge, UK).

A logging interval of 1 second was used during this experiment. Data stored from each of the two interfaces was logged as voltage differential. In order to obtain the resulting pressure data at time t from the raw data, the following relationship was used:

$$P_t = \frac{V_{supply}}{V_{logger}}\left(V_t - V_{ref}\right)C_{conv} \tag{3.1}$$

Where

P_t: Pressure at time t (Pa).

V_{supply}: Supply voltage from energy source (V)

V_{logger}: Operational voltage of the logging interface (V)

V_t: Output voltage at time t (V)

V_{ref}: Reference voltage, defined as the average of the voltage output during the first 30 seconds of recording (no fan power applied) (V).

C_{conv}: Conversion coefficient between the overall measuring pressure range and the voltage range of the sensor probe (Pa/V).

And

$$C_{conv} = \frac{P_{max} - P_{min}}{V_{max} - V_{min}} \quad 3.2$$

According to the manufacturer specifications, the ratio between the supply and logger voltage (V_{supply}/V_{logger}) is stablished as 2 and 1 for the type (1) and type (2) sensors probes, respectively. Figure 3.4 shows the recorded voltage output and its corresponding conversion to pressure. Voltage was recorded at eight different fan speeds over the whole duration of the monitoring period for a ± 1 and 2 H_2O inch range sensors (type (1)). Two sensor probes were located at 5 cm of distance inside the test section of the wind tunnel. Each visualised step correspond to a change on the fan speed, as indicated in Figure 3.4a. Additionally, velocity and pressure over time for each fan speed is assumed to be steady state, thus the time-averaged pressure was used for all the subsequent analysis. Each fan speed was averaged over at least 120 seconds of data recording.

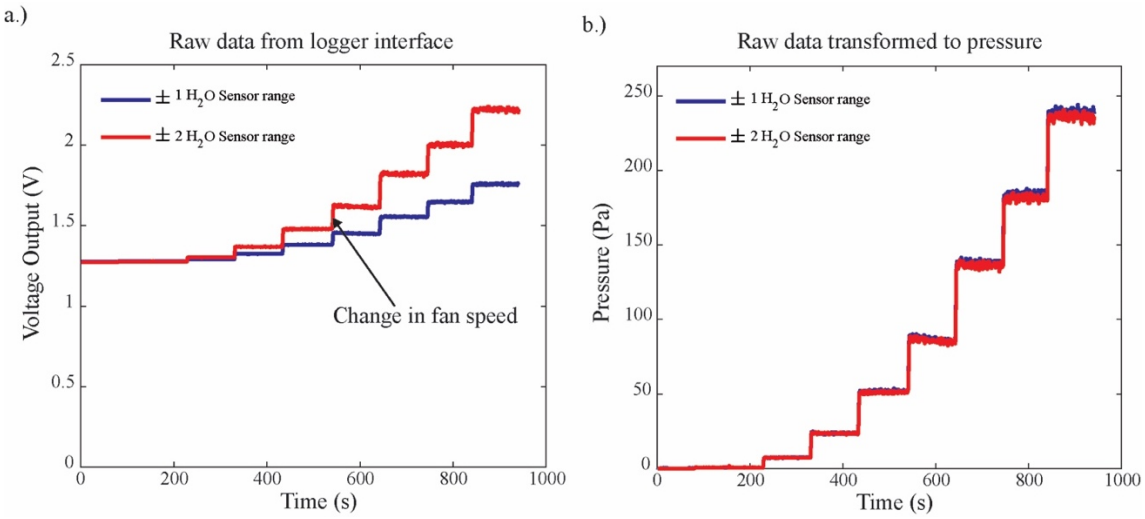

Figure 3.4: *Data logged at one second interval for two different range pressure sensors. Where a.) correspond to the voltage output raw data extracted from the logging system, and b.) is the converted pressure data by using the relationship described in equation 3.1.*

3.3. Experimental design

3.3.1. Pressure drop across a single vent

Type (1) pressure sensors were used to monitor differential pressure across each plate, placing each sensor probe to its corresponding pressure tap at the top of the test section, at 3.75 cm upstream and downstream from the plate according to the diagram in Figure 3.5. Point velocity was measured at the centre of the duct as indicated by the red dot in, and subsequently, the mean duct velocity was determined by using the relationship described in Figure 3.2c. This procedure was repeated at each fan speed, in triplicate.

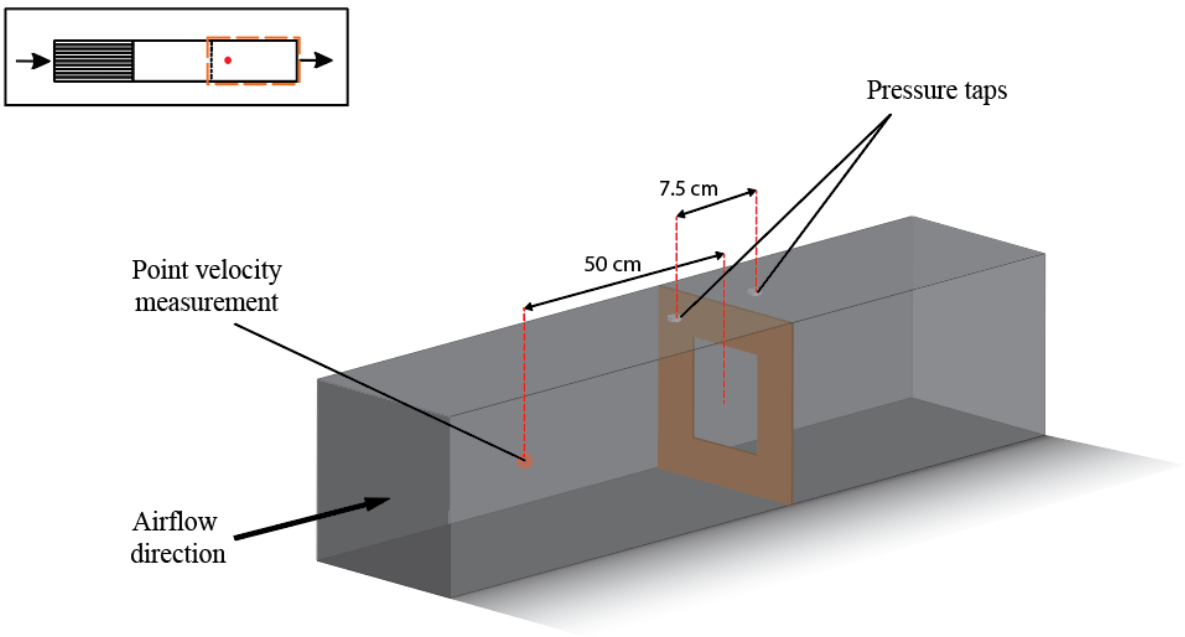

Figure 3.5. *Schematic diagram of the test section of the wind tunnel for a plate with 25% total open area (TOA).*

3.3.2. Pressure drop between multiple plates

Distance between plates, headspace cross-sectional area and number of plates are important parameters that can influence airflow resistance inside the wind tunnel. To visualise the effect of distance between plates and the cross sectional area of the headspace, a Face-Centered composite design (CCF) with three level factorial design (3^k) was developed, reducing the number of experiments without risking the visualization of the effect of any of these factors under study (Montgomery 2017). This CCF considered two factors: (1) the length of the box L (m), and (2) the internal cross sectional area of the headspace (m^2), which represents the internal composition of a package (bulk of produce) independent of the length between plates. Three different lengths were considered: 0.2, 0.3 and 0.4 m, as this dimensions are among the ranges of the commonly used packages in the kiwifruit industry. Additionally, three different headspace cross sectional areas were considered: 0.077, 0.047 and 0.017 m^2, resembling a filled, half filled, and empty package, respectively. Figure 3.6 shows the diagram of the CCD. From these two factors, 9 possible experiments were identified by a 3^k design, where k is the numbers of factors, in this case $k = 2$. After the analysis, the amount of experiments was reduced to 5(indicated by red stars; Figure 3.6). The resulting set of experiments are depicted in Figure 3.7.

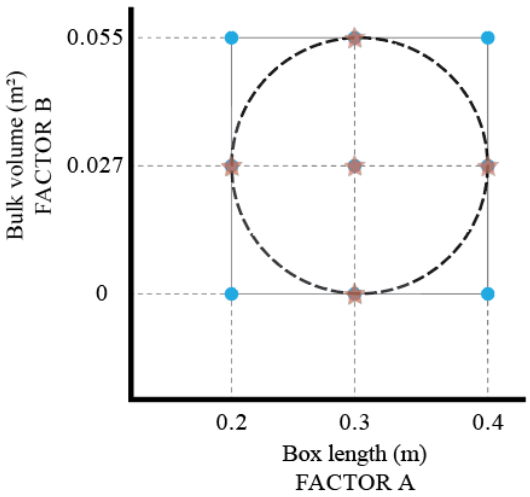

Figure 3.6: *Diagram of a three level Face Centered Composite Design (CCF) for 2 factors.*

Additionally, the effect of the number of consecutive plates on the airflow resistance was evaluated by placing three plates separated by 20 cm (Figure 3.7f). This resulted in a total of 6 experiments. A 6% total open area (TOA) vent size was selected for this experiment, as this vent area is usually within the range of vent designs managed in the kiwifruit industry (O'Sullivan 2016; Olatunji 2018).

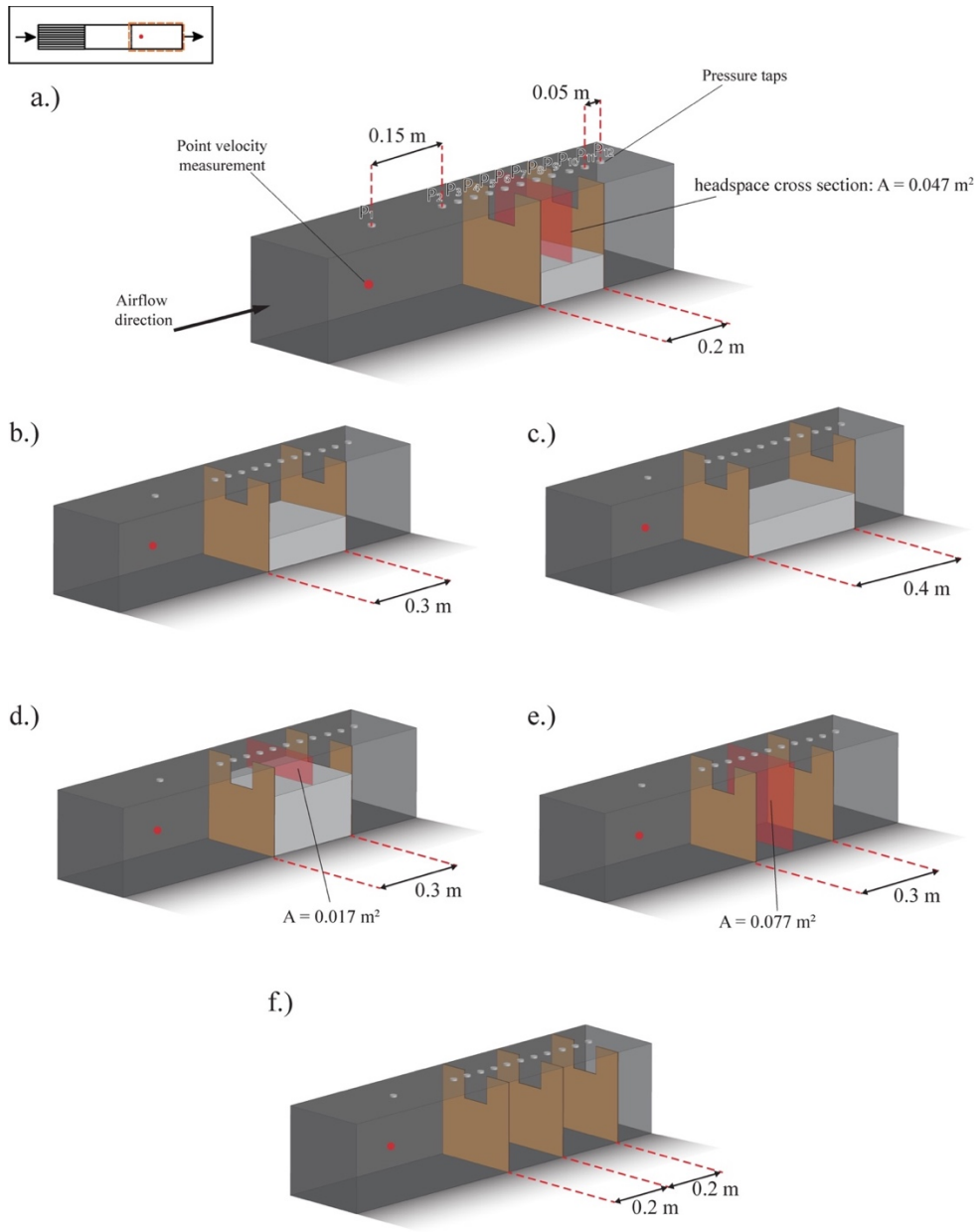

Figure 3.7. *Diagram of the experimental set-up of the test section inside the wind tunnel to measure the effect of length (a, b and c), internal headspace between plates (a, d and e), and number of plates (e and f) on the apparent airflow resistance.*

3.4. Data processing and analysis

The energy balance between two reference points *1* and *2* inside the duct is given by Bernoulli's equation:

$$z_1 g + \frac{p_1}{\rho} + \frac{v_1^2}{2} = z_2 g + \frac{p_2}{\rho} + \frac{v_2^2}{2} + \Delta H_m + \Delta H_f \qquad 3.3$$

Where,

z: Height of reference point (m)

p: Pressure at reference point (Pa)

ρ: Air density (kg/m^3)

g: Gravitational acceleration (m/s^2)

v: Mean duct velocity at reference point (m/s)

ΔH_m: Head loss due to minor losses

ΔH_f: Head loss due to friction

Air density at 25°C and 80% RH were chosen for this analysis as this environmental condition was set in the wind tunnel, and additionally, small differences in ambient conditions were considered to be not significant (Tsilingiris 2008). Moreover, no differences in height and friction losses within the air duct were considered. Equation 3.3 can be thus simplified considering only the changes in pressure as a result of accessories along the flow direction – such as an orifice plate – which directly affect the dissipation of kinetic energy into pressure loss. Thus, the pressure loss due to flow through an orifice plate is described by:

$$\Delta p = \rho_{air} k \frac{v^2}{2} \quad (3.4)$$

Where,

Δp: Pressure drop between the two reference points (Pa)

k: Apparent vent hole loss coefficient (-)

v: Air superficial velocity inside the duct (m/s)

A simplified representation of an airflow resistance is the loss coefficient (k) of a vent hole. This k value has been reported to be a function of the Reynolds number and the ratio between the orifice and the duct size, also known as the Total Open Area (TOA) ratio. A compendium from Idelchik (1987) gives commonly used relationships from the fluid flow disciplines, and describes the loss coefficient (k) of a sharp edged orifice (as depicted in Figure 3.8) of arbitrary dimensions inside a duct in its general form:

$$k = \left[k_D + k_C \cdot \left(1 + 0.707 \cdot \sqrt{(1 - TOA)} - TOA\right)^2\right] \cdot TOA^{-2} \quad (3.5)$$

Where,

k_D: Loss coefficient at the discharge of the orifice (-).

k_C: Loss coefficient of the stream jet contraction of the orifice (-).

TOA: Total open area. Ratio of the area of the orifice respect to the cross sectional area of the duct (-).

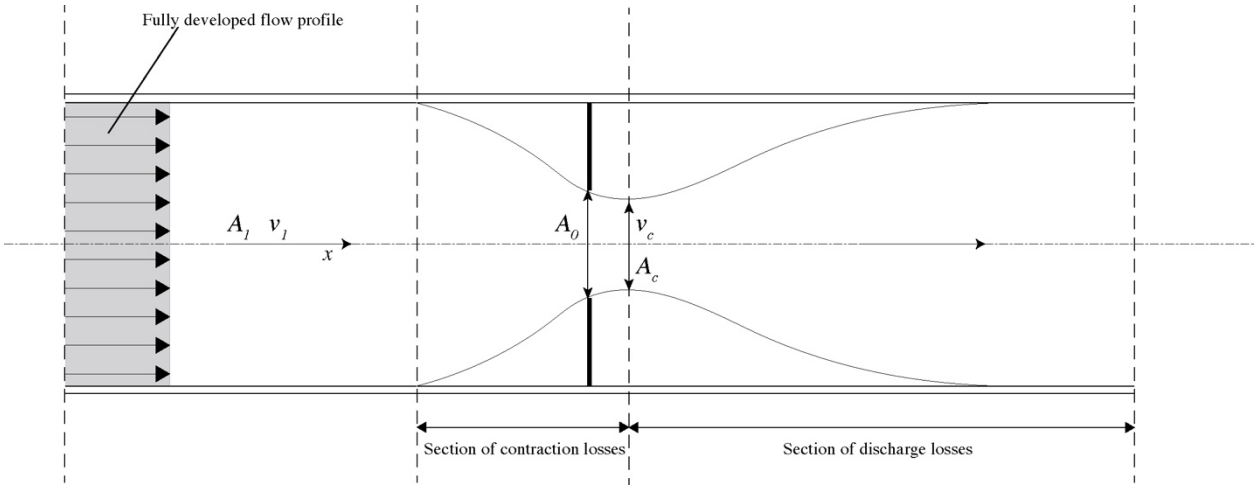

Figure 3.8: *Diagram of an ideal fully developed flow through an orifice plate.*

The variation of k_D and k_C as a function of an orifice TOA and Reynolds number for a given orifice size are shown according to the data obtained from Idelchik (1987) (Figure 3.9a). A shape-preserving piecewise cubic (*spline*) interpolation algorithm was performed in order to obtain values of k_D and k_C for all the studied TOA (Figure 3.9b).

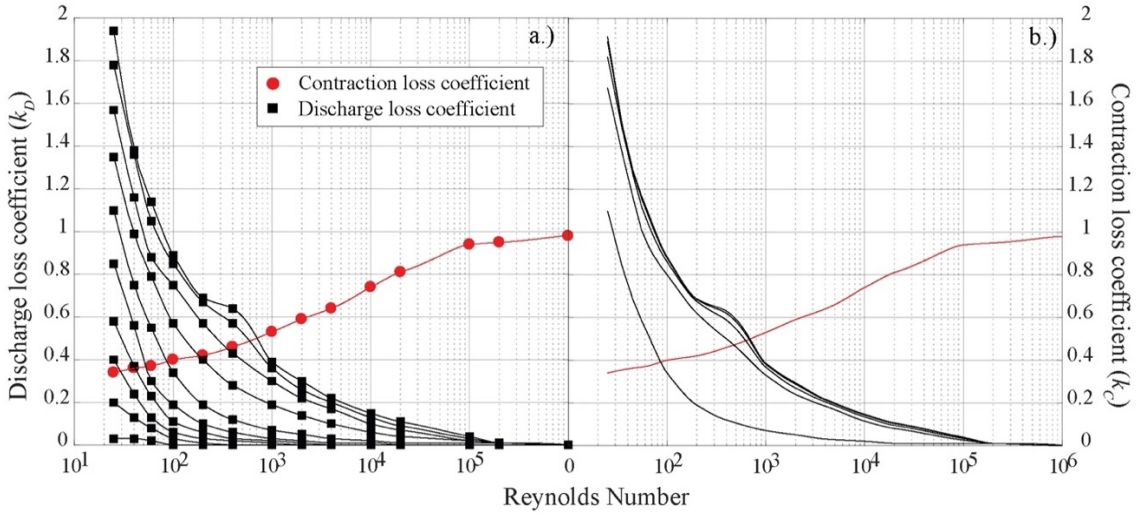

Figure 3.9: *Empirical (data points) and interpolated data (solid curves) for the discharge* (k_D)*, and contraction* (k_C) *loss coefficient of an orifice. a.) Data extracted from Idelchik (1994), where black curves represent different total open areas (TOA) (0.95, 0.9, 0.8, 0.7, 0.6, 0.5, 0.4, 0.3, 0.2, 0.0) (from bottom to top curves, and. b.) Interpolated data for the investigated TOA (0.5, 0.25, 0.15, 0.06 and 0.03) (from bottom to top curves).*

Typically, the flow regime of the refrigerated air during forced air cooling operations is turbulent, although transitional flow can be developed at locations of high resistance. During the wind tunnel

experiments, the Reynolds number at the second fan speed ranged from transitional to turbulent flow between 3 and 6% TOA. However, from 15 to 50% TOA the flow regime is assumed to be turbulent for all the studied fan speed. According to Figure 3.9, when the Reynolds number is approximately 10^5, the corresponding values of k_D and k_C starts to converge to 0 and 1, respectively. Thus, Equation 3.5 can be further simplified to:

$$k = \left(1 + 0.707 \cdot \sqrt{(1 - TOA)} - TOA\right)^2 \cdot TOA^{-2} \quad 3.6$$

An empirical approximated model was obtained by fitting the experimental data to Equation 3.4, using a Non-linear least squared algorithm. According to the raw pressure data output from the sensors (Figure 3.4b), mean pressure drop values were assumed to be normally distributed between repetitions. Moreover, a Kolmogorov-Smirnov normality test was performed to ensure normality (data not shown). The significance of differences between the empirical pressure loss coefficients were determined by using one-way analysis of variance (ANOVA) at 95% confidence interval. Multiple comparison test between treatments was performed by using Tukey's Honestly Significant Difference procedure at 95% confidence interval. Additionally, the Mean Absolute Percentage Error (MAPE) was used to compare the experimental and a predicted loss coefficient (calculated via Equations 3.5 and 3.6, depending on the Re number) as:

$$MAPE = \frac{1}{n}\sum_{1}^{n}\left(\frac{k_{exp} - k_{theory}}{k_{exp}}\right) \times 100 \quad 3.7$$

Where,

k_{exp}: Experimental loss coefficient obtained from Equation 3.4.

k_{theory}: Theoretical loss coefficient obtained from Equation 3.5 and 3.6 (-)

n: Number of experiment repetitions ($n = 3$)

3.5. Results and discussions

3.5.1. Effect of vent design parameters on the pressure loss coefficient

3.5.1.1. Vent size

The effect of the vent size ranging from 3 to 50% TOA on the consequent pressure loss are shown in Figure 3.10. As expected, as the total open area (TOA) increases, its corresponding loss coefficient decreases (as shown in Table 3.1). A lower apparent resistance to airflow implies that less kinetic energy is lost as turbulent dissipation, thus having a relative lower loss in pressure, in comparison to the smallest vent (Idelchik and Steinberg 1994; Ai and Mak 2013). Interestingly, differences in pressure drop between 3 and 6% TOA are up to 6.7% at the maximum fan speed, while the differences in superficial velocity are approximately doubled. This gives valuable information to consider when designing a package; increasing the vent of a package in the low size range can improve the airflow rate significantly with little pressure loss cost, hence, providing potential for an improvement in the cooling performance of an horticultural package. In practice, a bigger vent hole leads to a shorter cooling time of a produce. However, de Castro, Vigneault, and Cortez (2004) demonstrated that the half cooling time (HCT) does not improve significantly for vents bigger than a 14 % TOA.

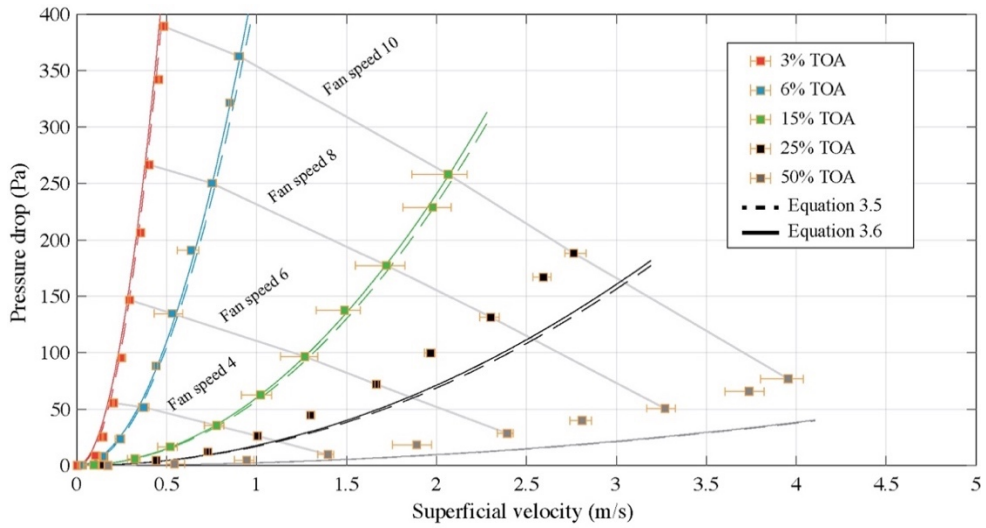

Figure 3.10. *Effect of vent size on pressure drop through an orifice plate. Data points represent the measured data with error bars representing the range of measured values. Dashed and solid lines represent theoretical pressure drop using the loss coefficient calculated by Equation 3.5 and 3.6, respectively. Grey lines represent the corresponding duct fan speed.*

Table 3.1: *Comparison of empirically fitted and theoretical loss coefficient values for all the studied total open areas (TOA).*

Total Open Area (TOA) (%)	$k_{exp}(\mu \pm \sigma)$	Prediction via Equation 3.5		Prediction via Equation 3.6 (for $Re > 10^5$)	
		k_{theory}	MAPE (%)	k_{theory}	MAPE (%)
3	2733.7 ± 38	3009.80	10.11	3085.1 1	12.87
6	744.3 ± 33.7	716.04	4.20	733.92	3.47
15	102.6 ± 13.9	97.81	8.87	100.24	8.79
25	41.5 ± 1.2	28.98	30.08	29.69	28.35
50	8.1 ± 0.3	3.91	51.92	4.00	50.78

Predictions of *k* were made using Equation 3.5 and 3.6, and the Mean Absolute Percentage Error (MAPE) between each prediction and the experimentally derived value was calculated (Table 3.1). Equation 3.6 was found to have the smallest MAPE value for all the studied vents, expect for the smallest size of vent (3 % TOA) (Table 3.1). Strictly, the simpler Equation 3.6 is only valid at Re numbers above 10^5. However, the MAPE error values for equation 3.6 are not dissimilar to the values from the more complex Equation 3.5 that has the parameters k_c and k_d, which depend upon Re number. This means that the simpler Equation 3.6 might be "good enough" for this application. This result opens the possibility to use a simplified relationship to predict the loss coefficient of an orifice plate without dependency on the Re number, which would greatly simplify the computation of loss coefficients in more complex airflow networks of packages, for example, as is found in a palletised arrangement. However, this statement is strictly only valid for flow regimes beyond the transition regime (high Re number). As the flow becomes laminar, this relationship does not hold to be accurate (Figure 3.15), therefore a more appropriated relationship to obtain a loss coefficient needs to be employed (Idelchik and Steinberg 1994; Rennels and Hudson 2012). In practice, laminar flows are likely to not occur during forced-draft cooling of palletised kiwifruit, however, laminar regimes zones can potentially be found in refrigerated shipping operations (Smale 2004).

Despite the overall good agreement, an evident lack of fitting between empirical and theoretical data was observed, where MAPE values around 50 and 28 % were found at 25 and 50% TOA, respectively. This is partly because the *k* value is much smaller at large TOA values, so even a small absolute error in *k* corresponds to a much larger relative error. However, as this project required more accurate *k* values, new parameters of k_D and k_C were fitted for Equation 3.6, accounting for the large TOA values. The fitting proceeded by determining new discharge and contraction coefficients, so that a new loss coefficient relationship was obtained (Equation 3.8). Figure 3.11 shows a comparison of the simplified loss coefficient relationship (Equation 3.6), and its subsequent adjustment, where a non-linear least squared algorithm was performed ($R^2 > 0.99$). Thus, a newly adjusted loss coefficient (k_{adj}) relationship for all our studied vent designs was defined as follows:

$$k_{adj} = \left[2 + 0.17 \cdot \left(1 + 0.707 \cdot \sqrt{(1 - TOA)} - TOA\right)^2\right] \cdot TOA^{-2} \qquad 3.8$$

By using the general form of the loss coefficient calculation (Equation 3.5), coefficients of discharge and contraction can be adjusted to a given system.

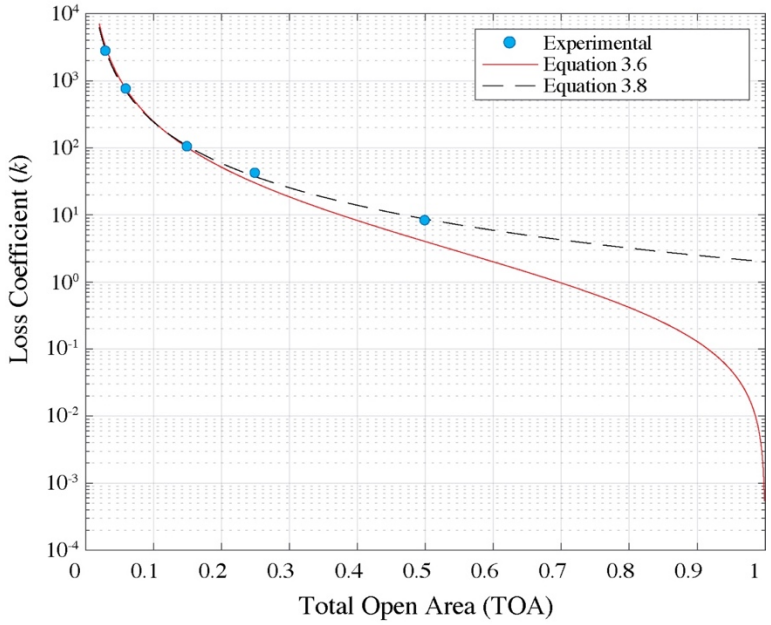

Figure 3.11. *Comparison between Equations 3.6 and 3.8 for predicting the vent loss coefficient, contrasted by empirical loss coefficient (k).*

3.5.1.2. Vent location

Vent location had no apparent effect on the pressure drop for plates with 3 and 6 % Total Open Area (TOA), according to Figures 3.12 and 3.13, respectively. However, the corresponding empirical loss coefficient shown in Table 3.2 revealed significant differences between some of the locations for both TOAs. The loss coefficients of the top and bottom vent locations are significantly different to all the other locations for a 3 % TOA plate (Figures 3.12b and 3.12c, respectively). Similarly, significant differences were found between top and centre vent locations for a 6 % TOA (Figures 3.13b and 3.13a). In addition to this, differences in superficial velocity between centre and top vents (Figures 3.13b and 3.13e) reached 13.8% at the highest fan speed, while there is only 2.14 % difference in pressure drop. This variability in superficial velocity could be caused by the close distance between the point velocity measurement location and the orifice plate. The flow profile in the cross sectional area of the duct changes as the flow approaches the orifice, changing the velocity distribution across the section of measurement. As

a result, this variability in superficial velocity at the top vent is greater with a smaller orifice (3 % TOA, Figure 3.12b), in comparison with a 6 % TOA at the same location (Figure 3.13b). Additionally, no apparent differences were found for the use of either Equation 3.5 or 3.6 to calculate the pressure loss coefficient for all the studied vents. However, the error related to the experimental data reaches approximately 50 and 20 % for the top vent with 3 and 6% Total Open Area (TOA), respectively.

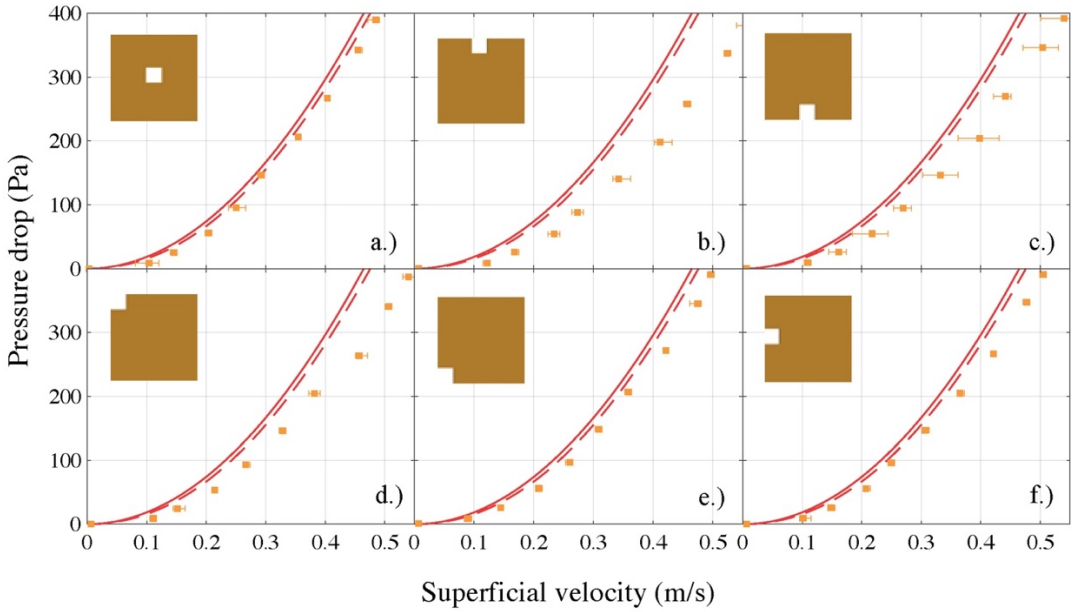

Figure 3.12. *Effect of vent location on the pressure drop for a 3 % Total open area (TOA) orifice plate. Dashed and solid lines represent theoretical pressure drop using the loss coefficient calculated by equation 3.5 and 3.6, respectively. Error bars represent the range of measured superficial velocity data.*

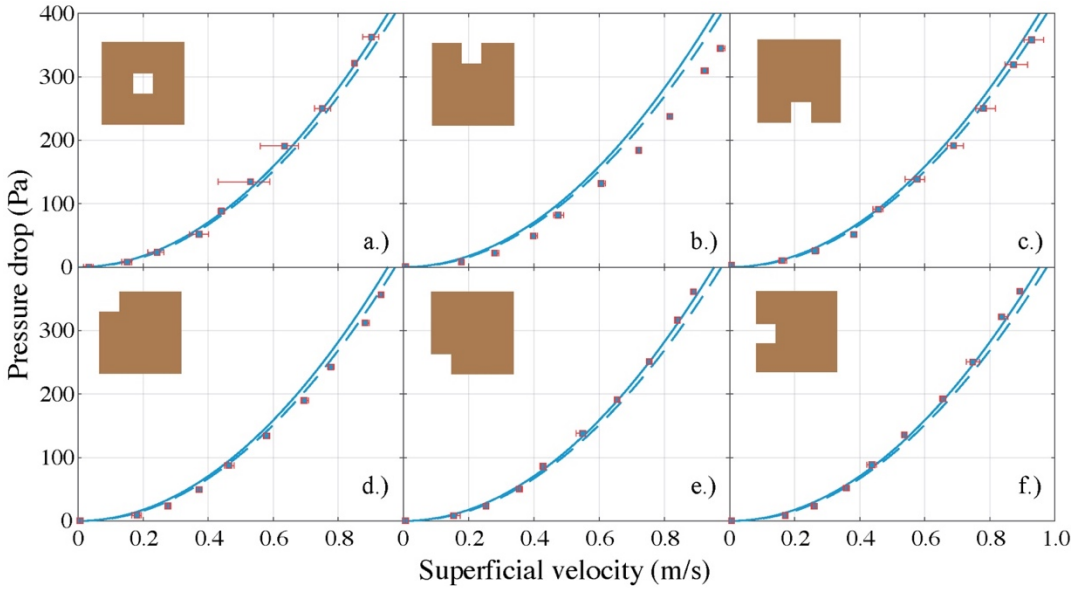

Figure 3.13. *Effect of vent location on the pressure drop for a 6 % Total open area (TOA) orifice plate. Dashed and solid lines represent theoretical pressure drop using the loss coefficient calculated by equation 3.5 and 3.6, respectively. Error bars represent the range of measured superficial velocity data.*

Optimising the vent location of a package has benefits in improving the uniformity and overall cooling performance of a porous media, however, changing the vent holes locations at constant total open area (TOA) does not necessarily imply a change in pressure drop (de Castro, Vigneault, and Cortez 2005). Nonetheless, this change in location does not account for potential obstructions of the vent hole. In practice, vents not located at the top of the box will possibly have fruit immediately in the airflow pathway, and similarly, a polyliner can fully or partially block the vent, thus affecting its loss coefficient.

Table 3.2. *Empirical loss coefficient of each vent location for 3 and 6% Total Open Area (TOA). Values of mean absolute percentage error (MAPE) are reported for each vent location respect of its corresponding theoretical loss coefficient for low (Equation 3.5) and high Reynolds (Equation 3.6) numbers. Means with the same superscript letter are not significantly different (p = 0.05).*

	3% TOA			6% TOA		
	$k_{exp}(\mu \pm \sigma)$	MAPE Eq. 3.5 (%)	MAPE Eq. 3.6 (%)	$k_{exp}(\mu \pm \sigma)$	MAPE Eq. 3.5 (%)	MAPE Eq. 3.6 (%)
Centre vent	2733.7 ± 38.0^{a}	10.05	12.87	744.3 ± 33.7^{ab}	4.21	3.47
Top vent	2011.1 ± 77.7^{b}	49.73	53.56	597.5 ± 5.9^{c}	19.16	22.84
Bottom vent	2252.9 ± 266.4^{b}	34.77	38.22	683.9 ± 43.1^{b}	5.76	7.60
Top left vent	2180.9 ± 65.7^{b}	38.02	41.55	668.6 ± 7.3^{b}	7.04	9.78
Bottom left vent	2590.2 ± 41.0^{a}	16.15	19.13	747.4 ± 4.5^{ab}	4.25	1.80
Centre left vent	2530.0 ± 25.9^{ab}	18.90	21.95	754.7 ± 13.8^{a}	5.16	2.74

3.5.1.3. Vent number

No significant differences were found between apparent loss coefficient when modifying the number of vents. However, the error of fitting the experimental data into both theoretical curves reaches up to 66 and 23 % for 3 and 6 % TOA, respectively (Table 3.3). Additionally, plates with a 3% TOA also presented higher MAPE values for all the studied vent numbers. Vigneault et al. (2004) previously found differences in pressure drop imparted by vent number at 25% total open area (TOA) plates. Those results suggest that pressure drop would increase with vent number at high TOA, but that study was conducted with the TOA distributed over a much larger number of vent holes. That is to say, that there might be a point at which the number of vents that the TOA is distributed over becomes significant regarding to pressure drop, but this number may be greater than the typically observed on kiwifruit packages (Olatunji 2018).

By modifying the number of vent holes of a package, the incoming airflow can be evenly distributed over the cross section of the food matrix, and thus optimising its cooling performance (Dehghannya, Ngadi, and Vigneault 2011). However, more complex package configuration such as polylined kiwifruit, implies a different thermodynamic approach, where natural convection of heat through the stagnant air trapped by the polyliner plays a more prominent role in the overall cooling performance (O'Sullivan 2016). Consequently, Olatunji (2018) empirically concluded that by increasing the number of vents, a better uniformity can be achieved, however, these results did not necessarily ensured a better cooling time.

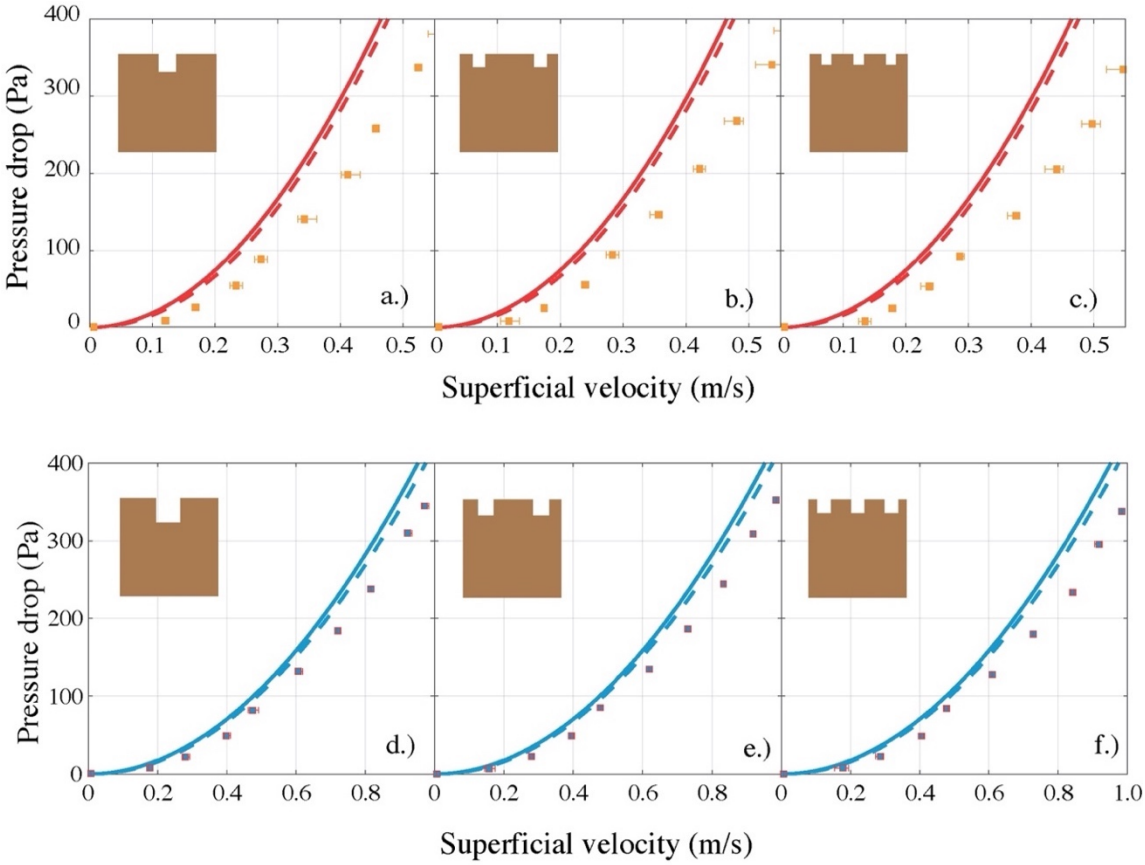

Figure 3.14: *Effect of vent number on the pressure drop for 3(a-c) and 6 %(d-f) TOA. Solid and dashed lines represent the theoretical pressure drop calculated by equations 3.5 and 3.6, respectively. Error bars represent the range of measured superficial velocity data.*

Table 3.3: *Empirical loss coefficient for 1, 2 and 3 vents for 3% and 6% total open area (TOA). Values of mean absolute percentage error (MAPE) are reported for each studied vent number for both low (Equation 3.5) and high (Equation 3.6) Reynolds number range. Means with the same superscript letter are not significantly different (p = 0.05).*

	Number of vents	$k_{exp}(\mu \pm \sigma)$	MAPE (%) $Re < 10^5$ (Eq. 3.5)	MAPE (%) $Re > 10^5$ (Eq. 3.6)
3 % TOA	1	2011.1 ± 77.66[a]	49.73	53.56
	2	1982.2 ± 134.95[a]	52.21	56.11
	3	1852.9 ± 108.38[a]	62.71	66.87
6 % TOA	1	597.5 ± 5.85[a]	19.77	22.84
	2	596.4 ± 0.7[a]	19.88	23.06
	3	598.3 ± 108.38[a]	19.65	22.71

Finally, vent location and number did not have a direct impact on the loss coefficient and its consequent pressure drop for the studied configurations. However, the loss coefficient does change with changing the vent size. Figure 3.15 summarises all the data obtained from the conducted experiments, where empirical correlations shows a reasonable agreement with the empirical data, and additionally, new relationships were developed where adjustment of loss coefficient where necessary (25 and 50 % TOA). Despite these findings, it shall be remarked that this information is valid mainly for turbulent flow regimes, as laminar flow behaves fundamentally different, and thus more appropriated flow measurements techniques shall be used in order to obtain deeper understanding of the respective airflow resistance. As the main goal of this project is to understand the forced-draft convection process, laminar regimes were not considered significant to be studied in depth. However, cold chain operations such as marine transport or storage can eventually present situations where laminar regimes are important to consider (Smale 2004), and thus the resistance through packages needs to be addressed accordingly (van der Sman 2017).

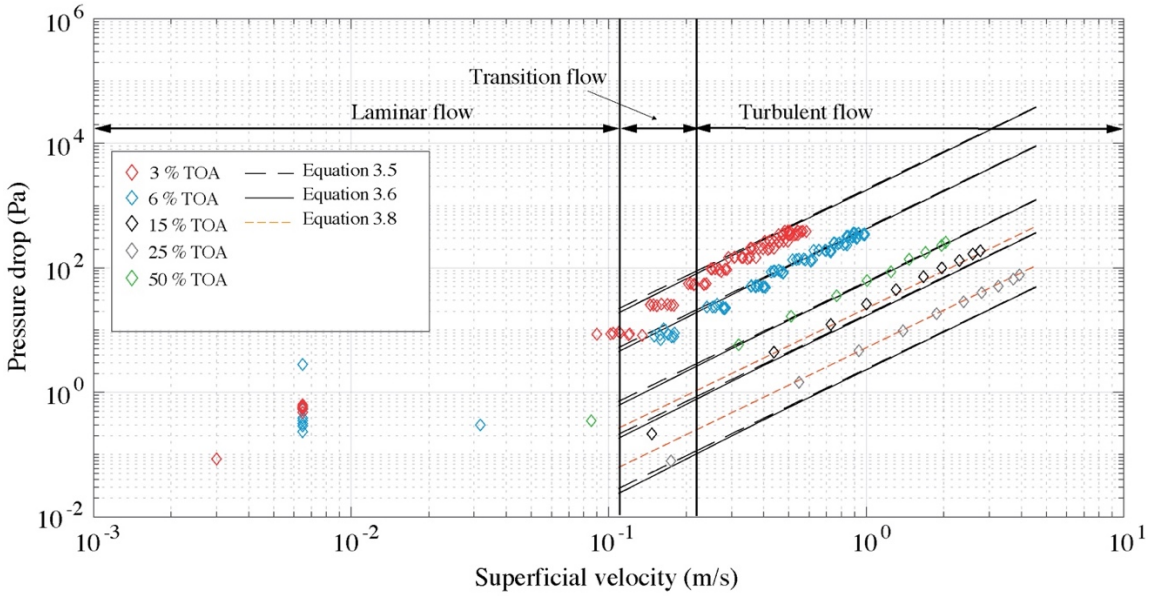

Figure 3.15. *Pressure-superficial velocity relationship of all the studied vent designs. Black lines represent the literature prediction of an ideal orifice plate. Orange lines represented the adjusted theoretical relationship of orifice of arbitrary flow conditions.*

3.5.2. Pressure drop between plates

High areas of pressure loss were identified to happen mainly across the plates, in comparison with the pressure loss due to friction in the duct walls (from 82 % of the total pressure drop, Figure 3.16c). In addition, pressure losses at the inlet plate were substantially major compared to the pressure loss at the subsequent plates within the duct, for all the studied systems (from 64 % of the total pressure drop, Figure 3.16c). In a similar way, Ambaw, Mukama, and Opara (2017) showed that during forced-draft cooling of palletised pomegranates, the pressure drops mostly at the box panels, neglecting the pressure loss due to the presence of produce, although this was conducted as a numerical simulation. Additionally, Adam et al. (2016) studied the pressure drop across a sharp edge orifice for hydraulic systems, showing that the overall pressure decay in a pipe occurs mostly due to the orifice plate, compared to the pressure loss due to friction.

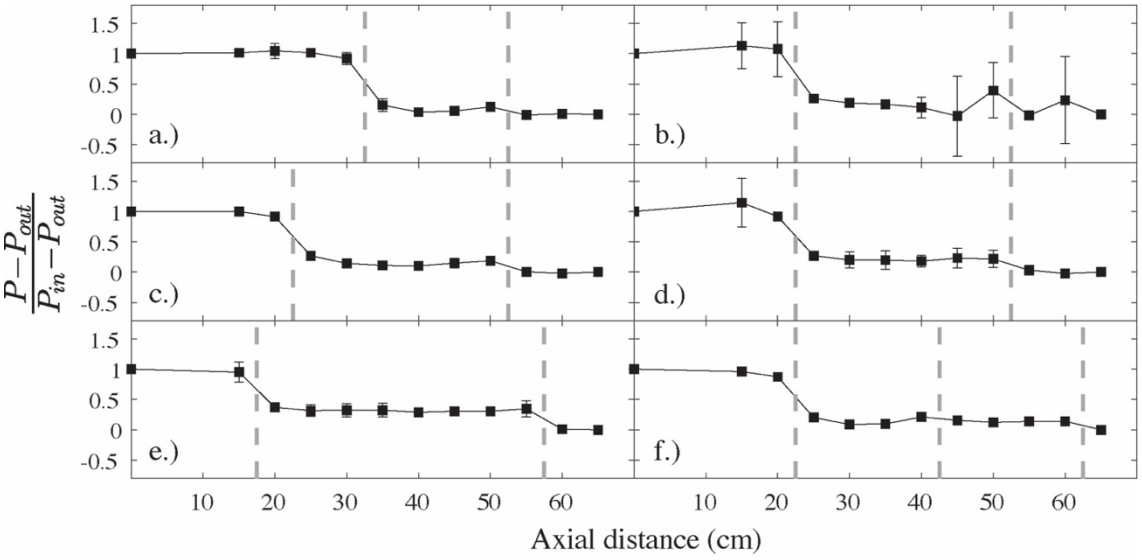

Figure 3.16: *Average scaled pressure decay across the test section of the wind tunnel over all measured fan speeds. Each diagram letter corresponds to the tunnel set-up outlined in Figure 3.7. Broken vertical lines indicate the location of the orifice plates. Error bars indicate the standard deviation, calculated over all fan speeds.*

3.5.2.1. Effect of the distance between plates on the airflow resistance

Comparison between having 0.2, 0.3 and 0.4 m of distance between plates (Figures 3.7a-3.7c, respectively) are shown in Figure 3.17. No apparent differences were found in the overall pressure drop through two plates for all the studied cases. Additionally, no differences were found between the apparent loss coefficient for all the studied cases (up to 2.7 % between distance of 0.2 and 0.3 m). When the pressure drop at each vent is analysed separately (Figure 3.18), most of the pressure drop occur at the inlet of the duct (up to 95.8% of the total resistance for a distance of 0.2 m). Additionally, an inverse relationship between the loss coefficient at the inlet/outlet and the distance between plates was observed.

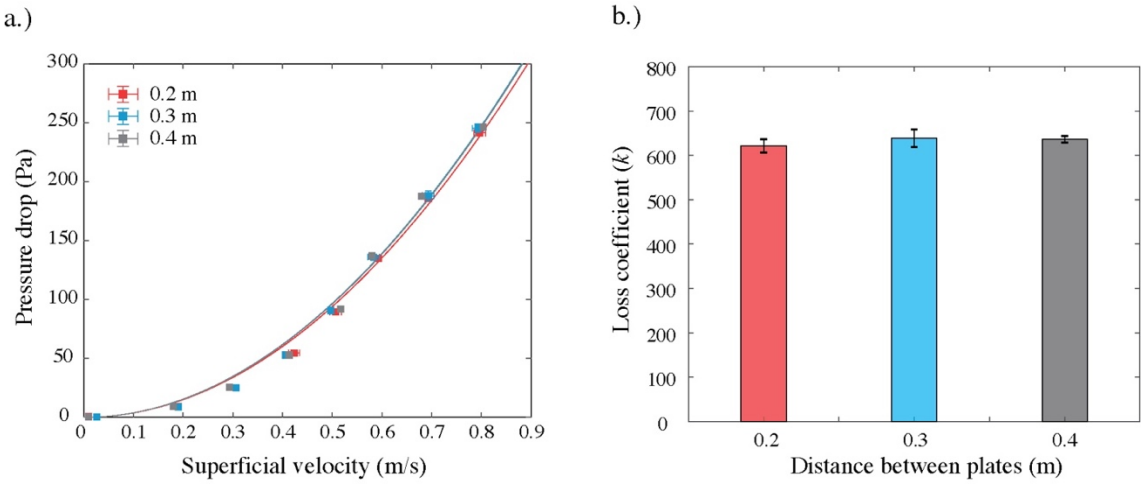

Figure 3.17. *a.) Velocity-Pressure relationship for different plates distances inside the wind tunnel. b.) Fitted vent loss coefficient for each distance between plates. For both diagrams, error bars represent the standard deviation of each value.*

As the distance between plates is increased, its corresponding loss coefficient at the inlet decreases (Figure 17b), and additionally, the loss coefficient at the outlet tends to increase (Figure 17d). By increasing the distance between plates, the available volume downstream of the plate gives sufficient space to the fluid to take a more uniform velocity profile, thus decreasing the entropy generation at the discharge of the plate, and subsequently, decreasing the loss coefficient at the

inlet. Similarly, a more uniformly developed fluid profile due to an increased distance between consecutive plates implicates a higher fluid contraction, thus generating a higher rate of entropy (and its consequent loss coefficient) at the outlet plate.

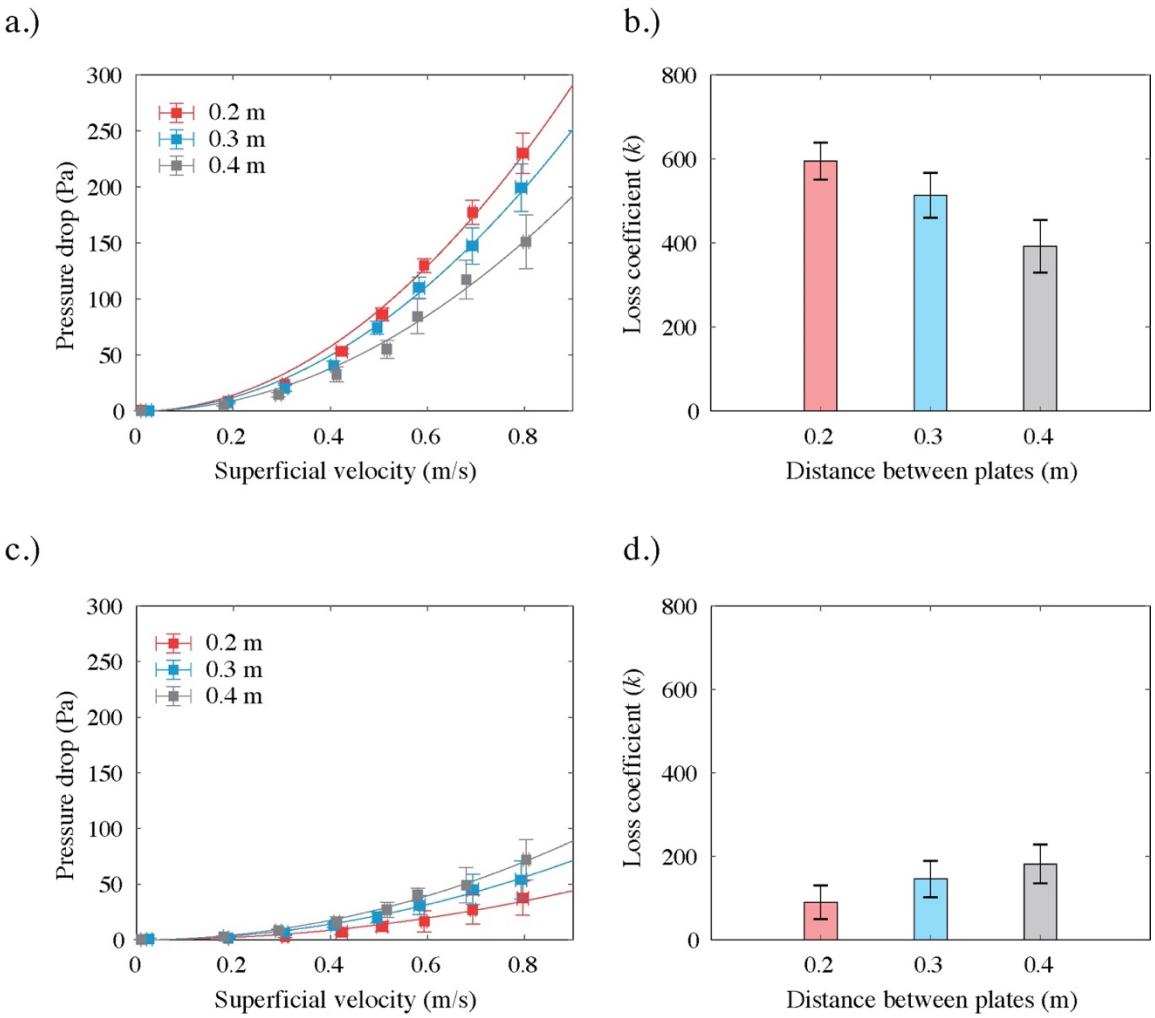

Figure 3.18. *Pressure curves at the inlet a.) and outlet b.) plates for 0.2, 0.3, and 0.4 m distance between plates.*

3.5.2.2. Effect of the headspace variation on the airflow resistance

No apparent differences on pressure and velocity were found when variations occur in the headspace cross section – as a consequence of placing a polystyrene block between plates (Figure 3.19a). Additionally, no apparent differences on the fitted apparent loss coefficient were found for the studied cases (up to 7.7 % difference) (Figure 3.19b). Nevertheless, a continuous relationship between loss coefficient and the available headspace is complex and requires further work.

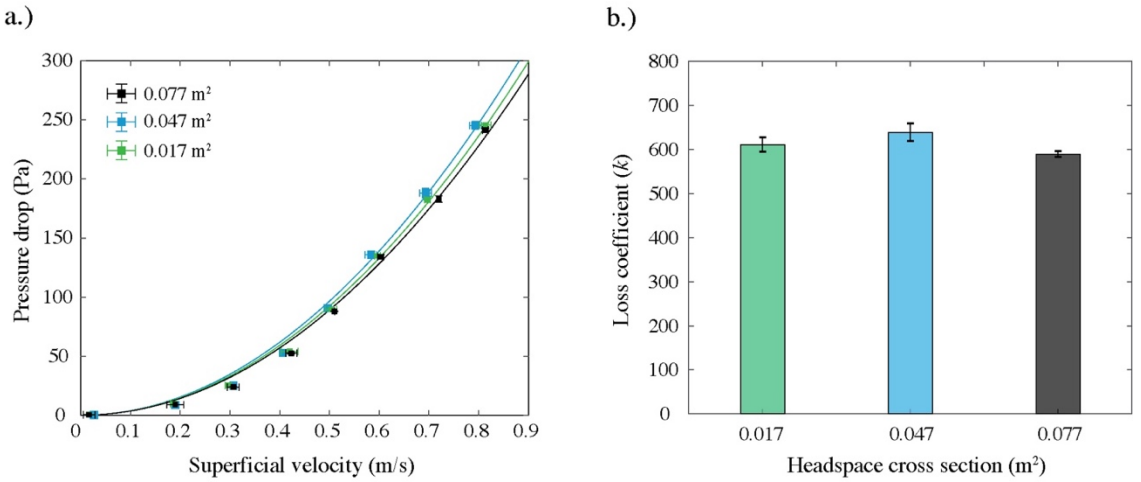

Figure 3.19. *a.) Velocity-Pressure relationship for different headspace cross sectional areas. b.) Fitted loss coefficient for each cross sectional area. Error bars represents the standart deviation of the measured fitted valuers. Distance between plates isfixed at 0.3 m.*

Similarly, no apparent significant differences were found between the fitted loss coefficients at the inlet and outlet of the plates (up to 6.30 and 29.4 % difference at the inlet and outlet, respectively) (Figures 3.20b and 3.20d). As the headspace inside a package is highly dependent on the bulk geometry, and the latter being variable for different stacking patterns (Olatunji et al. 2020), effects of headspace on the resulting airflow resistance can potentially be simplified without risking the accuracy of a pressure decay prediction.

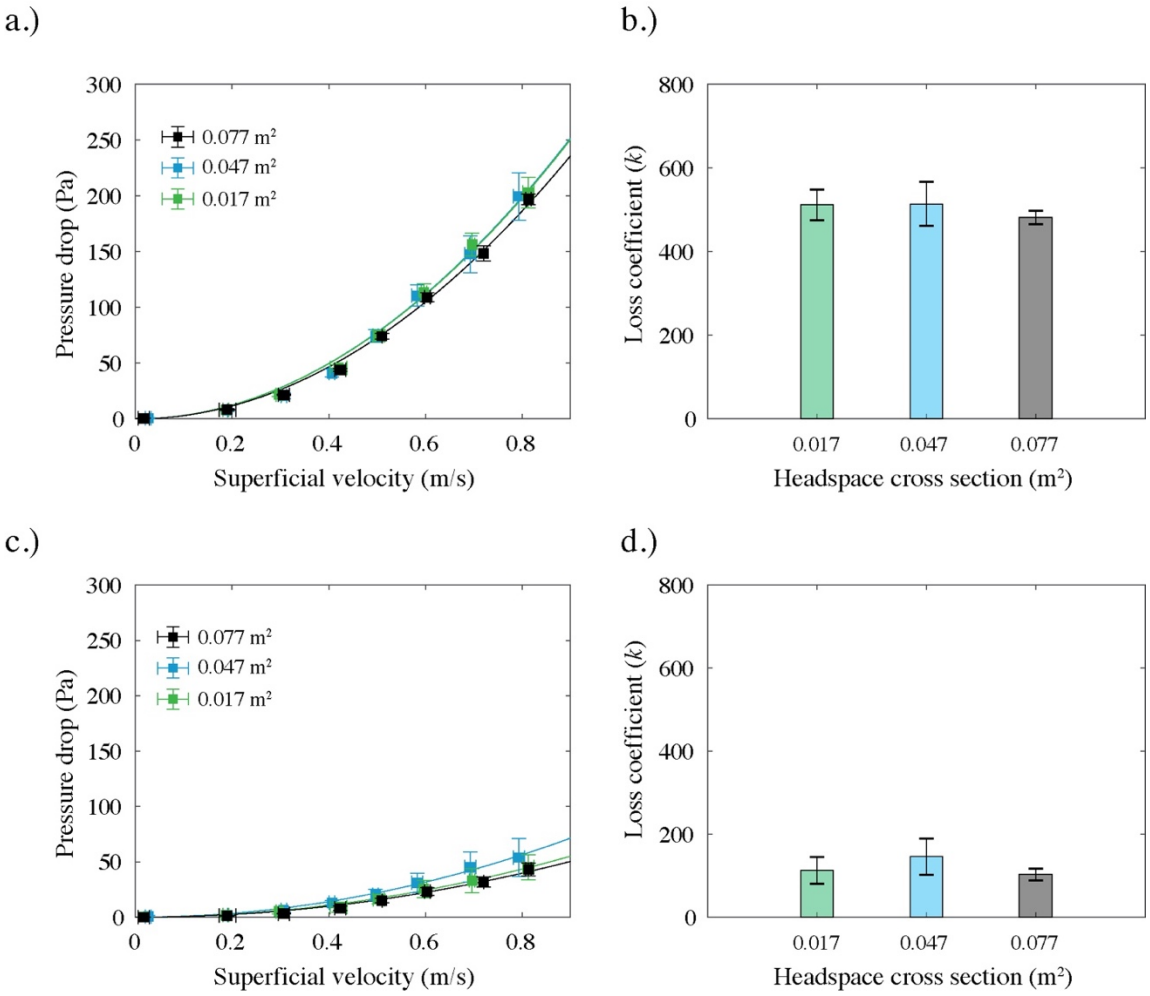

Figure 3.20. *Effect of the headspace cross sectional area variation on the pressure drop at the inlet-outlet plate, and its respective loss coefficient.*

3.5.2.3. Effect of the amount of plates on the resistance to airflow

As shown in Figure 3.21, no apparent differences were found on the pressure drop and superficial velocity when 1, 2 and 3 plates are placed in the duct, for all fan speeds. Similarly, no apparent significant differences were observed in the loss coefficient for the studied cases (up to 7.9 % differences). In addition, differences up to 14.48 % were observed between the apparent loss coefficient at the inlet plate between 1 plate and the inlet plate when 3 plates are inside the duct (Figure 3.22b). However, differences in loss coefficient at the outlet, between 2 plates and 3 plates were 20.27 and 54.40 % for the outlet and middleplates, respectively, when 3 plates are placed in the duct, although these differences were found to be not signifficant. These results differ from the results showed by Ai and Mak (2013), however, the distance between plates were higher than the 0.2 m studied in this instance, thus, the flow profile has more space to return to its uniform state. In reality, the distance between box panels is limited (between 0.2 and 0.5 m in the kiwifruit cold chain), thus there is and unlikely uniform flow profile, therefore the subsequent loss coefficient will be consistently different compared to the inlet loss coefficient.

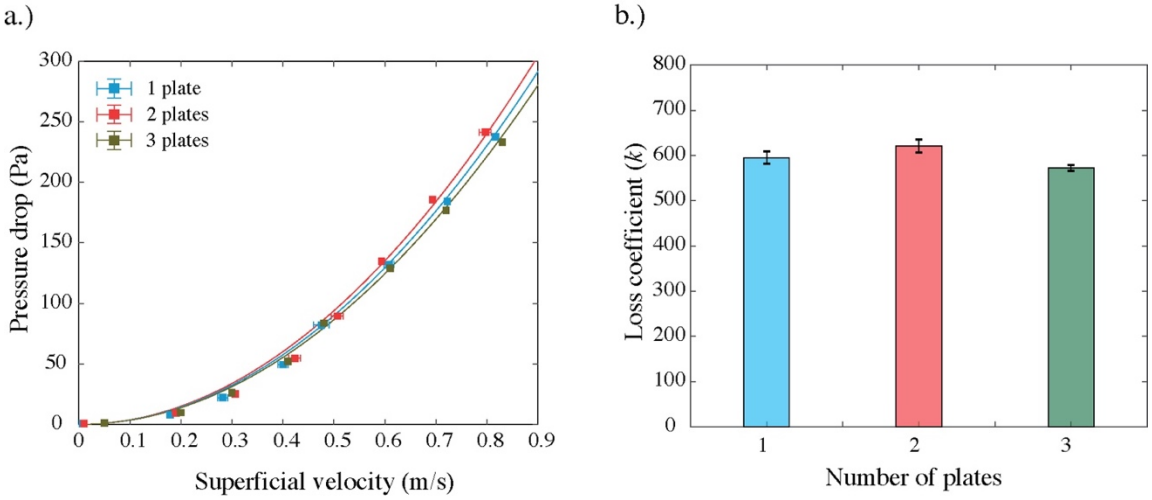

Figure 3.21. *a.) Velocity-Pressure relationship for different number of plates. b.) Fitted loss coefficient for each plate number. Error bars represents the standart deviation of the measured fitted valuers. Distance between plates is 0.2 m.*

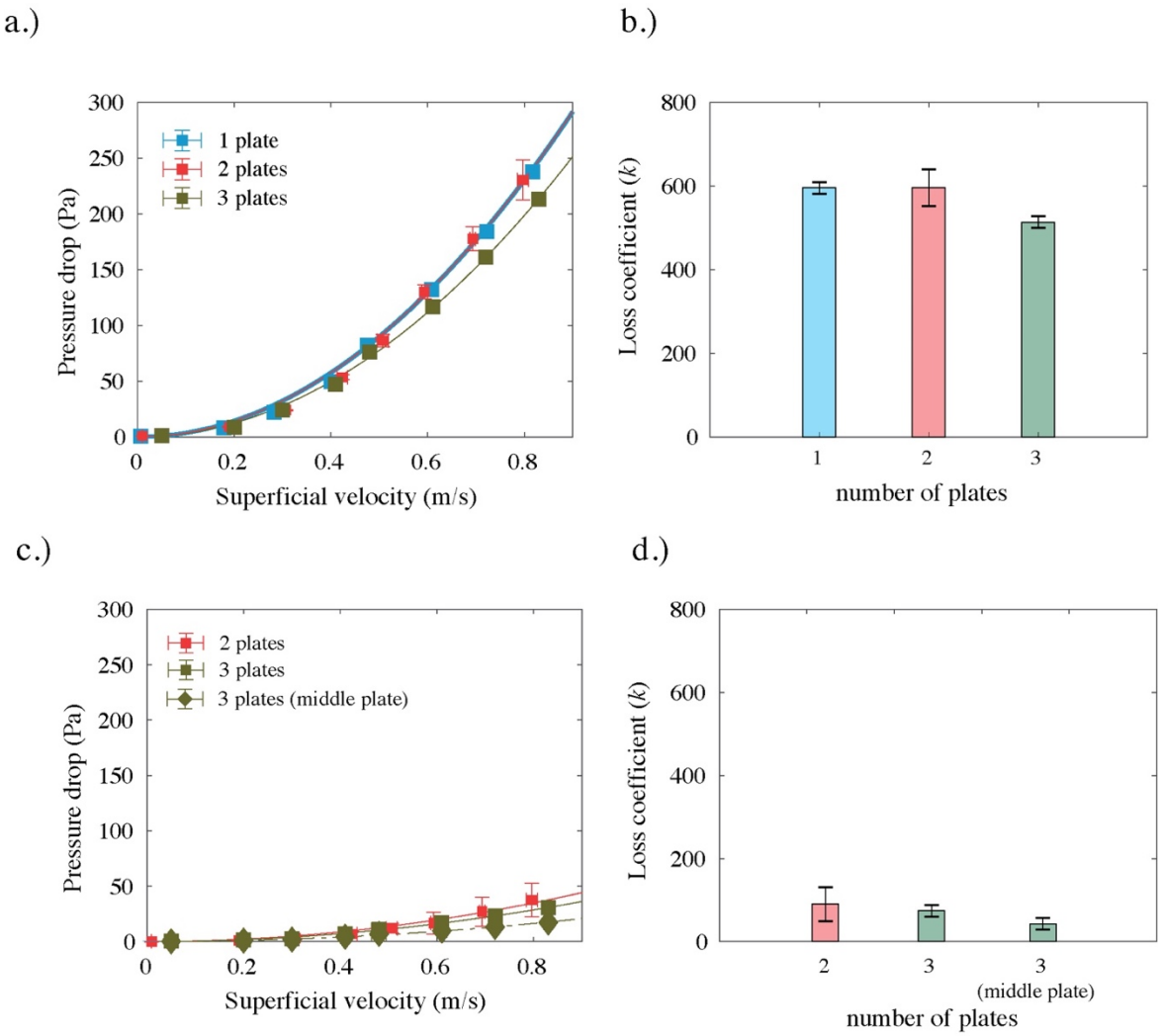

Figure 3.22. *Effect of the number of plates on the pressure drop at the inlet-outlet plate, and its respective loss coefficient.*

3.6. Conclusions

The consequent pressure drop through different vent designs was studied to determine the effect of vent design parameters (size, location, and number of vents). In addition to this, theoretical relationships to calculate the vent loss coefficient were compared to the empirical measurements. Firstly, as to be expected, as the vent size increases, the pressure drop, and hence, the pressure loss coefficient decreases. Interestingly, a comparison between 3 and 6% total open area (TOA) showed that this increase in the TOA significantly increases the superficial velocity by almost double with only a decrease of approximately 7% in the pressure drop at the highest fan speed. Secondly, vent location was found to have a minor effect on the pressure drop. However, significant differences were found at certain vent locations at constant TOA, specifically at the top and bottom vent locations, and top location for 3 and 6% TOA, respectively. And thirdly, vent number had no significant effect on the pressure loss and the subsequent pressure loss coefficient. In addition to this, large relative errors were found in the predicted vent loss coefficient at large TOA values. A 28 and 50% error was found for a 25 and 50% TOA, respectively. While for vent location, an error up to 50% was also found for a vent located at the top for a 3% TOA plate. In order to decrease the uncertainness, a new methodology to measure volumetric flowrate in the wind tunnel should be implemented. Lastly, the either use of Equation 3.5 or 3.6 to calculate the pressure loss coefficient can be used, as the error between both relationships was found to be approximately 5%. The advantage of using Equation 3.6 is that this relationship does not depend on the Reynolds number, simplifying the amount of variables that need to be accounted for in an airflow modelling routine, which is a major task of this thesis.

Pressure drop was investigated for multiple plates inside a duct. Representing a complete package with two faces in the line of flow, or a sequence of packages in the line of flow. First, it was found that at least 82% of the total pressure drop did occur through the plates That is, pressure drop, due to friction against the wind tunnel walls between the plates accounted for 18% of the observed

pressure drop. Additionally, it was found that at least 64 % of the total pressure drop occurred at the inlet plate inside the duct. That is, most of the pressure drop occurs in the first plate. Differences in apparent loss coefficient up to 2.7 % were found when the distance between plates varied between 0.2 and 0.4 m, And differences up to 6.3 and 29.4 % were found at the inlet and outlet plate, respectively. Similarly, no significant differences were found when variations occur in the headspace between two plates, with differences up to 7.7 % between the studied cases, and additionally, no differences were found at the inlet and outlet for these scenarios, with differences up to 6.3 and 29.4 %, respectively. Lastly, up to 7.9 % differences in the apparent loss coefficient were found when 1, 2 and 3 plates are placed in the duct separated by 0.2 m. Similarly, up to 14.48 % difference in apparent loss coefficient was found at the inlet plate for all the studied cases. However, differences up to 20.27 and 54.40 % were found between 2 and 3 plates at the outlet of the duct, and the middle plate for a 3 plates system in the duct, respectively.

The use of a simplified formula to calculate the loss coefficient of an orifice plate can be subsequently used to estimate resistance coefficients in palletised systems. Likewise, these resistances – by means of a vent loss coefficient – can be subsequently used as a driving force of a network algorithm that interconnects airflow pathways through aligned ventholes, independent of variables such as venthole shape, number and location for a box panel.

4. Empirical characterisation of airflow resistances during Forced-draft cooling.

4.1. Introduction

Obtaining a correlation to predict the loss coefficient of a given venthole is a fundamental part of developing a successful simplified airflow model through characterising the apparent airflow resistance. Although wide research has been done experimentally to characterise the forced-draft cooling performance of palletised produce (O'Sullivan et al. 2016; Ambaw et al. 2017; Defraeye et al. 2013; Han et al. 2018), this narrows the analysis to the temperature change over time, which is the ultimate cost function of a modelling scheme (Olatunji 2018). Additionally, empirical data libraries are used to validate mathematical models, mostly solved using computational tools such as Computer Fluid Dynamics (CFD) (Zhao et al. 2016). However, as the computational domain solves our most dedicated problems, little is known about the transport phenomena within our system under study. Specifically, a simulated airflow field is directly calculated to infer cooling performance, yet no study to date is dedicated to understand the airflow resistance in palletised systems.

Despite the lack of available information about airflow resistance and vent loss coefficients, important analysis has been performed to understand these resistances as a function of pressure loss. Notable work conducted by Van der Sman (2002), Ngcobo et al. (2012), and most importantly Smale (2004), used empirical relationships – such as the Darcy-Forchheinmer and Ergun equations – to describe airflow resistances.

Our previous chapter explored the impact of changing the vent design parameters on the overall airflow resistance inside a wind tunnel. While vent location and number had no significant impact on the overall pressure drop, differences in the flow condition and uniformity were discussed. However, vent size and number of subsequent panels does have a considerable impact on the airflow resistance. Therefore, an extrapolation approach to a pallet scale is necessary to fully understand the airflow resistances of a real pallet scale system, and subsequently obtain a loss coefficient relationship that can be incorporated in a simplified modelling scheme.

This chapter aims to develop an empirical technique to explore the pressure distribution across palletised kiwifruit system. Specifically, this chapter aims to:

- Investigate the effect of the internal packaging elements and stacking features (i.e. pallet orientation and presence of gaps) on the pressure loss coefficient and its consequent pressure distribution through a pallet layer of different kiwifruit packages.
- Develop an empirical correlation to predict the loss coefficient of a given venthole in a layer of palletised kiwifruit, based on the adjustment of a literature-based approximation using experimentally obtained data.

Ultimately, this chapter aims to characterise the impact of different packaging features on the airflow resistance, and subsequently, obtain an empirical venthole correlation that can be incorporated in a subsequent modelling approach.

4.2. Materials and Methods

4.2.1. Pre-cooler simulator environment

A pre-cooler simulator set-up was used to mount and monitor a pallet layer, as depicted in Figure 4.1. This simulator was located in the bioprocess laboratory at Massey University, where the measured pallet layer is enclosed inside a metallic rig and connected to a centrifugal variable speed control fan (AP0502AA5/16, Fantech, Wellington, NZ), previously developed by O'Sullivan (2016). Two pallet layers were constructed: the bottom layer being the monitored pallet layer, while the top layer acted as a dummy layer that contained the sensor probes (Figure 4.1b). Prior to the experiment, all inlet and outlet vents of the dummy layer were blocked with insulation tape, thus making sure that the incoming airflow enters only through the bottom layer. Polystyrene panels were used as insulation and to enclose the boxes to the simulator rig. Insulation tape was also used to block any potential gap between the boxes and the polystyrene panels, avoiding any undesirable airflow bypass.

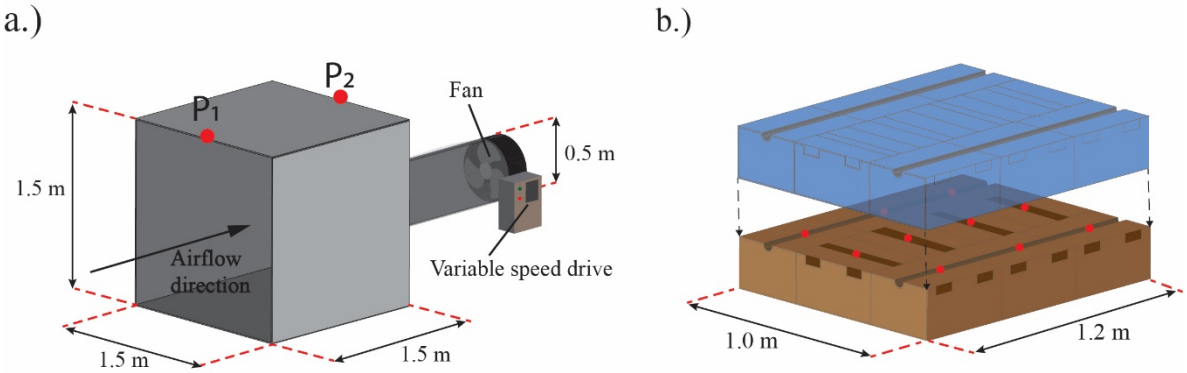

Figure 4.1. a.) Pre-cooler simulator rig, where pressure drop across the pallet layer was measured between points P1 and P2, and b.) pallet layer set-up for a kiwifruit Modular Bulk Package (MBP). Red dots (•) indicate the location of the pressure probes that monitors the pressure in each box within the system.

4.2.2. Studied package designs

Three different package designs typically used in the kiwifruit cold chain industry were studied, plus an alternatively new design (Figure 4.2). Each of these designs have different total open area (TOA) and dimensions. Table 4.1 summarises each of the packages characteristics.

Table 4.1. *Description of the studied packages. Length and width of the packages represent the long and the short side of the package, respectively.*

	Dimensions (cm)	Total venthole area, A_{vh} (cm^2)		Total Open Area, TOA (%)		Boxes per pallet layer
		Width	Length	Width	Length	
IT	50 x 30 x 6.5	-	30	-	9.2	8
ML	40 x 30 x 12	12.3	56	3.4	11.6	10
AML	50 x 30 x 12	12.3	60	3.4	10	8
MBP	40 x 30 x 19.5	12.3	56	2.7	7.2	10

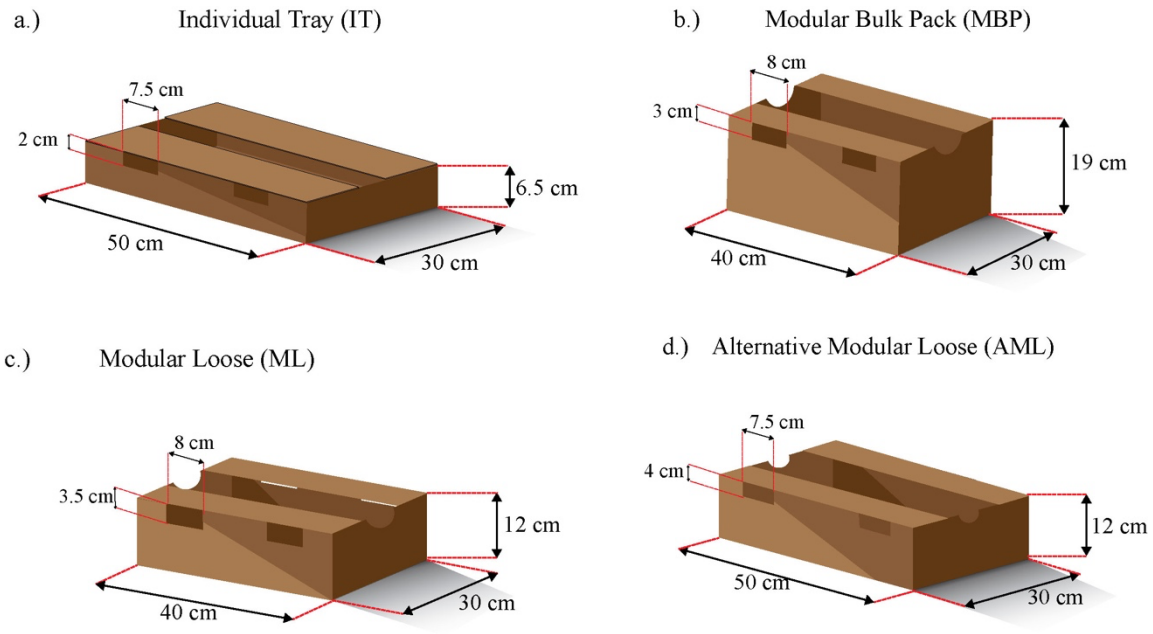

Figure 4.2. *Diagram of the studied packaging designs.*

4.2.3. Pressure and velocity measurements

Two types of piezoelectric pressure sensors sets were used to monitor pressure distribution in a palletised system: (1) One ±1 H_2O in range sensor (SSCSNBN002NDAA5, Honeywell, Morris Plains, USA), and (2) Ten ±1 H_2O in range sensors (P992-1B-A, Sensata-Kavlico, MA, USA). All sensors have the same reading accuracy of 2%. Conversion from input voltage to its equivalent pressure value was previously described in Section 3.1.3. Pressure drop across the pallet layer was measured by placing a differential type (1) pressure sensor between locations P_1 and P_2, as indicated in Figure 4.1. Type (2) pressure sensors were used to monitor pressure at the centre of each package. Pressure probes were attached to the centre of each package as shown in Figure 4.3. Air point velocity at the centre of each inlet vent was measured by a hot wire anemometer (9545 Velocicalc Air velocity meter, TSI, USA) with a range of 0 – 20 m/s and ±3% of accuracy.

The volumetric flowrate entering each box was determined by:

$$Q_{vent} = v_{vent} \cdot A_{vent} \tag{4.1}$$

Where,

v_{vent}: Measured point velocity at the centre of the vent hole (m/s)

A_{vent}: Vent hole area (m^2)

Thus, the total volumetric flowrate entering the pallet layer is determined by:

$$Q_{pallet} = \sum_{i=1}^{n} Q_{vent,i} \tag{4.2}$$

Where,

$Q_{vent,i}$: Volumetric flowrate at vent i (m^3/s)

n: Number of vents at the intake of the pallet layer

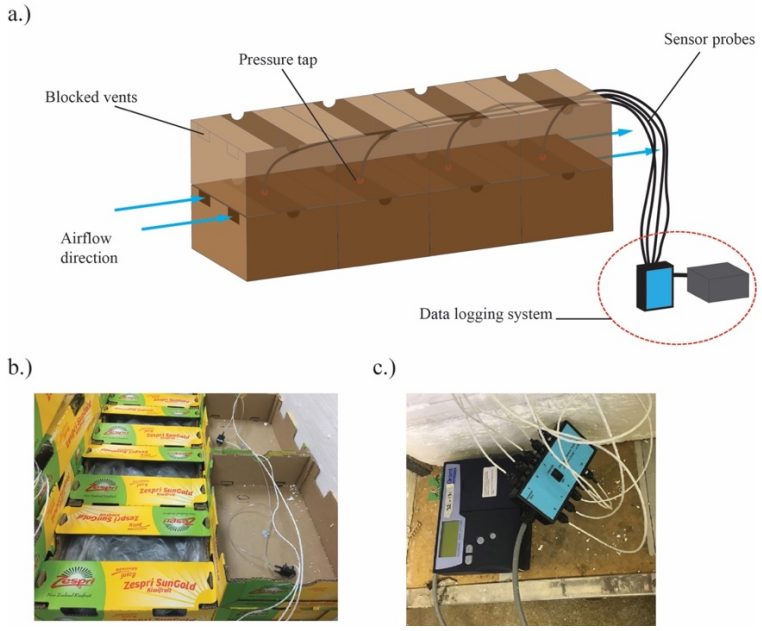

Figure 4.3. *a.) Diagram of sensor positioning in a row of boxes (example of boxes 1 to 4 in a MBP pallet footprint), b.) Picture of the top view of the sensor placemen in a pallet layer set-up, and c.) Data logger interface.*

4.3. Experimental design

The pallet footprints for each studied package design are shown in Figure 4.4. The pallet orientation was kept constant, in which the airflow enters the 1.0 m face (Figure 4.5a). One pressure differential sensor was attached to each box as shown in Figure 4.3, at the locations represented by the yellow points in Figure 4.4. The effect of the internal packaging elements on the pressure drop of three package designs (Figures 4.4a - 4.4c) was assessed by testing four different internal packaging elements:

- Empty packages.
- A flat surfaced polystyrene block that leaves a 3.5 cm headspace, thus avoiding any vent hole obstruction.
- A randomly arranged kiwifruit-like fruit simulators wrapped in a polyliner bag and folded underneath the bulk.
- A randomly arranged kiwifruit-like bulk without polyliner – resembling a semi-porous media inside the package.

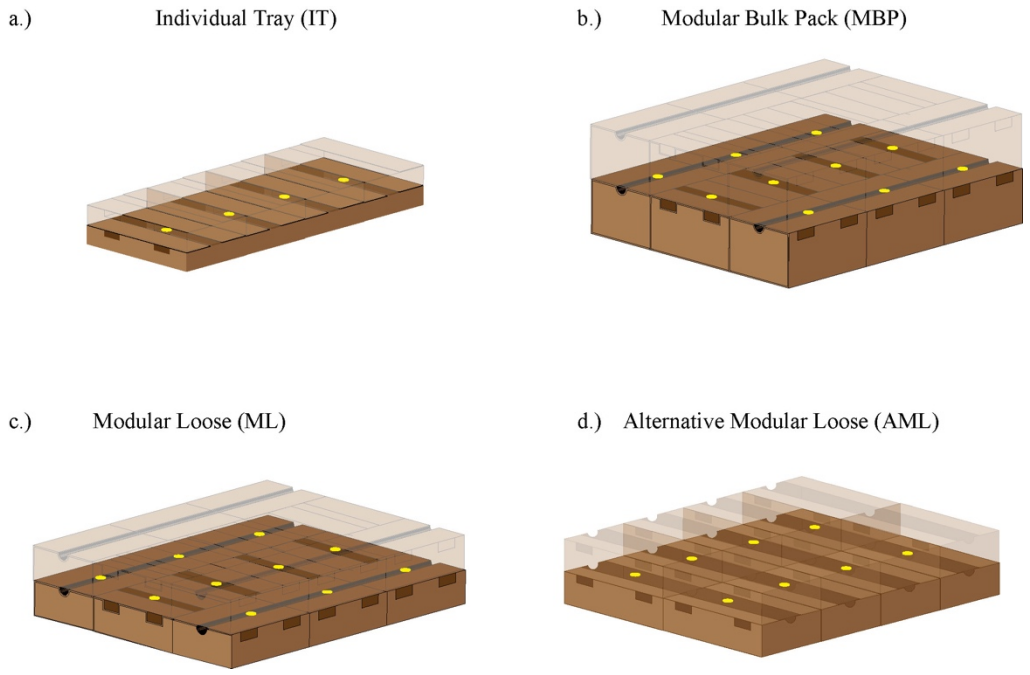

Figure 4.4. *Pallet footprint of each studied package design. Yellow dots (•) represents the location of the pressure taps at the center of each box.*

The effect of the pallet stacking configuration on the consequent pressure drop was studied only for the Modular Bulk Package (MBP) design (Figure 4.4b). The pressure distribution inside the pallet was measured at: (1) airflow entering the 1.0 m face, and (2) airflow entering the 1.2 m face of the pallet layer (Figure 4.5). The pallet arrangements were studied with empty and polylined fruit simulators, separately. The effect of gaps between pallets on the pressure distribution was

conducted only for the polylined package configuration, by leaving a 2cm gap at each side of the pallet. The premise for leaving only 2 cm gap at each side was derived from an industry survey work conducted by Shim et al (2016). Additionally, two additional measurements of point velocity were performed at the centre of each side gap. Table 4.2 summarises the total amount of experiments that were needed for this study.

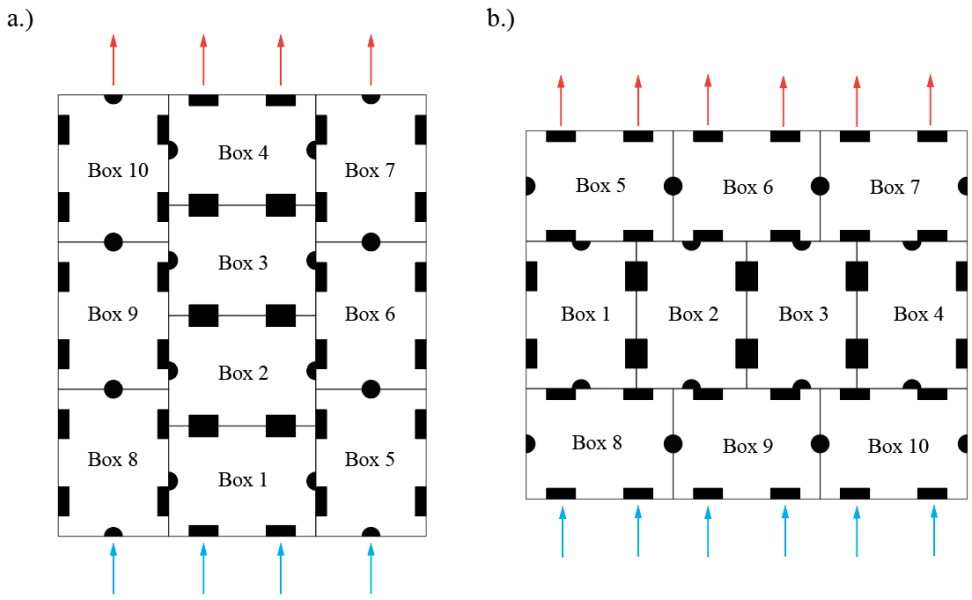

Figure 4.5. *Palletised kiwifruit modular bulk package (MBP) footprint. Airflow entering through a.) 1.0 m face and b.) 1.2 m face.*

The airflow resistances of two different package designs were studied by comparing an empty Alternative ML and the current Modular Loose (ML) package design, both shown in Figure 4.2c and 4.2d, respectively. The basis for this prototype design is based on an hypothesis that having a wider headspace dimension preserving the height of the package, more surface of the bulk is exposed to the incoming airflow, thus enhancing the convective cooling performance. Pressure and velocity data were measured at three different fan speeds: 600, 900 and 1200 rpm. All experiments were conducted in triplicate – re-assembling the pallet layer at each repetition to account for the error related to the experimental set-up.

Table 4.2: *Summary of the experimental design of each studied package and pallet footprint.*

Package design	Empty	Polystyrene block	Fruit + polyliner	Fruit bulk
IT	X	X	X	X
MBP	X	X	X	X
ML	X	X	X	X
AML	X			
MBP (1.2 m face)	X		X	
MBP + gaps			X	

4.4. Data processing and analysis

4.4.1. Experimental data

Time-averaged velocity and pressure were used to analyse pressure differential through the pallet layer, and subsequently, the pressure drop between packages. The classic Bernoulli equation describes the mechanical energy balance between two reference points in a giving domain as following:

$$z_1 g + \frac{p_1}{\rho} + \frac{v_1^2}{2} = z_2 g + \frac{p_2}{\rho} + \frac{v_2^2}{2} + \Delta H_m + \Delta H_f \qquad 4.3$$

Where

z: Height of reference point (m)

p: Gauge pressure at reference point (Pa)

ρ: Fluid density (kg/m^3)

g: Gravity acceleration (m/s^2)

v: Mean velocity at reference point (m/s)

ΔH_m: Head loss between the referenced points due to accessories (such as ventholes)

ΔH_f: Head loss between the referenced points due to friction losses

Within a palletised system, the potential and the kinetic energy terms are simplified, as there is no change in elevation between referenced points and cross sectional area, respectively.

Alternatively, general losses are included, containing potential losses due to friction and fitting components (i.e. package ventholes of arbitrary shape and size), thus resulting in the following relationship:

$$\Delta p = \rho k \frac{v^2}{2} \tag{4.4}$$

Where,

Δp: Pressure drop between the two referenced points (Pa)

k: Venthole loss coefficient (-)

v: Mean air superficial velocity (m/s)

By merging equation 4.4 and the relationship $Q = vA$, we obtain:

$$\Delta p = k\rho \frac{Q^2}{2A^2} \tag{4.5}$$

Where,

Q: Estimated volumetric airflow rate through the pallet layer or venthole (m^3/s)

A: Total cross sectional area of the ventholes in the box panel (m^2)

The pressure drop between adjacent packages was defined as the absolute difference between its corresponding pressure readings (gauge pressure). Figure 4.6 shows the diagram of two packages, where the pressure drop between P_1 and P_2 is defined as $\Delta P_{1-2} = |P_1 - P_2|$.

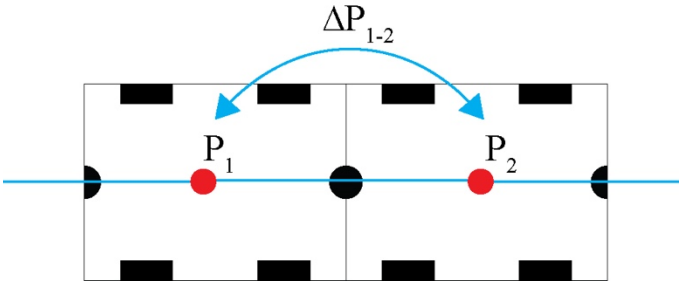

Figure 4.6. *Diagram of pressure readings (P_1 and P_2) between two adjacent packages.*

During forced draft cooling of palletised kiwifruit, the airflow is pulled in one direction – from the inlet to the outlet of the pallet. For ease of estimation, the airflow is assumed to flow through each column from inlet to outlet, neglecting air exchange between column of boxes in the airflow direction. Through numerical simulation, O'Sullivan (2016) calculated the exchange of airflow between column of packages to be ≈ 4% for a layer of palletised polylined kiwifruit. Thus, the apparent venthole loss coefficient (k) of each venthole for all studied pallet configurations was estimated by fitting the experimental data of volumetric airflow rate (Q) and Pressure drop (ΔP) according to Equation 4.5.

4.4.2. Venthole loss coefficient correlations

When the incoming airflow enters a package, its flow profile contracts as entering the package through a venthole, reaching its minimum at the vena contracta, and subsequently expanding inside the package. Following this scheme, Idelchik (1987) developed an approximation of the apparent loss coefficient (k) as a function of its total open area (TOA). This correlation resembles to a flow through a sharp-edged orifice of arbitrary shape characteristic. The loss coefficient of airflow through a venthole between packages was defined as $k_{orifice}$, and was calculated by:

$$k_{orifice} = \left[\underbrace{k'(1-TOA)}_{Inlet} + \underbrace{(1-TOA)^2}_{Outlet} + \underbrace{\tau\sqrt{(1-TOA)}(1-TOA) + k_{fr}}_{vena\ contracta}\right] \cdot (TOA)^{-2} \quad 4.6$$

Where,

k': Loss coefficient of the inlet stretch of the orifice (-)

k_{fr}: Loss coefficient due to friction in the orifice (-)

τ: Coefficient depending on the orifice inlet shape, thickness and flow conditions through the orifice stretch and vena contracta (-).

TOA: Total Open Area. Ratio between the area of the orifice and the area of the duct (-)

The overall loss coefficient of the stretch was segmented by its resistance at the intake of the venthole, through the vena contracta, and at the outtake, where the airflow fully enters the package. Similarly, by simplifying the intake and outtake terms of Equation 4.6, the loss coefficient of a venthole at the inlet and outlet of a pallet layer can be approximated by the following relationships:

- Loss coefficient through a venthole located at the inlet of the pallet layer:

$$k_{inlet} = [k' + (1-TOA)^2 + \tau(1-TOA)] \cdot TOA^{-2} \quad 4.7$$

- Loss coefficient of a venthole located at the outlet of the pallet layer:

$$k_{outlet} = \left[1 + k'(1-TOA) + \tau\sqrt{(1-TOA)}\right] \cdot TOA^{-2} \quad 4.8$$

The applicability of these relationships for studying airflow resistances in palletised package systems was assessed by fitting Equations 4.6 to 4.8 on all the measured ventholes that corresponded to the same pallet dimensions (1.0 x 1.2 m) using a Non-linear Least Squared algorithm. The contribution of each section on the overall airflow venthole resistance was assessed in terms of their fitted loss coefficient component at the inlet (k'), vena contracta (τ) and friction (k_{fr}) of the ventholes, within the range of the studied venthole dimensions (2.7 – 11.6 % TOA). The fitness of each model respect to the experimental data was assessed by calculating the Root Mean Squared Error ($RMSE$) of each studied correlation according to the formula:

$$RMSE = \sqrt{\frac{\sum_1^n \left(k_{predicted} - k_{empirical}\right)^2}{n}} \qquad 4.9$$

Where,

$k_{predicted}$: Loss coefficient predicted by the model (-)

$k_{empirical}$: Apparent loss coefficient of the venthole given by the measured data (-)

n: Total number of estimated loss coefficients .

4.5. Results and discussion

4.5.1. Effect of the package design and internal packaging elements on the overall airflow resistances

Pressure drop through a pallet layer at 600, 900 and 1200 rpm for all the studied packages and internal packaging configurations are shown in Figure 4.7. At the highest fan speed (1200 rpm), Average differences on pressure drop between internal packaging configurations were found to be 0.73, 0.94 and 1.53 % for the IT, ML and MBP, respectively. Additionally, at the sane fan speed, averaged differences in volumetric flowrate of 7.52, 15.08 and 7.92 % were found for the IT, ML, and MBP package designs, respectively. Table 4.3 shows the apparent loss coefficient of each studied palletised system. A lower value of k was observed for the IT, in comparison to the ML and MBP designs. This difference can be influenced by two factors: (1) the IT package has the highest total open area among all the studied packages (11.4 % TOA), and (2) the amount of packages composing the pallet layer under monitoring (4 for the IT, in comparison to 10 for the ML and MBP designs). This indicates that not only the TOA but the number of packages composing a pallet layer can potentially influence the resulting pressure drop and consequent loss coefficient. Additionally, the empty packages resulted in the lowest loss coefficient for the ML and MBP designs. This agrees with Gruyters et al. (2020), who found that an empty single package of pears had less relative resistance to airflow in comparison to a package filled with pears. For the ML and MBP packages, the polylined bulk represented the highest additional resistance to airflow. Similarly, Ambaw et al. (2017) and Mukama et al. (2020) found that by adding a plastic liner into the palletised packages of pomegranates resulted in higher resistance to airflow, and consequently, a higher energy was required to achieve the seven eights cooling time. Ngcobo et al. (2012) found that the presence of a plastic liner increased the relative airflow resistance of palletised table grapes. Moreover, the presence of perforations in the liner implicated a decrease of the apparent airflow resistance, and hence, its loss coefficient.

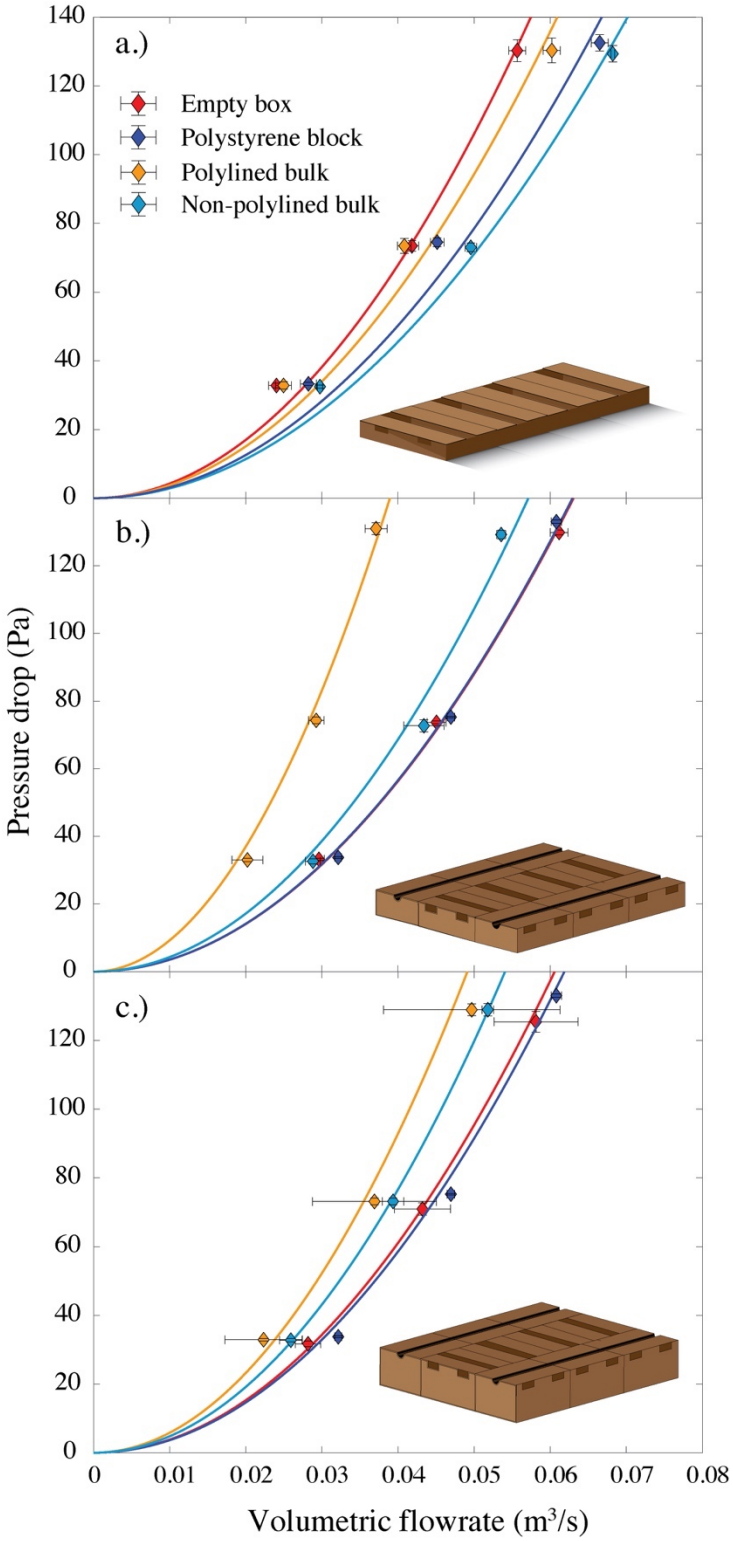

Figure 4.7. *Pressure drop through palletised kiwifruit with different internal package elements. a.) IT tray; b.) Modular loose; and c.) Modular Bulk Pack (MBP) packages. Data points represent the measured data and the solid line represent the fitted curve according to Equation 4.5. Error bars represent the standard deviation of the measured data.*

Table 4.3. *Averaged values of fitted values of apparent loss coefficient (k) for all the studied pallet configurations.*

	Loss coefficient (k)		
	IT tray	Modular Loose (ML)	Modular Bulk Pack (MBP)
Empty package	68.8	838	2278
Flat surface	58.6	842	2185
Polylined bulk	59.9	2198	3465
Non-polylined bulk	50.3	1021	2860

Equation 4.5 successfully described the measured relationship between volumetric flowrate and pressure drop, thus accounting for the resistance coefficient in one parameter (k). This is a significant benefit in comparison the classical Ramsin (see section 2.2.2) and the Darcy-Forchheimer equations (see section 2.3.2), where both require two unknown empirical terms. Results of Ambaw et al. (2017) infer that the contribution of friction losses on the total pressure drop through palletised pomegranates can be practically neglected, in comparison to the inertial loss term of the Darcy- Forchheimer equation. Finally, these results are narrowed to the kiwifruit packaging system only. Given that in this case the venthole total open area (TOA) changes within a small range (from 2 to 11 % TOA) – and these are located only to align with the headspace of the package – it would be interesting to further understand the effect of simple loose packed of any produce (i.e. citrus, pears, apples), as well as more complex systems, such as clamshells (in the case of blueberry), sealed liners (cherry) and perforated liner (grapes) on their airflow resistances during forced-drafted cooling.

Apparent differences in pressure distribution and pressure drop between packages along the airflow direction are shown in Figures 4.8 and 4.9, respectively, for all the studied designs and all internal packaging elements, at the highest fan speed (1200 rpm). High regions of pressure drop were identified at the inlet of the pallet layer for the IT design (average of 58% of the total pressure drop through the column of boxes), while pressure decreases towards the interior of the system (about 5% of the total pressure drop for all internal packaging elements). Similarly, approximately 55 % of the total pressure decays at the inlet of the system for both the ML and MBP designs (Figures 4.9a-b and 4.9c-d, respectively). Increased pressure drop at the outlet was found when the geometry in the headspace is rather irregular (polylined and non-polylined bulk), where the decay in pressure is up to 56 and 31 %, for the ML and MB packages, respectively. Smale (2004) investigated the pressure drop through a series of boxes filled with apples for various venthole total open area (TOA), showing that the mayor pressure decays occur at the outlet, and additionally, the pressure drop through internal vents between packages were minor in comparison to the inlet and outlet of the packaging stack. In addition, Ambaw, Mukama, and Opara (2017) showed a high pressure drop at the inlet of the pallet face of pomegranates using a Direct Numerical Simulation (DNS) approach.

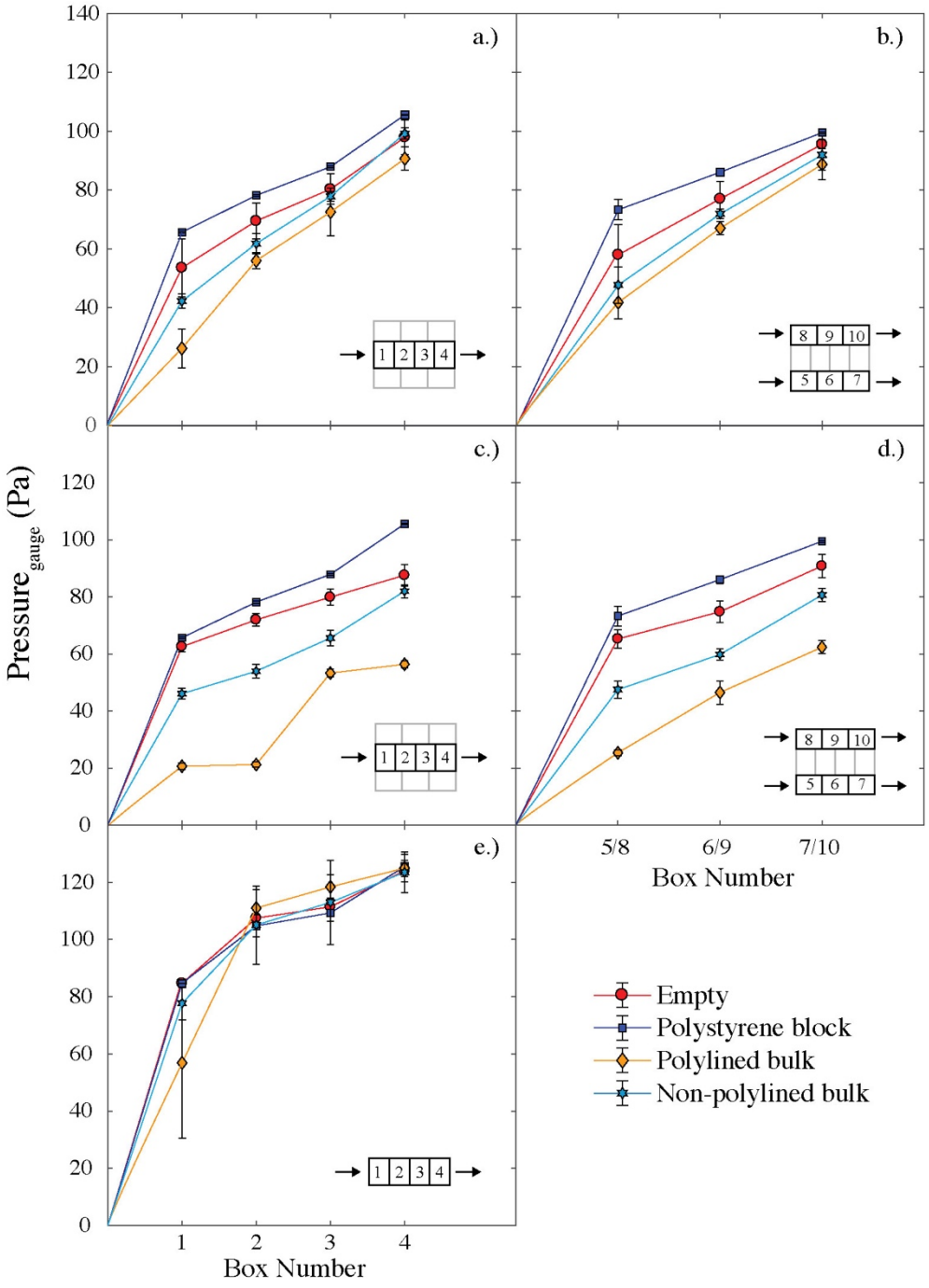

Figure 4.8. *Gauge pressure distribution through a pallet layer at high fan speed (1200 rpm) of: a-b.) Modular Bulk Pack (MBP), c-d.) Modular Loose (ML), and e.) Individual Tray (IT), for different internal packaging configurations. Error bars represent the standard deviation of the measured data.*

The produce geometry resulted in relatively small influence on the resistance to airflow (Figure 4.9). Interestingly, the pressure drop differences between packages with a polylined packaging configuration are less consistent in comparison to the results of other internal packaging elements – as depicted by the yellow bars in Figure 4.9. As the polyliner bag has the ability to flap with the air movement, this creates internal geometrical variability over time. Additionally, venthole obstruction is possible, in addition to changes in the headspace geometry, and thus the local loss coefficient. The added tortuosity to the airflow path inside the non-polylined packages – shown by the light blue bars in Figure 4.9 – adds additional resistance to airflow, due to an increase in turbulent dissipation forces through the system (Bejan 2013). Evidence of this can be observed with the slight increases in pressure drop for the polylined and non-polylined bulk configurations in the central box location (Figures 4.9a, 4.9c, 4.93).

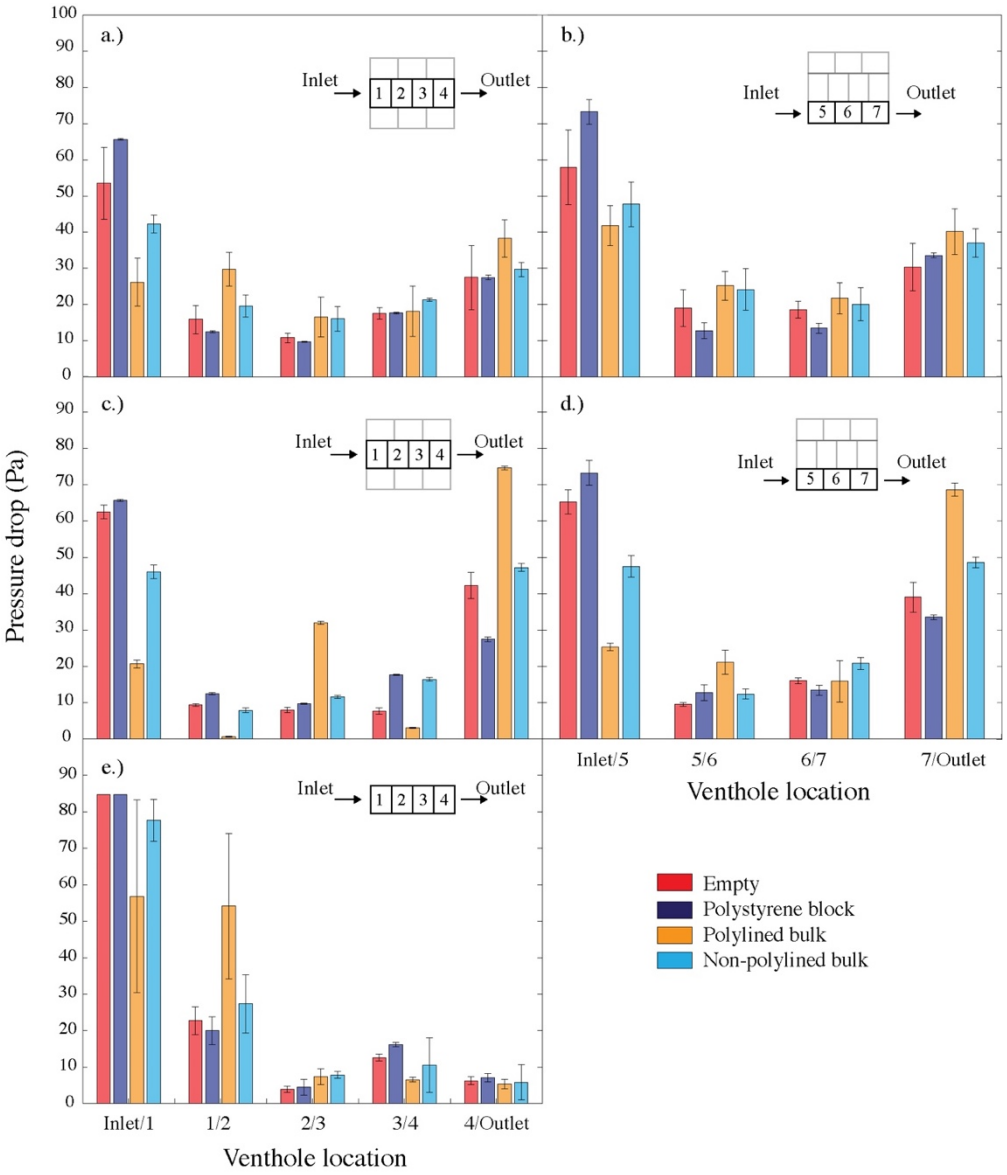

Figure 4.9. *Pressure drop between packages on the airflow direction at high fan speed (1200 rpm) for: a-b.) Modular Bulk Pack (MBP), c-d.) Modular Loose (ML), and e.) Individual Tray (IT), for different internal packaging configurations.*

4.5.2. Effect of the pallet orientation and presence of gaps on the airflow resistances

Changing the pallet orientation towards the 1.2 m face perpendicular to the airflow resulted in a lower overall apparent airflow resistance, for an empty and a polylined pallet layer (Figure 4.10). While minor differences were found in pressure drop (1.6 and 5.3 % for empty and polylined bulk, respectively), mayor differences were observed in volumetric flowrate (56 and 54 % for the empty and polylined bulk, respectively). Previously, O'Sullivan (2016) studied the pressure drop through a half pallet of polylined Modular Bulk Package (MBP) design, showing that the 1.2 m face perpendicular to the airflow had a lower resistance in comparison to the 1.0 m side. When the 1.2 m face is perpendicular to the airflow entering the pallet, the air passes through 1.0 m length of palletised bulk, decreasing the amount of energy dissipation per unit distance within the pallet layer. In addition, the 1.2 m pallet orientation has a higher total open area (TOA) at the inlet of the pallet layer, in comparison to the 1.0 m orientation (7.4 and 4.3 % TOA, respectively). Similar results were found for grapes (Ngcobo et al. 2012) and pomegranates (Mukama et al. 2017), showing that the inlet TOA is a highly sensitive parameter that affects the airflow resistance in a palletised stack.

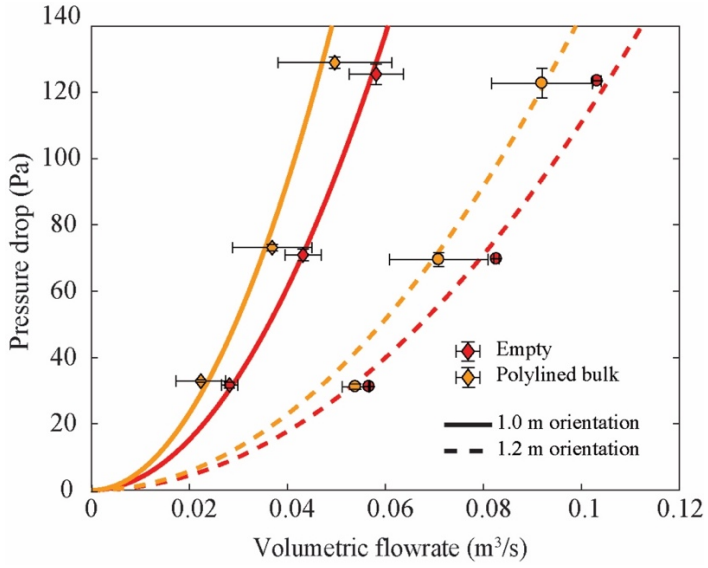

Figure 4.10. *Effect of the pallet orientation on the pressure drop through a pallet layer of empty and polylined Modular Bulk Package (MBP). Error bars represent the standard deviation of the measured data.*

The pressure distribution when the airflow enters through the 1.2 m face of the pallet showed a different trend in comparison to the standard orientation (Figure 4.11). Areas of low pressure drop were observed at the inlet and outlet for a pallet layer of empty packages (14.1 and 5.3 % of the total pressure drop, respectively), with the maximum pressure drop observed between the first and second row of boxes on the airflow direction (51 and 47 % of the total pressure drop) (Figures 4.11a and 4.11b). In comparison to the empty packages, the pallet layer of polylined bulk resulted in a different pressure drop distribution (Figures 4.11c and 4.11d), where a higher pressure drop at the outlet of the pallet layer for both columns of boxes was observed (49.2 and 41.2 % of the total pressure drop). Ambaw, et al. (2017) obtained a similar trend in pressure drop in loosed and polylined stacks of boxes when simulating the pressure decay through a pallet of packed pomegranates. In that case, the contribution of the produce to the pressure drop within the packages was found to be minimum.

Typically, the partial obstruction of vent holes in the airflow direction due to the change in stacking pattern decreases the effective available venthole TOA, consequently resulting in a higher pressure decay. In comparison, when the pallet is orientated for the air to enter the 1.0 m face, the TOA remains constant throughout all the column of boxes along the airflow direction. Therein, the TOA had an important impact on the airflow resistance, showing consistency with previous research by Van der Sman (2002), Vigneault, et al. (2006) and Delele et al. (2008). Consequently, an increase in the effective TOA along the airflow direction can potentially increase the cooling performance of the produce, by means of an enhanced airflow rate through the produce.

With respect to the polylined bulk (Figures 4.11c and 4.11d), Smale (2004) showed a similar trend, where mayor pressure drop at the outlet was observed for a column of packages filled with apples (around 38% of the total pressure drop), thus arguing that internal content of a package does have a contribution on the airflow resistance. In conclusion, the internal content of the packages has an impact on the pressure distribution within the pallet layer, and a potential high pressure decay within the pallet

layer. This can affect either the cooling performance of the produce or the energetic efficiency of the process, while no significant effect was observed on the overall pressure drop through the pallet.

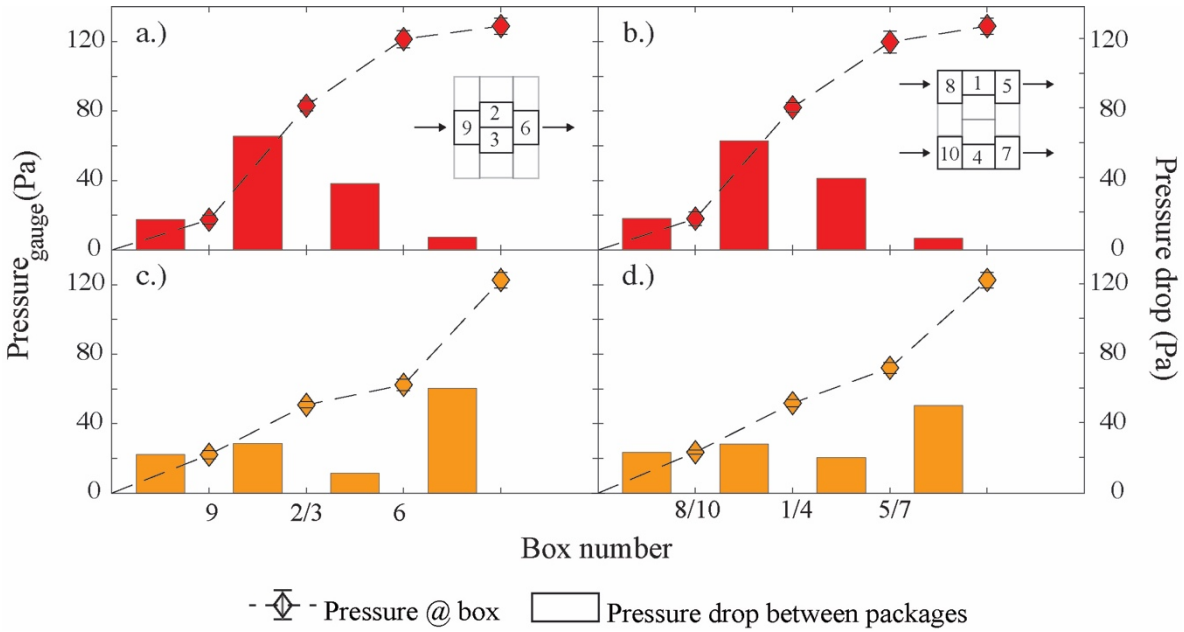

Figure 4.11. *Pressure distribution between packages along the airflow direction of a pallet layer with the 1.2 m face perpendicular to the airflow at high fan speed (1200 rpm) for: Empty (a. and b.) and polylined bulk (c. and d.) packages. Error bars on data points represent the standard deviation of the measured data.*

Similarly to the pallet orientation effect, the presence of gaps represented an apparent lower resistance to airflow, with differences of 24.7 and 61.4 % in pressure drop and volumetric flowrate, respectively (Figure 4.12). Additionally, there was an effective 94.2 % increase on the available TOA when gaps are introduced, thus decreasing the overall airflow resistance. To the authors knowledge, little research is available that studies the impact of gaps between pallets that can occur during industrial application of forced convection of horticultural produce. In survey work, Shim et al. (2016) found that 80% of gaps were found to be < 15 mm – in kiwifruit cool stores – with the gaps being highly variable between facilities.

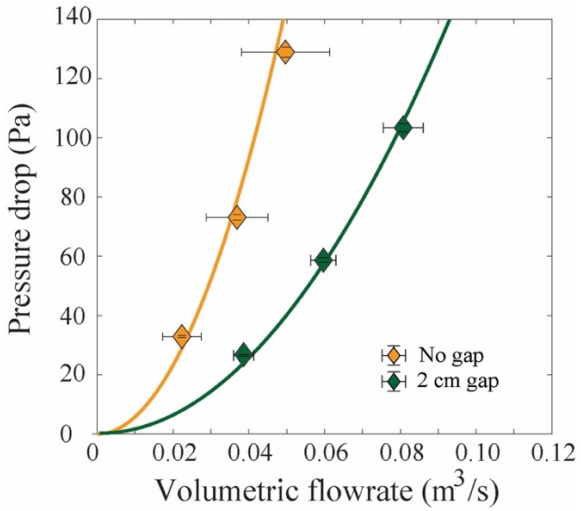

Figure 4.12. *Effect of the placement of gaps on the pressure drop through a pallet layer of polylined MB packages. Error bars represent the standard deviation of the measured data.*

The occurrence of gaps in the industry is mostly an involuntary phenomena that happens when two or more palletised produce are placed in the precooling units. While the produce is transported to each operation by using forklifts, slights displacement may occur due to the inherent inaccuracy of the transport vehicles. When gaps are present on the sides of the pallet arrangement, high pressure drop towards the second package of the column of boxes was identified (Figure 4.13) (38 % of the total pressure drop). Interestingly, a minimum pressure drop was identified between box 2 and 3 (only 1.2 Pa) (Figure 4.13a). Moreover, 70% of the total airflow bypassed the pallet layer at the highest fan speed, as the gaps allowed lower airflow resistance, in comparison with the vent holes and the typical airflow pathways within the pallet arrangement.

The implementation of a package design with considerable low airflow resistance – such as a single tray with a porous net – can improve the cooling performance of the produce (Defraeye et al. 2013). However, a constrain to be accounted for is that to some scenarios, the airflow bypasses the produce surface through undesirable gaps with lower resistance to airflow, in detriment of an effective cooling (Ferrua and Singh 2009a).

The addition of gaps has been poorly investigated to the date. However, a lateral airflow bypass can potentially deliver cold air into the boxes located at the back of the pallet, thus potentially improving the cooling performance of a given palletised system. Therefore, cooling data is still needed in order to obtain a feasible proof of benefit for future industrial applications.

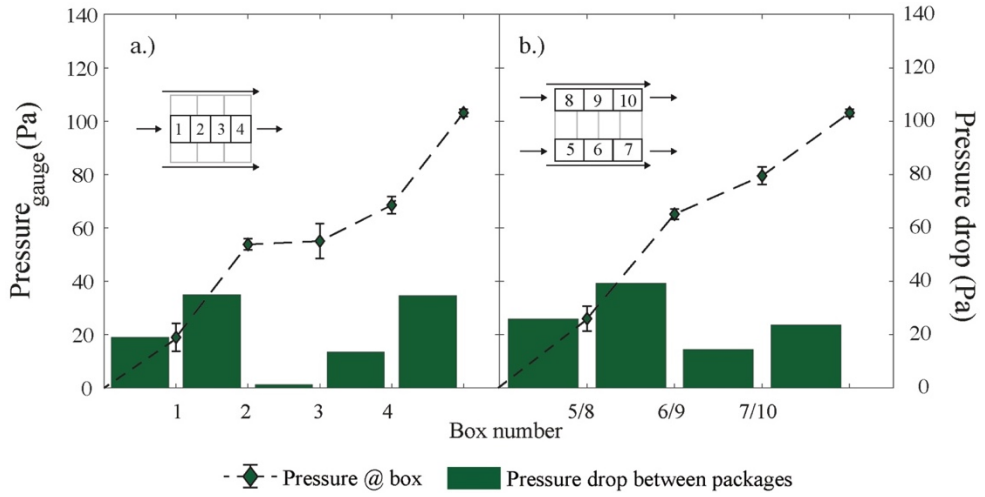

Figure 4.13. *Pressure distribution through a pallet layer with 2 cm gaps on the sides of the pallet for an MB package design at high fan speed (1200 rpm). Error bars represent the standard deviation of the measured data.*

4.5.3. Effect of an alternative package design on the airflow resistances

A relative lower, yet not significant overall resistance to airflow was observed for an alternative package design (Figure 4.14a). Difference of 13.4 % in volumetric flowrate between both designs at the highest fan speed was observed, although this difference was not significant. Similarly to the *status quo* ML design (Figure 4.9c), a high pressure drop at the intake of the pallet layer was identified (42.7 % of the total pressure drop) (Figure 4.14b). Additionally, no overall apparent differences on pressure distribution were identified between both package designs, therefore they showed similar resistance to airflow. However, this information by itself cannot directly guarantee a benefit by replacing the current

package. Cooling data that can ensure an additional benefit on cooling performance is therefore required for a more informed analysis.

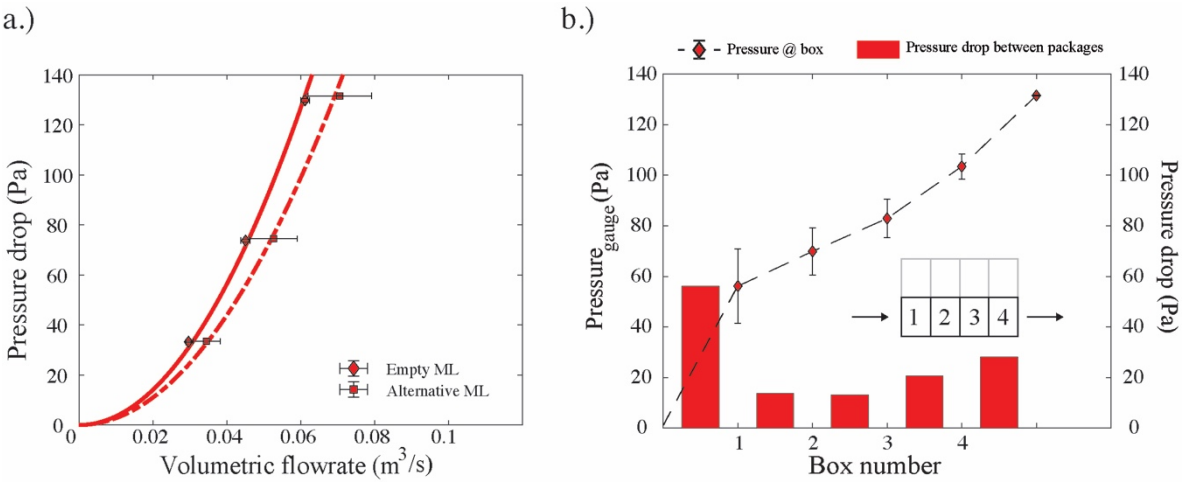

Figure 4.14. *a.) Pressure drop through a pallet layer of empty ML and Alternative ML designs. b.) Pressure distribution through a pallet layer of Alternative ML Package design. Error bars represent the standard deviation of the measured data.*

4.5.4. Vent hole loss coefficient correlations

The apparent venthole loss coefficients obtained by Equation 4.5 are shown in Table 4.4, for all studied pallet configurations and all internal packaging elements. As shown previously in Figure 4.9, high pressure drop was observed at the inlet and outlet of the pallet layer as a consequence of high loss coefficient values at those locations, while lower loss coefficients were obtained between packages within the pallet layer. There was a consistent difference in loss coefficient for a MBP design (Figures 4.15a and 4.15b) for the polylined bulk, in all studied sections within the pallet footprint, apart from the inlet stretch. As the polyliner flaps throughout the forced-draft cooling operation, partial obstruction of the ventholes might occur, thus adding extra resistance to airflow.

Table 4.4 *Fitted values of venthole loss coefficient according to equation 4.5 for all the studied package designs and internal packaging configurations.*

		Venthole apparent loss coefficient, k (-)								
		Middle column					Side column			
		In/1	1/2	2/3	3/4	4/Out	In/5	5/6	6/7	7/Out
Individual Tray (IT)	Empty	4.00	1.17	0.17	0.54	0.32				
	Polystirene block	2.04	0.50	0.12	0.42	0.17				
	Polylined bulk	1.71	1.65	0.23	0.22	0.17				
	Non-polylined bulk	1.81	0.69	0.19	0.22	0.12				
Modular Loose (ML)	Empty	1.51	0.31	0.24	0.50	0.57	2.12	0.71	0.58	1.55
	Polystirene block	1.75	0.34	0.27	0.48	0.75	2.18	0.39	0.41	0.99
	Polylined bulk	0.75	0.65	0.42	0.41	1.03	1.71	0.99	0.87	1.66
	Non-polylined bulk	1.67	0.81	0.49	0.83	1.13	1.96	0.97	0.81	1.53
Modular Bulk (MBP)	Empty	1.77	0.27	0.21	0.20	1.39	1.85	0.28	0.47	1.16
	Polystirene block	1.58	0.31	0.24	0.43	0.66	3.49	0.62	0.65	1.60
	Polylined bulk	1.82	0.36	1.97	0.27	6.34	1.95	1.46	1.20	5.21
	Non-polylined bulk	1.64	0.42	0.42	0.58	1.71	1.75	0.46	0.79	1.80
Alternative Modular Loose (AML)	Empty	1.57	0.56	0.37	0.73	1.00				

Relationship between size (TOA) and apparent loss coefficient (k) at the inlet, orifice between packages, and outlet were correlated separately, as shown in Figure 4.15, Figure 4.16 and Figure 4.17, respectively. All values of apparent loss coefficient are related with the venthole TOA described in Table 4.1, according to each package design. Additionally, fitted coefficients of inlet stretch (k'), venthole section (τ) and friction (k_{fr}) within the passage and $RMSE$ were also reported in Table 4.5,Table 4.6, and Table 4.7.

At the inlet section of the pallet, major values of loss coefficient attributed to the inlet stretch (k') were observed for all internal packaging configurations, in comparison to the coefficient related to the vena

contracta due to venthole characteristics (Table 4.5). Negative values of τ were observed for all the studied systems, where uniform flow profiles are hardly possible due to irregular internal geometry, as well as highly turbulent systems due to sudden flow contraction and immediate expansion into the package. Additionally, relative short distance between the inlet and the subsequent venthole along the airflow direction does not allow the flow profile to become uniform before contracting into the subsequent venthole. Resulting values of $RMSE$ were reported for all the studied internal packaging elements individually and for all systems altogether. While minor $RMSE$ of 0.25 was obtained for the empty packages, major $RMSE$ value of 0.50 was reported when all packaging elements were fitted simultaneously. Despite these fitting results, Figure 4.15 showed that apart from the polystyrene block – which presented the highest RMSE of all studied packaging elements – all other studied systems presented poor fitting, considering the nature of the resistance to airflow, in terms of its phenomenology. As the TOA becomes smaller, the loss coefficient k shall increase exponentially, tending to infinite as the TOA approaches 0, as shown in Figure 4.15b. This overall poor shape of the fitted correlations is due to unclear relationships on k and TOA of the studied package designs. Despite the higher relative values of TOA (3.4 and 2.7 % for the ML and MBP design, respectively), the ML design presented higher values of k compared to the MBP designs for the empty and non-polylined systems, respectively (Table 4.4). For instance, the tortuous solid matrix as a result of loosely placed kiwifruit simulators creates extra airflow channels, where losses in kinetic energy occur inside the semi-porous media, being potentially imperceptible for the pressure probe. Additionally, the placement of fruit simulators, together with an even partial obstruction near the ventholes, can create an extra resistance that can be unrelated to the TOA of the package design, thus influencing the resulting loss coefficient k.

Although all coefficients were fitted according to the measured empirical data, these are somewhat a function of each other, thus aiding the better fit, and not necessarily reflected the underlying phenomena within the flow regime by their own merit. Additionally, these correlations were preliminary reported as ideal hydraulic systems, where an ideal, fully developed flow were the main premise for this approximation – an scenario that is hardly ideal in stacked, packaging systems.

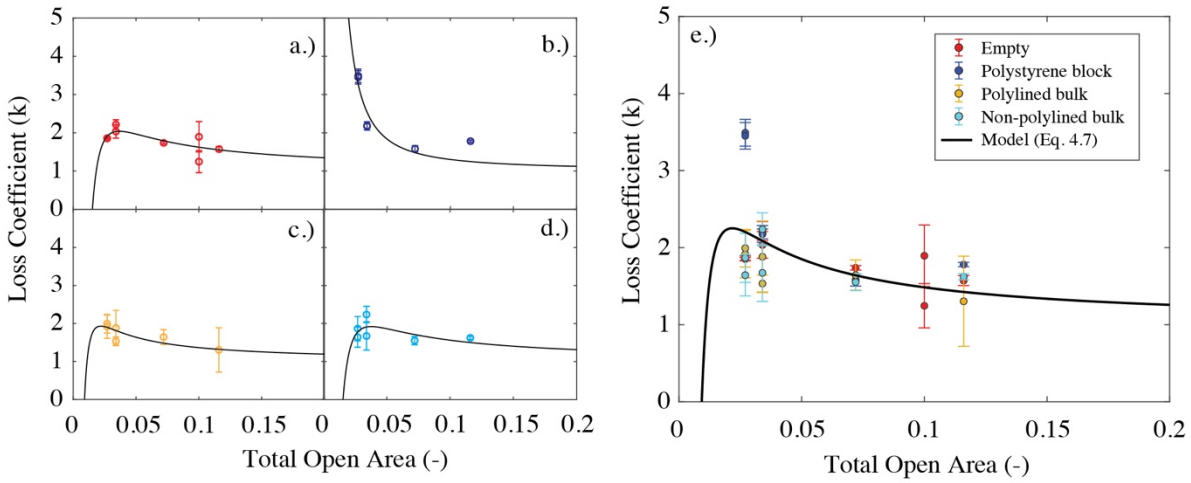

Figure 4.15: *Loss coefficient correlation at the inlet section of the pallet footprint according to Equation 4.7 for: a.) Empty packages, b.) Polystyrene block, c.) Polylined bulk, d.) Non-polylined bulk, and e.) all internal packaging configurations. Error bars represent the standard deviation of the obtained data.*

Table 4.5: *Mean fitted inlet loss coefficients according to Equation 4.7 for each packaging configuration.*

	k'	τ	$RMSE$
Empty	1.07	-2.08	0.25
Polystyrene block	1.02	-2.02	0.40
Polylined bulk	1.04	-2.04	0.35
Non-polylined bulk	1.07	-2.07	0.29
All configurations	1.05	-2.08	0.50

For the loss coefficient on venthole through stacked packages, the fitted coefficients of contraction at the inlet (k'), through the venthole (τ) and due to friction (k_{fr}) within the venthole were presented in Table 4.6. Major fitted coefficients of k' were found on the empty packages, where the flow profile is contracted the most to enter the venthole, in comparison to the other packaging systems. Furthermore, large differences in k' was found to the polylined bulk, where disturbances due to flapping polyliner occur due to fluctuations in local flow velocity through the cooling process, provoking constant changes

in internal geometry and potential venthole obstruction. Consequently, the polylined bulk presented the largest values of τ and k_{fr}, in comparison to the other internal packaging configurations. However, the variability within the presented data as a consequence of the polyliner resulted in the largest $RMSE$, due to poor fitting of the model. On the other hand, minor value of RMSE was observed when a polystyrene block is present within the package arrangement, and as a result, the polystyrene block resulted in the best shaped curve in comparison to the other studied systems (Figure 4.16b). As a difference to the loss coefficient at the inlet of the pallet arrangement, when all packaging configurations are fitted simultaneously, the model replicates the desired curve behaviour (Figure 4.16e). This is an advantage when using this correlation for modelling purposes, as this relationship is able to predict the loss coefficient of partially obstructed ventholes as a result of the alignment of two packages in different orientations – as it is the case of the standard kiwifruit pallet footprint (Figure 4.5).

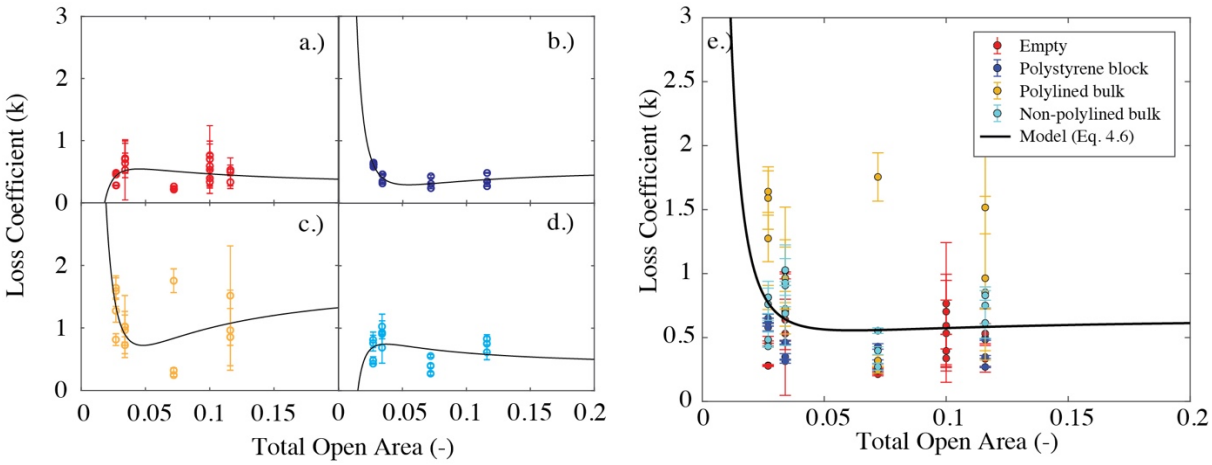

Figure 4.16: *Apparent loss coefficient correlation at the orifice between packages within the pallet footprint, according to Equation 4.6 for: a.) Empty packages, b.) Polystyrene block, c.) Polylined bulk, d.) Non-polylined bulk, and e.) all internal packaging configurations. Error bars represent the standard deviation of the obtained data.*

Table 4.6: *Mean fitted venthole loss coefficients according to Equation 4.6 for each packaging configuration.*

	k'	τ	k_{fr}	$RMSE$
Empty	0.75	-1.85	0.10	0.24
Polystyrene block	-0.40	-1.05	0.44	0.08
Polylined bulk	-4.81	1.94	1.87	0.52
Non-polylined bulk	0.35	-1.59	0.23	0.26
All configurations	-0.76	-0.82	0.56	0.40

The fitted curves and its corresponding coefficients for the ventholes at the outlet of the pallet arrangement were presented in Figure 4.17 and Table 4.7 for all the studied packaging configurations. Similarly to the inlet stretch of the pallet, larger values of k' were found, in comparison to the coefficients at the venthole τ for all the studied systems. Additionally, minor $RMSE$ values were reported for the polystyrene block, reflected in the curve shape in Figure 4.17b, and the largest $RMSE$ value was presented for the polylined bulk. Similarly to the previous fittings, the source of error was found to be due to the use of the polyliner, which adds extra variability into the systems introducing partial obstructions during the cooling process, as well as airflow that enters and goes out of the polylined bulk. Additionally, the polyliner can also potentially block momentarily the measuring probe at the top of the package. Finally, $RMSE$ values of 0.4 was reported when all packaging configurations were fitted. However, the model had poorly shaped curve, where the loss coefficient tends to decrease at TOA values below the studied ventholes.

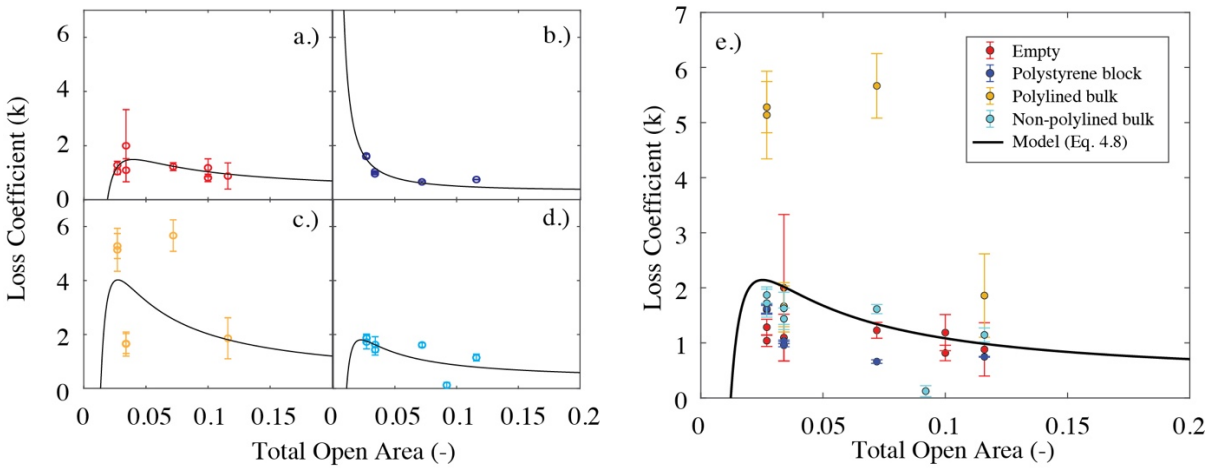

Figure 4.17: *Apparent loss coefficient correlation at the outlet section of the pallet footprint, according to Equation 4.8 for: a.) Empty packages, b.) Polystyrene block, c.) Polylined bulk, d.) Non-polylined bulk, and e.) all internal packaging configurations. Error bars represent the standard deviation of the obtained data.*

Table 4.7: *Mean fitted outlet loss coefficients according to Equation 4.8 for each packaging configuration.*

	k'	τ	$RMSE$
Empty	0.80	-1.80	0.52
Polystyrene block	0.96	-1.96	0.21
Polylined bulk	0.58	-1.59	2.41
Non-polylined bulk	0.86	-1.86	0.50
All configurations	0.81	-1.81	1.40

The models on Equations 4.6, 4.7 and 4.8 were fitted on the measured data with differences that mostly depended on the internal packaging configurations – notoriously in the case of the polylined bulk. Additionally, these equations were fitted on all measured data, including all packaging configurations simultaneously (Figure 4.15e, Figure 4.16e and Figure 4.17e). The potential of building a simplified airflow model that accounts for all corresponding airflow resistances shall at this stage account for a simplified, uniform geometry, considering venthole size. However, these fitted models are limited to a

minimum TOA for a given package design. For ease and consistency with the measured data, these correlations are limited to packages with minimum TOA of 2.7 % in any of their panels.

Likewise, the fitted model in Figure 4.16e can account for typically encountered obstructions due to overlapping ventholes in palletised arrangements. Finally, these newly obtained correlation, although not theoretically consistent to the detail, brings a simplified approximation for the venthole loss coefficient. This quantitative notion of the airflow resistance associated to a specific pallet footprint, gives the necessary information to proceed to a simplified modelling approach based on the airflow resistances.

4.6. Conclusions

The relative effect of package design, internal packaging elements, and pallet footprint (pallet orientation and placement of gaps) was investigated in a pilot-scale forced-draft cooling simulator. No apparent difference in pressure drop through a pallet layer was observed when packaging elements are changed, for all the studied designs. Average differences in pressure drop of 0.73, 0.94 and 1.53 % for the IT, ML, and MBP, respectively. Additionally, average differences of .52, 15.18 and 7.92 % were observed in the measured volumetric flowrate for the IT, ML and MBP, respectively. Overall, pressure loss was largely influenced at the inlet of the pallet layer, where average of 58 % of the total pressure decay at the inlet venthole, between all the internal packaging elements for the IT package design. Moreover, about 55 % of the total pressure drops at the inlet section of the pallet layer for both the ML and MBP designs.

Additionally, up to 5.3 and 56 % differences in pressure drop and volumetric flowrate were observed when the pallet orientation is changed to the 1.2 m size perpendicular to the airflow direction. Thus, concluding that the TOA had large influence on the resulting effect in airflow resistances (7.4 against 4.3 % TOA, for the 1.0 and 1.2 m, respectively). Consequently, while the pressure decay at the inlet and outlet represented 14.1 and 5.3 %, respectively, a maximum of 51 % of the total pressure dropped at the centre of the pallet layer. This caused majorly by an overlapping of ventholes in these sections of the pallet, thus decreasing the effective TOA. Differences up to 24.7 and 61.4 % were found in pressure drop and volumetric flowrate when 2 cm gaps are placed on the sides of the pallet. The latter mostly attributed to the lower resistance offered by the gaps, where the TOA available increased by 94.2 %. Additionally, about 38 % of the total pressure drops towards the second package of the central row of boxes, although about 70 % of the total airflow bypassed the packages through the gaps.

By implementing an alternative package design, a 13.4 % higher volumetric flowrate through the pallet was observed, largely influenced by the available TOA at the inlet, in comparison with the pallet of ML. And additionally, 42.7 % of the total pressure drop was observed at the inlet of the pallet layer. However, by solely comparing airflow related data, a recommendation about implementing a new package design is still not possible without direct cooling data over time.

Subsequently, relative high values of loss coefficient were found at the inlet and outlet of the pallet layer, in comparison with the ventholes within the pallet layer, for the IT, ML, AML and MBP packages. Thus, based on the correlations of vent loss coefficient found in the literature, a new venthole loss coefficient approximation were performed based on empirically obtained values of loss coefficient k. Among all the studied internal packaging configurations, the packages with polystyrene block showed a better fitting into Equations 4.6, 4.7 and 4.8. Likewise, values of RMSE of 0.40, 0.08 and 0.21 were found at the inlet, venthole between packages, and at the outlet of the pallet, respectively. On the other hand, the model had poor performance for the other studied scenarios, specially when the polylined

bulk was placed inside the packages. RMSE values of 0.35, 0.52 and 2.41 were found at the inlet, venthole between packages, and at the outlet of the pallet, respectively. Finally, the model was fitted on all the studied packaging configurations simultaneously, where RMSE values of 0.50, 0.40 and 1.40 were found at the inlet, venthole between packages, and at the outlet of the pallet, respectively. Moreover, the model found its limitation to packages only above 2.7 % TOA, corresponding to the smallest studied venthole size. However, smaller ventholes as a result of obstructed ventholes between packages can be projected.

These approximations will aid to approximate the venthole loss coefficients as a function of its size, taking part in a resistance network modelling approach that aims to predict airflow distribution in a pallet arrangement for a given by package design.

5. Airflow model development

5.1. Introduction

In Chapter 2, it was determined that a good modelling approach for our current system that is fast, robust, and flexible is the resistance network model of airflow. In this approach, resistances had to be estimated prior to the iteration of the airflow distribution of a given network. Subsequently, Chapter 4 investigated airflow resistances in stacked packages, specifically those resistances associated to the package design features such as venthole and package dimensions.

As multiple packages are stacked together to form a pallet layer of produce, potential venthole obstruction may occur as some packages are rotated within the system, thus influencing airflow distribution and its consequent effect in cooling performance (Ambaw et al. 2017; O'Sullivan et al. 2017). Another important feature to consider is the potential of coupling an airflow model with a heat transfer model such as a zonal approach (Olatunji 2018; Tanner 1998; Tanner et al. 2002), thus enabling optimisation routines to maximise cooling performance of a polylined package design.

This chapter aims to describe the mathematical basis of the resistance network model for airflow prediction in a palletised system. Additionally, a geometrical model was constructed to calculate potential vent obstructions and the effective venthole areas involved in a given pallet footprint.

The objectives of this chapter are:

- To develop a geometrical model algorithm that provides the pallet footprint information based on the venthole and package design parameters.

- Implement and incorporate a previously approximated formula to predict the venthole loss coefficient in a pallet layer arrangement, as a function of the effective venthole size.

- Develop and apply a resistance network modelling approach to predict the airflow distribution within a pallet layer during forced-draft cooling operations.

5.2. Problem definition

The scope of this thesis is to develop a simplified modelling approach to predict airflow distribution in palletised polylined wrapped produce. Therefore, an optimal package design shall create an optimum airflow distribution, thus resulting in an effective convective heat transfer, minimising heterogeneity between packages during cooling performance. Additionally, some preliminary assumptions and boundary conditions are defined before proceeding with the mathematical development of the model:

- This modelling routine predicts the airflow distribution of a single layer of palletised kiwifruit in packages.
- Null thickness is assumed for all packages. As the priority of the model is to predict airflow distribution, the resistance associated to each venthole is determined by its relative size respect to the package face.
- The forced-draft cooling process is assumed to be a steady state process. Thus, although small fluctuations of velocity and pressure occur during this operation, time-averaged values were used.

- Airflow is assumed to enter at the inlet of the pallet layer with a turbulent, fully developed flow. Likewise, refrigerated air enters only through the ventholes, and flows from inlet to outlet only. That is to say, no airflow leakage through the bottom or top of the pallet layer.
- The packages are assumed to fit perfectly in the pallet layer, thus leaving no gap between each of the boxes.
- The headspace of the packages acts as a closed conduit, interconnected only by the package ventholes.
- The top and bottom of the packages are assumed to be a continuous and uniform solid during the process. Although cardboard is likely to bend due to mechanical stress, this is assumed to not highly influence an airflow pattern during precooling.

A resistance network modelling approach will be adapted to this scenario, inspired by the work of (Smale 2004). However, this methodology has been previously applied to solve hydraulic engineering problems for water distribution in pipes (Ateş, 2017; Ellis, 1996).

5.2.1. Transport phenomena

As this problem is fundamentally a requirement to quantitatively describe a distribution of a fluid within a physical domain, transport phenomena involved must be therefore identified. Firstly, as the main principle of a forced-draft process consists of circulating refrigerated airflow aided by a centrifugal fan (Thompson et al. 2008), the physical domain acts as an airflow resistance. As a result, a pressure differential is thus imposed within the pallet layer domain. Consequently, a momentum balance over the studied domain must be constructed, where physical variables are subjected to analysis. Thus, based on the problem boundary conditions, the overall model containing the significant variables was decomposed into several airflow relationships, representing small segments within the domain.

5.2.1.1. Airflow resistances

Previously in Chapter 4, it was concluded that the most significant variable that affected the airflow resistance was the venthole size, determined by the total open area (TOA). However, these relationships between resistances differ in magnitude, depending on the location of the venthole in the palletised domain. Subsequently, an approximation to calculate the venthole loss coefficient was developed for the inlet, venthole between packages, and outlet of the palletised domain, inspired by the general form of an orifice loss coefficient (Idelchik 1994). Thus, the following correlations were identified as follows:

$$k_{inlet} = [1.05 + (1 - TOA)^2 - 2.08(1 - TOA)] \cdot TOA^{-2} \quad 5.1$$

$$k_{orifice} = \left[-0.76(1 - TOA) + (1 - TOA)^2 - 0.82\sqrt{(1 - TOA)}(1 - TOA) + 0.56\right] \cdot (TOA)^{-2} \quad 5.2$$

$$k_{outlet} = \left[1 + 0.81(1 - TOA) - 1.81\sqrt{(1 - TOA)}\right] \cdot TOA^{-2} \quad 5.3$$

Where,

k: Venthole loss coefficient (-)

TOA: Ratio between the venthole and package face area (-)

5.2.1.2. Mechanical energy equations

A mechanical energy balance is necessary to relate all the relevant variables interconnected between a finite number of segments. Firstly, by following the law of conservation of mass, it is expressed – for a given reference point – that the refrigerated air entering an established node, must be equal to the air leaving the same node, thus:

$$\sum \dot{Q}_{in} - \sum \dot{Q}_{out} = 0 \tag{5.4}$$

Where,

$\dot{Q}_{in}$: Total of refrigerated air volumetric flowrate entering a node (m^3/s)

$\dot{Q}_{out}$: Total of refrigerated air volumetric flowrate leaving a node (m^3/s)

Subsequently, Bernoulli's equation is used to express all forces involved in the airflow motion between nodes within the palletised domain. This considers potential, kinetic, viscous, and non-viscous forces, as shown in Equation 5.5. Additionally, head losses due to fittings and friction are merged as a single loss due to turbulent dissipation between segments.

$$z_1 g + \frac{p_1}{\rho} + \frac{v_1^2}{2} = z_2 g + \frac{p_2}{\rho} + \frac{v_2^2}{2} + \underbrace{\Delta H_m + \Delta H_f}_{\substack{Turbulent \\ dissipation\ losses}} \tag{5.5}$$

Where,

z: Height of reference point (m)

p: Gauge pressure at reference point (Pa)

ρ: Fluid density (kg/m^3)

g: Gravity acceleration (m/s^2)

v: Mean velocity at reference point (m/s)

ΔH_m: Head loss between the referenced points due to minor losses

ΔH_f: Head loss between the referenced points due to friction losses

Subsequently, the pressure differential between two nodes is described as:

$$\Delta p = R\dot{Q}^2 \tag{5.6}$$

Where the airflow resistance (R) term is introduced, thus:

$$R = \frac{k\rho}{2A^2} \tag{5.7}$$

And,

Δp: Pressure drop between segments (Pa)

Q: Volumetric airflow rate (m^3/s)

ρ: Air density (kg/m^3)

k: Venthole loss coefficient (-)

A: Venthole area (m^2)

These relationships are based on mass conservation and Newton's second law of energy conservation, serving as a mathematical basis for the construction of our network algorithm. Figure 5.1 shows a basic diagram of a simple channel network. Firstly, it should be noted that this network interconnects a series of flow channels ($\dot{Q}$); associated to a given resistance (R), from two extreme fixed nodes (n_1^f and n_2^f), which values are known. Each node – denoted in red – is defined as the point of flow which may diverge or converge into one or a series of channels. Finally, a loop is a pathway enclosed by a series of nodes, and marked as a clockwise directed sets of nodes.

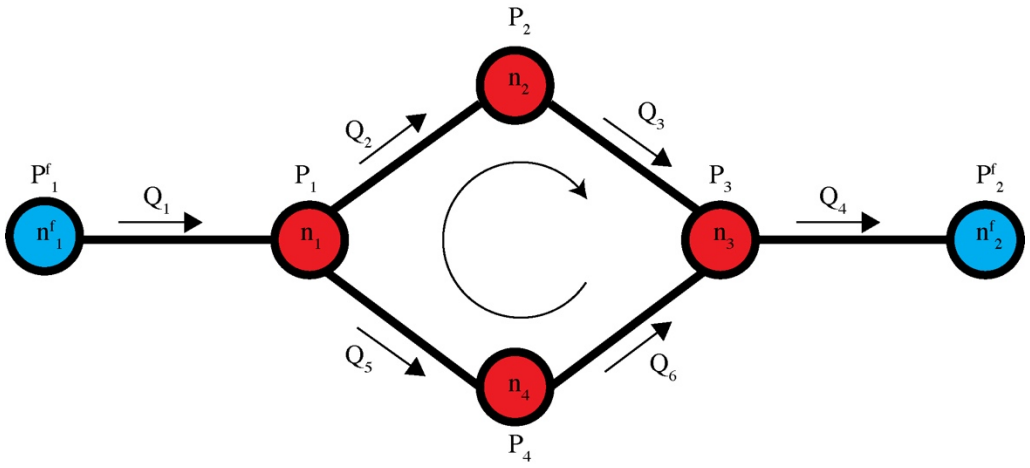

Figure 5.1. *Diagram for a simple flow channel network.*

Thus, following the reasoning of Equation 5.4, a node equation for n_1 is defined as follows:

$$\dot{Q}_1 - \dot{Q}_2 - \dot{Q}_5 = 0 \tag{5.8}$$

Subsequently, a loop equation is established from n_1 to n_4 by Equation 5.6 and 5.7:

$$\Delta P_{1-2} + \Delta P_{2-3} - \Delta P_{4-3} - \Delta P_{1-4} = 0 \tag{5.9}$$

$$R_2 \dot{Q}_2^{\,2} + R_3 \dot{Q}_3^{\,2} - R_6 \dot{Q}_6^{\,2} - R_5 \dot{Q}_5^{\,2} = 0 \tag{5.10}$$

Finally, the pressure difference between two fixed nodes is equal to the sum of the pressure differential between nodes, for any pathway between fixed nodes. The following relationship reflects this as follows:

$$\Delta P^{f}{}_{1-1} + \Delta P_{1-2} + \Delta P_{2-3} + \Delta P_{3-2^{f}} = \Delta P^{f}{}_{1-2} \qquad 5.11$$

These mathematical relationships are the logical basis of the resistance network modelling approach. In principle, the distribution of a given volumetric air flowrate is weighed by the resistance associated to each flow channel. Therefore, the importance of having an accurate approximation of such resistances is vital. These are defined in Equation 5.7, and determined by equations 5.1, 5.2 and 5.3.

5.3. Development of a geometric model

The venthole design of a horticultural package is the main feature that allows refrigerated air to cool horticultural produce to its storage temperature. A model that can predict the effective venthole area between packages in a pallet arrangement as a function of design parameter such as size, location and number of vents, as well as the number and location of the package in the palletised stack is therefore needed. A flow diagram of the geometric model is presented in Figure 5.2 for a given package design. In the subsequent sections, each of the operations involved in the model will be described in detail. Additionally, each operation will be described mathematically, expressing the variables as space-coordinates of all ventholes.

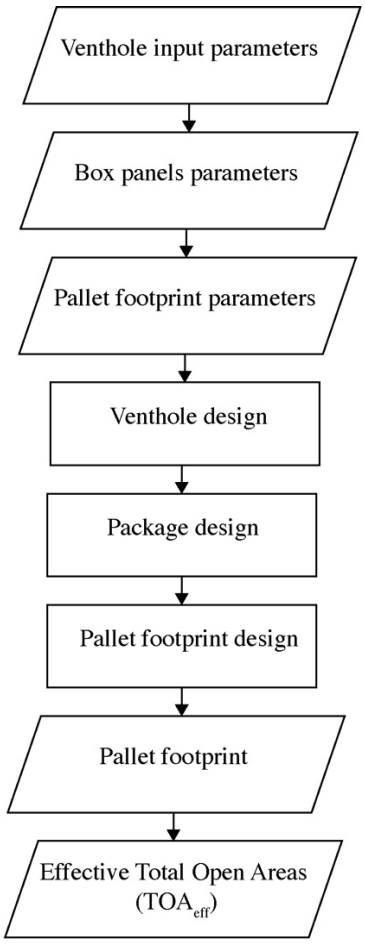

Figure 5.2. *Structure of the geometric model to predict effective venthole area within a palletised stack. Input /Output variables are outlined as rhomboids, and model operations are outlined as rectangles.*

5.3.1. Venthole design

The construction of a vent of arbitrary dimensions had to be discretised in a finite number of points, and subsequently, placed into our physical domain. Two simplified shape designs present in the kiwifruit industry were considered: A rectangular, and a semicircular shape, as shown in Figure 5.3, for a kiwifruit Modular Bulk Package (MBP). Subsequently, an arbitrary number of discretization points (N) was considered for all venthole shapes. This allows assignment of a finite number of coordinates to each vent, taking the origin of the Cartesian plane as a reference, creating a representation of a given venthole.

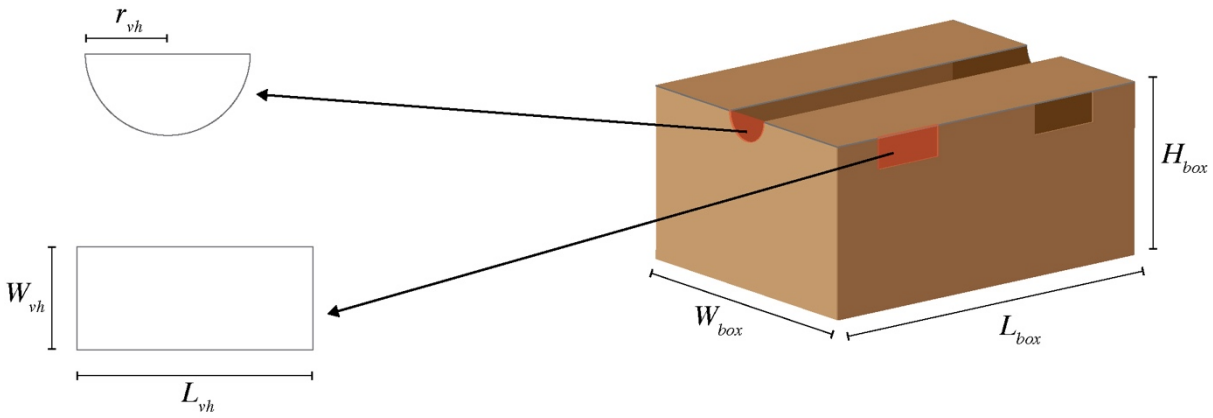

Figure 5.3: *Diagram of venthole design in a standard kiwifruit modular bulk package (MBP). a.) endface venthole design. b.) frontface venthole design.*

For the endface of the package, preliminary geometric indicators such as apparent length (L_{vh}) and perimeter (P_{vh}) were estimated as follows:

$$L_{vh} = 2 \cdot r_{vh} \tag{5.12}$$

$$P_{vh} = \pi \cdot r_{vh} + L_{vh} \tag{5.13}$$

Where r_{vh} is the venthole apparent radius (m). Subsequently, the amount of discretization points was distributed separately in two segments; the top line and the semi-circle segments of the venthole, taking

as a reference the shape described in Figure 5.3. These segments were transformed separately into Cartesian coordinates. The semi-circle segment of the venthole was preliminary characterized in polar coordinates. The amount of points of this segment was firstly described in polar coordinates, where all points of this segment were separated by the same angle θ, and is described as:

$$\theta = \frac{P_{vh}}{N \cdot r_{vh}} \tag{5.14}$$

Thus, the discretization points of this segment in polar coordinates of the form $P(r_{vh}, \theta_i)$ is:

$$\theta_i = \sum_{i=1} \pi + \theta \cdot (1 - i), \quad \pi \leq \theta_i \leq 2\pi \tag{5.15}$$

And the transformation to Cartesian coordinates of the form $P(x_i, y_i), \forall\, i \in \{1, \dots, N_{semi-circle}\}$ were accomplished by:

$$P(x_i) = r_{vh} \cdot \cos\theta_i \tag{5.16}$$

$$P(y_i) = r_{vh} \cdot \sin\theta_i \tag{5.17}$$

Subsequently, the coordinates of the top part of the venthole of the form $P(x_i, y_i), \forall\, i \in \{1, \dots, N_{top}\}$ were obtained by the following relationship:

$$P(x_i) = \sum_{1}^{N_{top}} -r_{vh} + \left(\frac{2r_{vh}}{N_{top}}\right) \cdot (i - 1) \tag{5.18}$$

$$P(y_i) = 0 \tag{5.19}$$

Finally, the coordinates corresponding to both segments of the venthole were concatenated, such as the direction of the venthole coordinates were oriented clockwise. The final space of venthole coordinates is defined as $P(x_i, y_i), \forall\, i \in \{1, \dots, N\}$.

Similarly to the end face, dimensions of the venthole such as venthole length (L_{vh}) and width (W_{vh}) were considered for the venthole on the front face panel, as well as the number of discretization points (N). Firstly, the venthole perimeter (P_{vh}) was described by:

$$P_{vh} = 2 \cdot (L_{vh} + W_{vh}) \tag{5.20}$$

Subsequently, the total number of discretization points was calculated for the length (N_L) and width (N_W) of the venthole, where $N_L \wedge N_W \in \mathbb{N}$. Thus:

$$N_L = \frac{L_{vh} \cdot N}{P_{vh}} \tag{5.21}$$

$$N_W = \frac{W_{vh} \cdot N}{P_{vh}} \tag{5.22}$$

Likewise, the distance between discretization points in the length and width of the venthole is defined:

$$d_L = \frac{L_{vh}}{N_L} \tag{5.23}$$

$$d_W = \frac{W_{vh}}{N_W} \tag{5.24}$$

Finally, the resulting array of venthole coordinates for the front face of the package design is therefore defined as $P_{frontface}(x, y)$. These coordinates were orientated in the clockwise direction, where N points were calculated for each coordinate axis, $\forall\, i \in \{1, \dots, N\}$.

$$\begin{aligned}
P(x_i) &= -\frac{L_{vh}}{2} + (i-1)\cdot d_L && , i \le N_L \\
P(x_i) &= \frac{L_{vh}}{2} && , N_L < i \le (N_L + N_W) \\
P(x_i) &= \frac{L_{vh}}{2} - (i - N_L - N_W - 1)\cdot d_L && , (N_L + N_W) < i \le (2\cdot N_L + N_W) \\
P(x_i) &= -\frac{L_{vh}}{2} && , i > (2\cdot N_L + N_W)
\end{aligned} \tag{5.25}$$

And,

$$\begin{aligned}
P(y_i) &= \frac{W_{vh}}{2} && , i \le N_L \\
P(y_i) &= \frac{W_{vh}}{2} + (i - N_L - 1)\cdot d_W && , N_L < i \le (N_L + N_W) \\
P(y_i) &= -\frac{W_{vh}}{2} && ,(N_L + N_W) < i \le (2\cdot N_L + N_W) \\
P(y_i) &= -\frac{W_{vh}}{2} + (i - 2\cdot N_L - N_W - 1)\cdot d_W && , i > (2\cdot N_L + N_W)
\end{aligned} \tag{5.26}$$

Examples of both ventholes are shown in Figure 5.4, where a number of 10, 60 and 180 discretisation points were considered for each venthole. A decreased amount of points affects the precision in the venthole representation in the end face of the package. Increasing the amount of discretization points creates a more realistic representation of the venthole shape, while potentially decreasing the computational efficiency of the model.

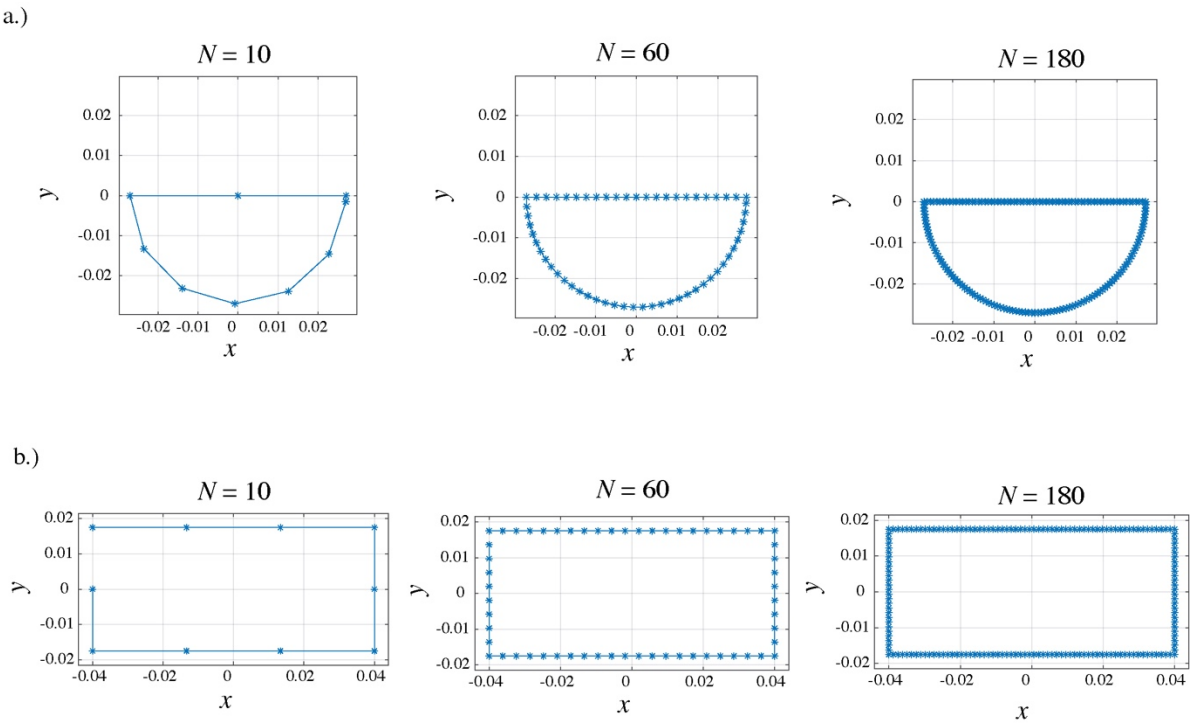

Figure 5.4: *Venthole coordinates with 10, 60 and 180 discretization points. a.) Endface vent, b.) Frontface vent.*

The effect of the number of discretization points on the simulated venthole area is shown in Figure 5.5. The area of the venthole was calculated by using the MATLAB function *polyarea*. This function calculates the area of a polygon of the form $P(x, y)$. As the rectangle form venthole only needs 4 points to represent the vertices of the shape, the area was accurately calculated. In comparison, with the semi-circle shape, a more accurate calculation is achieved as the discretization points increased.

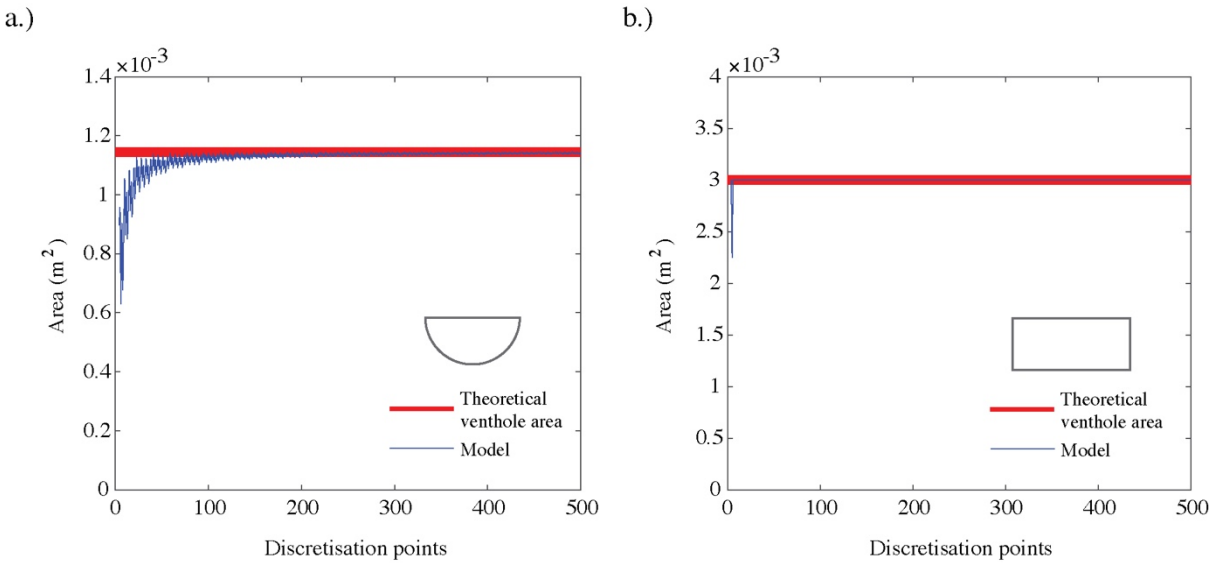

Figure 5.5: *Effect of the amount of the discretization points on the calculation of the venthole area. a.) Endface vent and b.) frontface vent.*

5.3.2. Package design

Once the overall design parameters of the ventholes were transformed into a finite number of physical coordinates of the form $P(x_i, y_i)$ —for the end and front face of the package— a procedure to obtain a preliminary sketch of the package design was developed. At this stage, variables such as the package length (L_{box}), width (W_{box}) and height (H_{box}) were incorporated. Additionally, a number of ventholes n defined for each panel as $n_{endface}$ and $n_{frontface}$ was also considered. The center point of the venthole with respect to the panel — which acts as a reference point — was defined as an $C(x_j, y_j), \forall\, j \in \{1, \dots, n\}$, for the end and front panel, respectively. Thus, the new ventholes coordinates for each panel are defined as follows:

$$P(x_i, y_i)_j = P(x_i + C(x_j), y_i + C(y_j)) \qquad 5.27$$

Where $i \in \{1, \ldots, N\}$ and $j \in \{1, \ldots, n\}$, accounting for the number of discretization points of the ventholes, and the number of ventholes in the panel, respectively. Figure 5.6 shows different panel configurations for a kiwifruit Modular Bulk Pack (MBP). Where the standard status quo design is illustrated in Figure 5.6a. An increase on the venthole size by two times is illustrated in Figure 5.6b, where only one venthole was considered for the front face panel. Finally, an increase in the number of vents, whilst maintaining the overall total open area of the package was illustrated in Figure 5.6c. Thus, the algorithm is capable of illustrating an arbitrary venthole design, where its relative size, location and number can be introduced as separated variables.

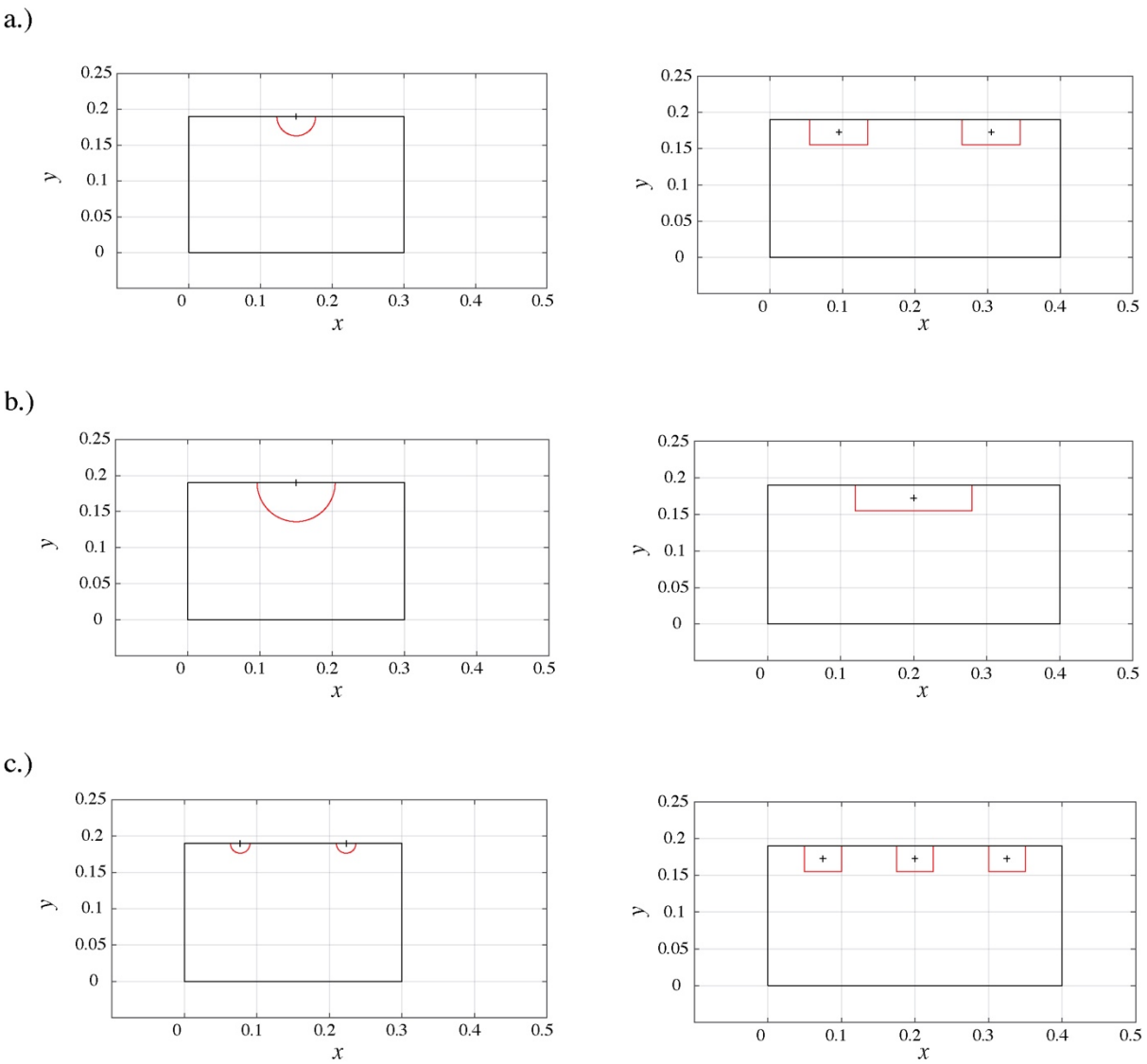

Figure 5.6: *Diagram of different venthole designs for a Modular Bulk Package (MBP).*

5.3.3. Pallet footprint

Once the package has been created in a quantifiable space, the next operation is to construct the pallet footprint. Firstly, and subsequently to the creation of the considered ventholes in each box panel, these were placed in each of the panels that conform the final package in the three dimensional space. Figure 5.7 shows the labelled faces of the package with the numbers 1 and 3 for the large panels of the package (front view), and 2 and 4 the small panels (end view).

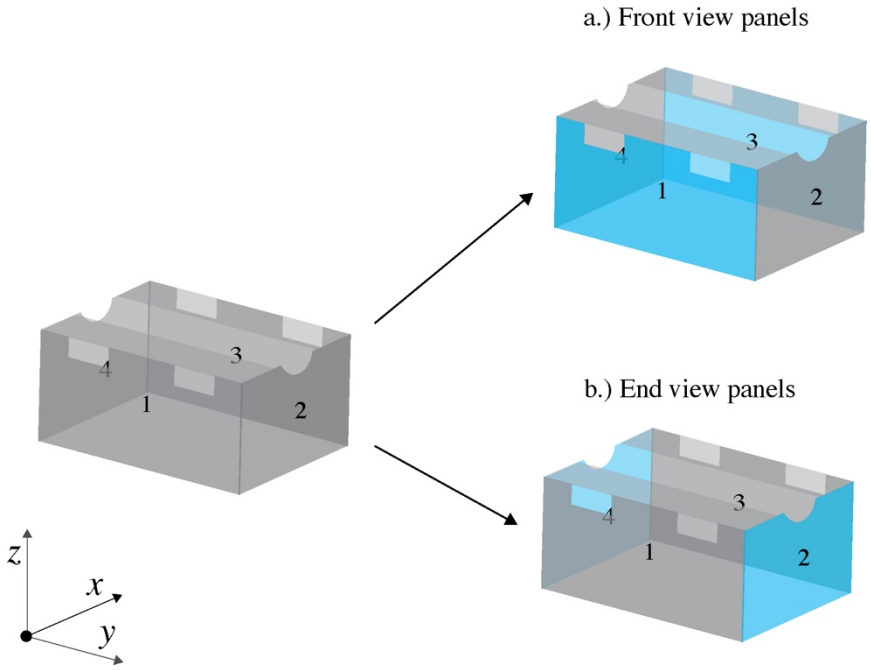

Figure 5.7: *Labeling of the panels that conforms a single package.*

The pallet width, length and height are represented in the x, y and z axis, respectively (as shown in Figure 5.7). The venthole coordinates were placed accordingly under this new space orientation. An imperative procedure is therefore to represent each of the panel ventholes in each of the package panels, correspondingly. A superscript notation was considered in order to identify the panel label into our mathematical scheme. Thus, panels 1 and 3; corresponding to the front view of the package, were described of the form $P(x_i, y_i, z_i)_j, \forall\, i \in \{1, .., N\} \wedge j \in \{1, .., n\}$.

$$P^1(x_i, y_i, z_i)_j = P_{frontface}(z_i, x_i, y_i)_j \quad 5.28$$

$$P^3(x_i, y_i, z_i)_j = P_{frontface}(z_i + W_{box}, x_i, y_i)_j \quad 5.29$$

Similarly, panels 2 and 4 were descripted by:

$$P^2(x_i, y_i, z_i)_j = P_{endface}(x_i, z_i, y_i)_j \quad 5.30$$

$$P^4(x_i, y_i, z_i)_j = P_{endface}(x_i, z_i + L_{box}, y_i)_j \quad 5.31$$

Where N is the number of discretization points of the ventholes and n is the number of ventholes of each panel. The resulting panels in the three dimensional space can be found in Figures 5.8a and 5.8b, for the end and front view of the package, respectively.

a.)

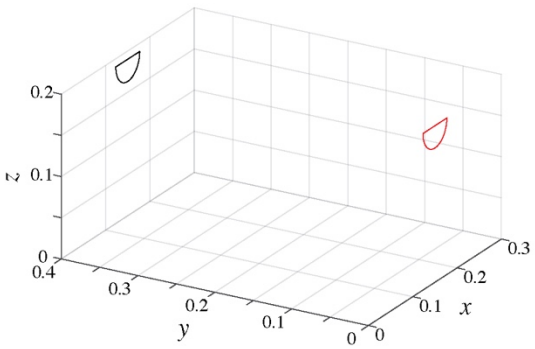

b.)

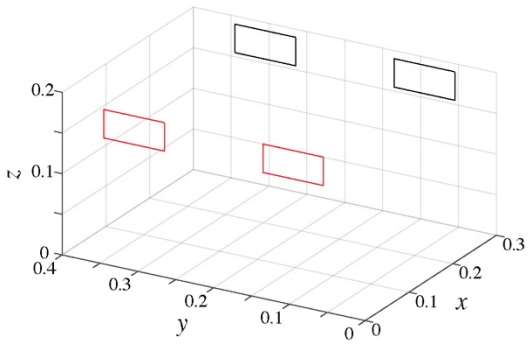

Figure 5.8: *Venthole coordinates of the endface (a) and frontface (b) of the package. Ventholes of panels 1 and 2 red are market in red for identification purposes.*

Once the venthole coordinates were obtained for each of the panels that compose the package, the desired pallet footprint was constructed. Firstly, two input vectors were considered for this operation, both in binary logic. A vector that indicates how many packages were considered in the pallet layer (up to 10 packages), and a vector of package rotation, that indicates which of the packages are rotated in 90° respect to the origin. Both the package inclusion and rotation vector, respectively, are described as follows:

$$I_k = \begin{cases} 1, & \text{if package } k \text{ is included in the pallet footprint.} \\ 0, & \text{otherwise} \end{cases} \quad 5.32$$

$$R_k = \begin{cases} 1, & \text{if package } k \text{ is rotated orthogonally in } 90° \text{ respect to the } z-\text{axis} \\ 0, & \text{otherwise} \end{cases} \quad 5.33$$

At this stage, each of the ventholes corresponding to each package were identified with a series of coordinates for all ventholes within the package. The general form of a package coordinates is defined as the catenation of all panel ventholes from 1 to 4, in the jth dimension, described as follows:

$$P_k(x_i, y_i, z_i)_j = \left(P^1 || P^2 || P^3 || P^4\right)_j \quad 5.34$$

Where k is the package number, dictated by the logical integer of the vector index ($k \in I_k = 1$). However, this mathematical description makes sense only for a package that is not subjected to rotation. To account for this feature, a 90° matrix rotation respect to the z axis was required (Equation 5.35). Thus, the coordinates of a rotated package are described in Equation 5.36.

$$R_{z_{90°}} = \begin{bmatrix} cos(90°) & -sin(90°) & 0 \\ sin(90°) & cos(90°) & 0 \\ 0 & 0 & 1 \end{bmatrix} \quad 5.35$$

$$P_{rot} = P(x_i, y_i, z_i)_j \cdot R_{Z_{90°}} \quad 5.36$$

However, by only this operation, the obtained rotated package venthole coordinates were placed in the second quadrant of the plane. To account for this, the following adjustment was needed, thus resulting in the coordinates of a rotated package ventholes:

$$P_{rot}(x_i)_j = P_{rot}(x_i)_j + L_{box} \quad 5.37$$

All the pertinent steps to accomplish a package rotation are shown in Figure 5.9, where the package illustrated in Figure 5.9a was rotated preliminary as shown in Figure 5.9b. Finally, the resulted package is shown in Figure 5.9c.

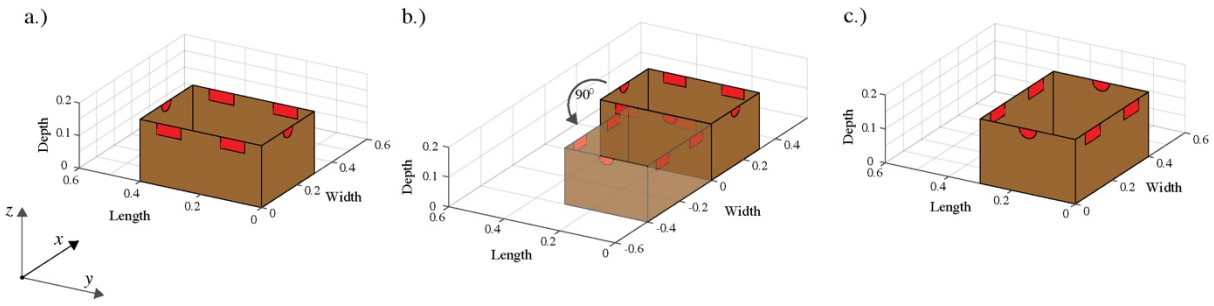

Figure 5.9: *Diagram of a package rotation of a standard Modular Bulk Package (MBP).*

Now that the package orientation was accounted for, the subsequent placement of all the relevant packages in the pallet footprint had to be accomplished. Here, each package was translated accordingly using a displacement constraint in the x and y direction, namely Δx and Δy, respectively. These constraints are dependent on the location of the adjacent packages towards the plane origin, thus these quantities can be automatically modified when these packages are rotated. The general form of a venthole coordinates of a given package k, $\forall\, k \in I_k = 1$ is described as:

$$P_k = P(x_i + \Delta x, y_i + \Delta y, z_i)_j \tag{5.38}$$

Or its analog for a rotated packaged,

$$P_k = P_{rot}(x_i + \Delta x, y_i + \Delta y, z_i)_j \tag{5.39}$$

Where P_k is an array that contains all coordinates i, of the ventholes j, for the package k. Table 5.1 shows the different displacement constraints for each of the packages of the pallet footprint, independently of their orientation. Likewise, Figure 5.10a shows a sample pallet layer where no package had been rotated, while Figure 5.10b shows a *state of the art* pallet footprint of kiwifruit Modular Bulk Packages (MBP), where packages 1 to 4 were rotated in 90°.

Table 5.1. *Displacement constrains in the width (Δx) and length (Δy) for all packages.*

	Δx	Δy
P_1	$\max(P_5(x_i))$	0
P_2	$\max(P_6(x_i))$	$\max(P_1(y_i))$
P_3	$\max(P_6(x_i), P_7(x_i))$	$\max(P_2(y_i))$
P_4	$\max(P_7(x_i))$	$\max(P_3(y_i))$
P_5	0	0
P_6	0	$\max(P_5(y_i))$
P_7	0	$\max(P_6(y_i))$
P_8	$\max(P_1(x_i))$	0
P_9	$\max(P_2(x_i))$	$\max(P_8(y_i))$
P_{10}	$\max(P_3(x_i), P_4(x_i))$	$\max(P_9(y_i))$

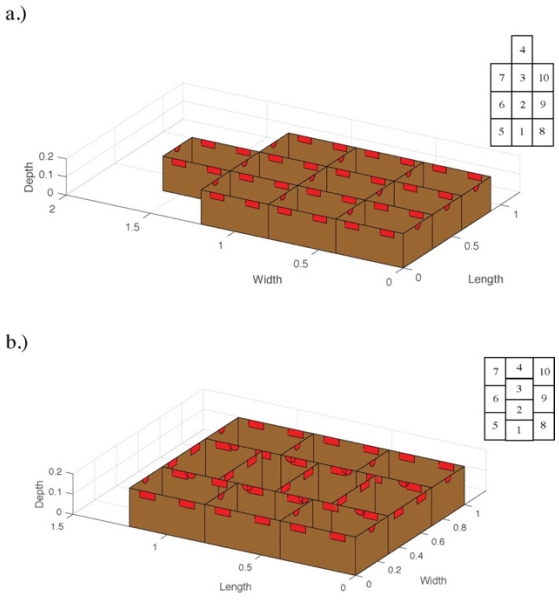

Figure 5.10: *Pallet footprint diagram of a Modular Bulk Package (MBP).*

5.3.3.1. Pallet orientation and column exchange

Additional pallet footprint adjustment such as pallet orientation and column swapping were accounted for. Firstly, it is mandatory to establish a preliminary pallet design, as the column swapping is specified for specific scenarios. By adding two characteristic distances, two columns of packages can be exchanged, originating a new pallet footprint, which can eventually improve the airflow rate and distribution of a given package design. Relationships in Equations 5.40 and 5.41 served as an example of two adjacent columns being swapped with respect to a predefined footprint shown in Figure 5.11a. These are displayed in Figure 5.11c and Figure 5.11e, respectively.

$$\Delta x_1 = max\big(P_1(x_i)\big) - max\big(P_5(x_i)\big) \tag{5.40}$$

$$\Delta x_2 = max\big(P_5(x_i)\big) \tag{5.41}$$

Where,

Δx_1: Characteristic displacement of column 1 (m)

Δx_2: Characteristic displacement of column 2 (m)

Subsequently, this characteristic displacement is added to each of the packages conforming each column. Thus, the coordinates of each package were modified as follows:

$$P_k(x_i) = P_k(x_i \pm \Delta x_1), \qquad \forall\, k = \{5,6,7\} \vee \{8,9,10\} \tag{5.42}$$

$$P_k(x_i) = P_k(x_i \pm \Delta x_2), \qquad \forall\, k = \{1,2,3,4\} \tag{5.43}$$

Alternatively, pallet orientation change in 90° anticlockwise can be achieved by using a rotation matrix such as Equation 5.35, although applied to all the packages conforming the pallet footprint, and subsequently adjusting the corresponding coordinates in the *x* axis (Figure 5.11b). These operation is described as follows:

$$P_k = P_k \cdot R_{Z\,90^\circ}, \qquad \forall\, k \tag{5.44}$$

$$P_k(x_i)_j = P_k(x_i)_j + L_{pallet}, \quad \forall\, k, i, j \tag{5.45}$$

This algorithm allows a free choice of package inclusion and rotation. However, these must be used in consideration of the desired pallet footprint. The architecture of this routine is based on various possible pallet footprints previously existing in the postharvest cold chain for different produces (e.g. Ambaw et al. 2017; Defraeye et al. 2013; East et al. 2013; Han et al. 2018; O'Sullivan et al. 2017). The pallet footprint design shall follow the standard ISO pallet dimensions (1.0 x 1.2 m). The algorithm that constructs the pallet footprint was written in MATLAB, and follows the structure outlined in the diagram of Figure 5.12.

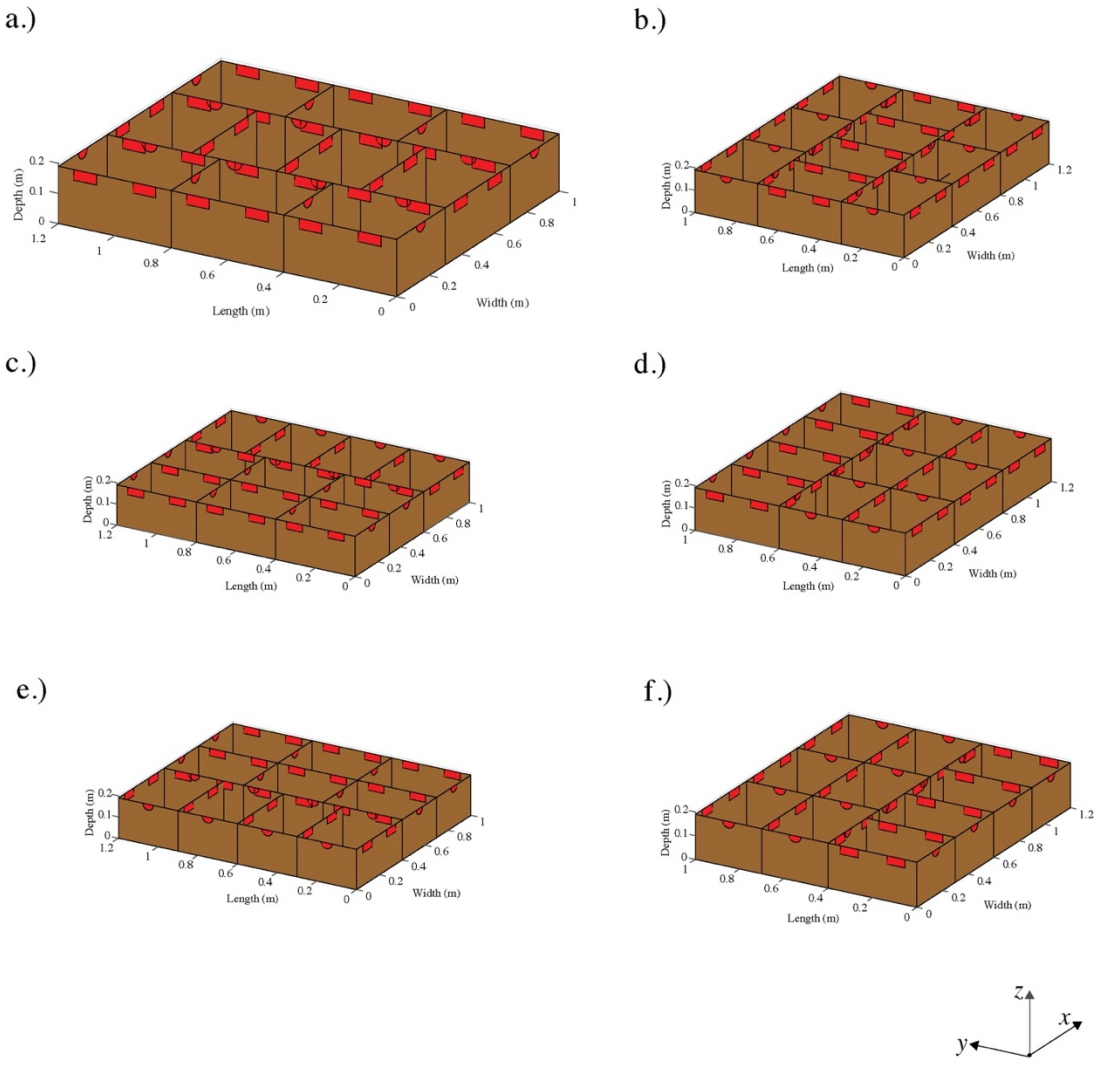

Figure 5.11. *Different pallet footprints for a pallet layer of Modular Bulk Package (MBP).*

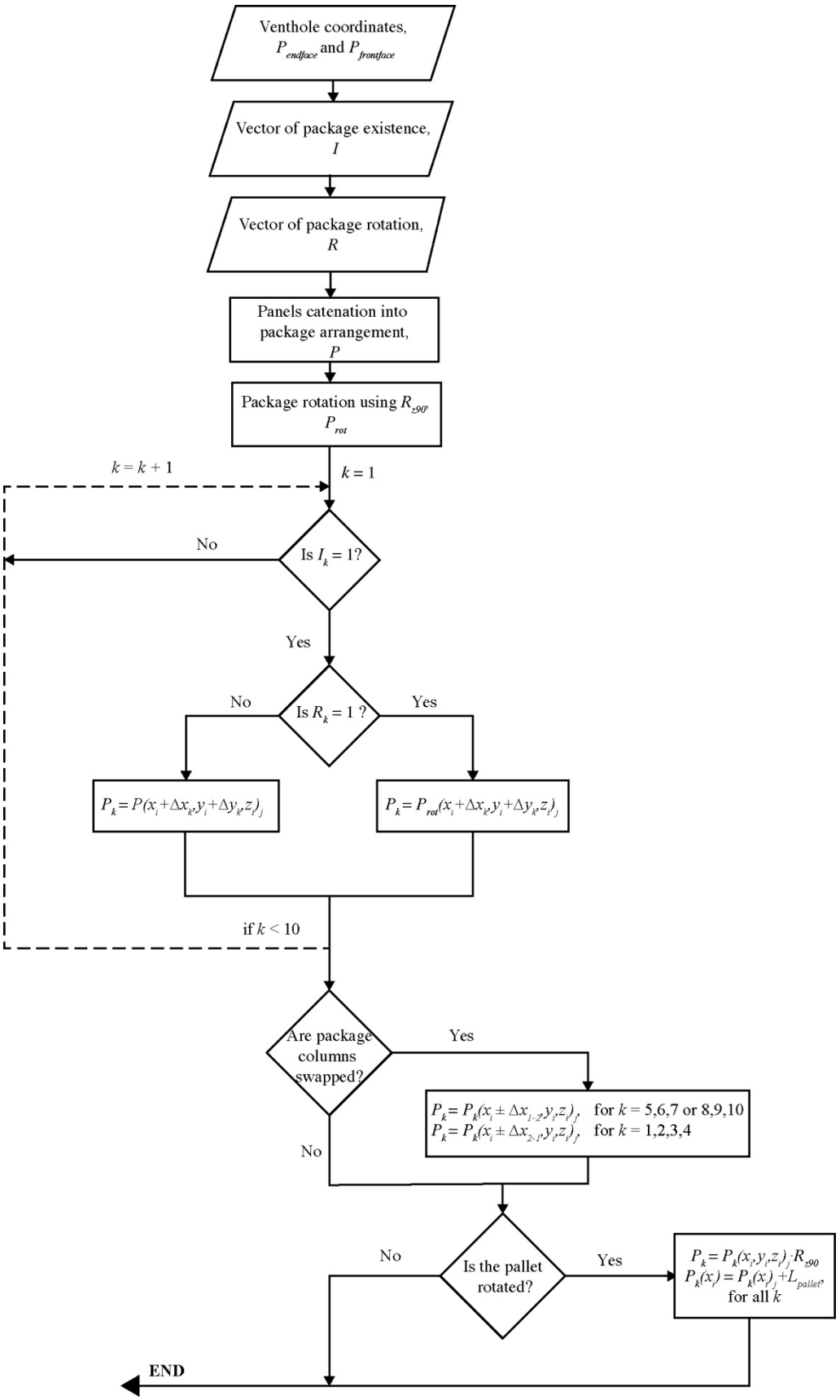

***Figure 5.12**. Flow diagram of the pallet footprint algorithm.*

5.3.4. Vent obstructions and effective venthole area

Once our pallet footprint has been characterized in our physical space, the interaction of these within the pallet layer between adjacent packages, had to be somewhat accounted for. When two or more adjacent packages are symmetrically aligned, so are they ventholes; creating an ideal airflow bypass between packages (Figure 5.13). However, there exists a risk of overlapping one or more ventholes within two package panels, or inclusively, obstruct them entirely. These obstructions directly affect the effective available area of the venthole, thus affecting its resistance, and consequently, influencing the pressure drop to the detriment of the airflow render (Ambaw et al.2017).

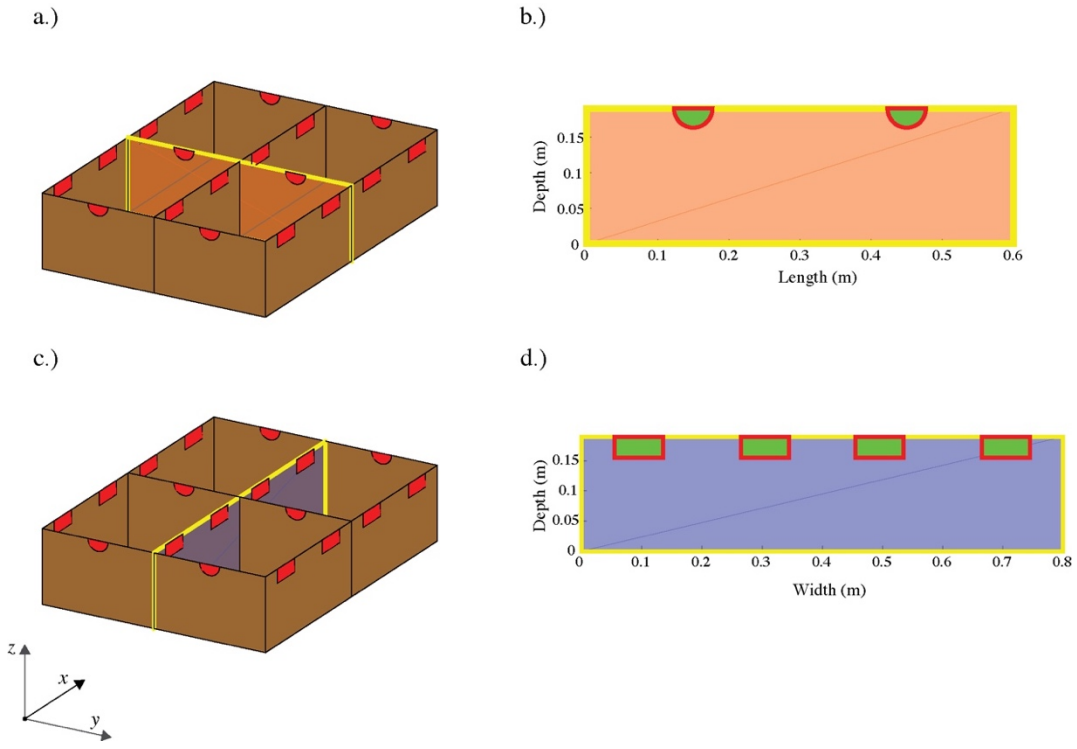

Figure 5.13. *Diagram of vent intersection in the length (a.) and b.)), and the width (c.) and d.)) of a 4 package stack.*

In all interactions between packages, there is at least one panel that interacts with another package panel. Therefore, these interactions were identified automatically in the width and length of the pallet layer. Thereof, the general form of interacting two sets of ventholes was defined as P_m and $P_n, \forall\, m \wedge n \in k$. Additionally, the panels are superposed to each other when $P_m(x_i) = P_n(x_i) \vee P_m(y_i) = P_n(y_i)$, for the Width (x-axis) and Length (y-axis), respectively.

When two of more ventholes are overlapped, it must be identified whether any venthole coordinates are inside or on the polygons formed by all the venthole coordinates, for each panel. This procedure was aided by the MATLAB function *inpolygon*. Therefore, the overlapping of two ventholes is defined as the intersection of all coordinates of P_m into P_n, and vice versa, as shown in the following definition:

$$P_m \cap P_n \begin{cases} 1, & P_m(x_i, y_i, z_i) \text{ is located inside the polygon formed by } P_n \\ 0, & \text{otherwise} \end{cases} \quad 5.46$$

$$P_n \cap P_m \begin{cases} 1, & P_n(x_i, y_i, z_i) \text{ is located inside the polygon formed by } P_m \\ 0, & \text{otherwise} \end{cases} \quad 5.47$$

Subsequently, the coordinates of the effective venthole $P_{eff}(x, y, z)$, between P_m and P_n was denoted as:

$$P_{eff} = (P_m \cap P_n) \cup (P_n \cap P_m) \quad 5.48$$

However, these coordinates were not ordered clockwise. To account for this, polar coordinates of the form $P_{eff}(r, \theta)$, and Pythagorean mathematics were used. The reference origin for the polar plane is defined as the intersection of the lines of the form $y = m \cdot x \pm n$ conformed by the maximum and minimum in the horizontal orientation and for the corresponding maximum and minimum on the

vertical orientation, as shown in Figure 5.14a. Consequently, the coordinates of the reference origin point in the polar map $O(x_o, y_o)$, were defined as:

$$x_o = \frac{n_2 - n_1}{m_2 - m_1} \quad 5.49$$

$$y_o = m \cdot x_0 \pm n \quad 5.50$$

Where,

m: Slope of the line formed by extremes values in the horizontal (m_1) and vertical (m_2) of the effective venthole coordinates.

n: Intersection of the line with the *y*-axis, formed by extremes values in the horizontal (n_1) and vertical (n_2) of the effective venthole coordinates.

Subsequently, the resulting components of the polar coordinates of the effective venthole P_{eff}; where θ is the angle of the reference directions (radians), and d is the distance between the origin point to the venthole edge (m) (Figure 5.14b). By using the Pythagorean theorem, the distance d from the origin to the edge of the venthole for each discretisation point was defined as:

$$d_i = \sqrt{(x_i - x_i)^2 + (y_i - x_o)^2 + (z_i - y_o)^2} \quad 5.51$$

Similarly, the distance of all points of the venthole for a venthole on the *x*-*z* plane is:

$$d_i = \sqrt{(x_i - x_o)^2 + (y_i - y_i)^2 + (z_i - y_o)^2} \qquad 5.52$$

Additionally, the angle or orientation θ for all points of the effective venthole is defined as:

$$\theta_i = \begin{cases} \cos^{-1}\left(\frac{y_i - x_o}{d_i}\right), & x_o \leq y_i \ \wedge \ y_o \leq z_i \\ \pi - \cos^{-1}\left(\frac{x_o - y_i}{d_i}\right), & x_o > y_i \ \wedge \ y_o < z_i \\ \pi + \cos^{-1}\left(\frac{x_o - y_i}{d_i}\right), & x_o > y_i \ \wedge \ y_o > z_i \\ 2 \cdot \pi - \cos^{-1}\left(\frac{y_i - x_o}{d_i}\right), & x_o < y_i \ \wedge \ y_o > z_i \end{cases} \qquad 5.53$$

Finally, aided by the MATLAB function *sort*; the angles θ were sorted in the desired orientation, while the distance d was sorted in case the values of angles were identical. By using these functions, the same output order was applied to the venthole coordinates in Cartesian form. Subsequently, all coordinates were sorted clockwise. The MATLAB function *polyarea* was used to calculate the effective venthole area A_{eff} (Figure 5.15b).

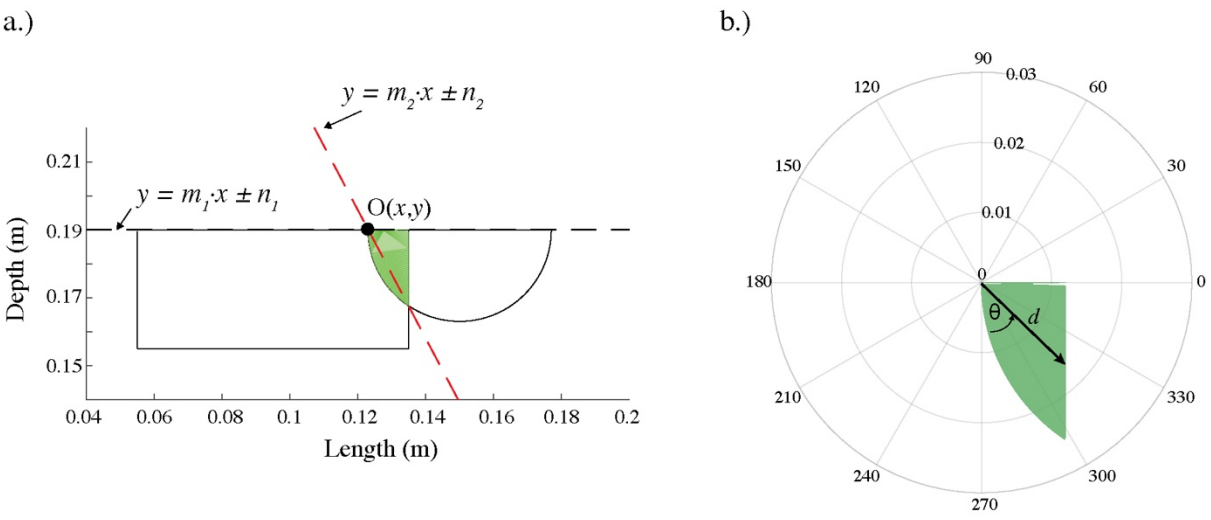

Figure 5.14. *a.) Diagram of the reference point of the polar plane. b.) Characterisation of the polar coordinates of the effective venthole.*

a.) b.)

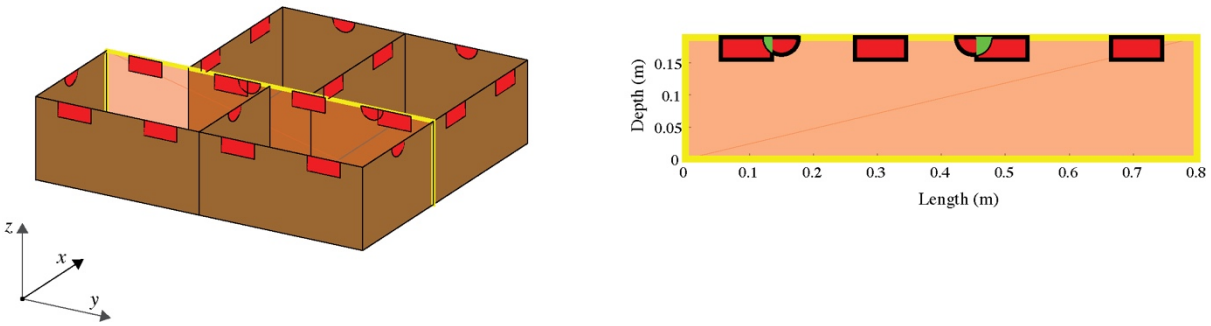

Figure 5.15. *Diagram of the effective venthole area resulted by partial venthole obstruction between packages.*

5.4. Network builder

Now that the effective venthole areas within the pallet footprint were obtained, these were used to characterize the airflow resistances and thus build a network of interconnected pathways. Figure 5.16a shows a two dimensional sketch of a standard Modular Bulk Pack (MBP) pallet footprint, where nodes were indicated for each of the packages within the stack. Additionally, a node diagram is shown in Figure 5.16b, where the sign convention is adopted whether the airflow mass flux is either entering (positive) or exiting a given node (negative). Subsequently, Figure 5.16c shows the airflow pathway network for the pallet footprint, where a single pathway was defined as the interconnection between two nodes. Finally, two fixes nodes of known pressure quantities are denoted at the inlet and outlet of the pallet layer (marked as blue nodes). Typically, there is a line of symmetry, unifying the lateral packages within the pallet footprint. However, it was decided to preserve the original pallet footprint, thus increasing the amount of loops and node equations for better mathematical convergence when solving the airflow distribution.

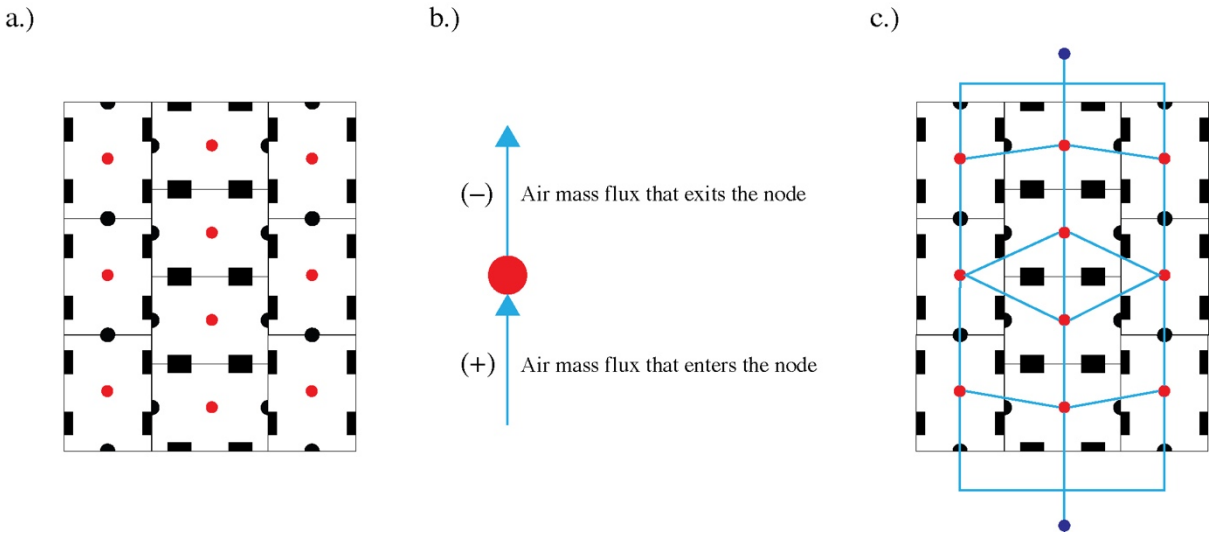

Figure 5.16. *a.) Two-dimensional plane of a standard kiwifruit Modular Bulk Package (MBP). b.) Sign convention for mass balance of each node. c.) All possible airflow pathways between nodes in a MBP pallet footprint.*

An airflow pathway network can be characterized in a set of equations; these called node, loop and path equations (Section 5.2.1.2) — which represents the Newton laws of conservation of mass and energy. These equations, form a system of equations that can be solved iteratively (Smale 2004). For a given pallet footprint, the amount of airflow entering each pathway within the system can be estimated, thus the subsequent cooling efficiency can be somewhat quantified (Olatunji 2018). Therefore, these set of equations were arranged in a matrix-like manner, which is the mathematical representation of the system of equations in a computational environment. To account for this, a topological analysis of the pallet footprint was developed by using graph theory (Bondy and Murty 1976). A given network can be arranged in a set of matrices which can be generated automatically, aiding our airflow model to be subsequently coupled with a heat transfer approach, and integrated in an automated routine that can evaluate the cooling performance of a given packaging configuration (Ferrua and Singh 2009b; Olatunji 2018). Figure 5.17 shows a network diagram for a classic MBP pallet footprint. Firstly, the base reasoning to tackle this problem is to establish the airflow direction respect to a given node. Thus, it was stated that an airflow path is positive when this enters a node, while an airflow path must be negative when leaving this node, as represented in Figure 5.16b. Secondly, each package conforming the pallet

footprint represents a node. These nodes of unknown static pressure P served as a conceptual base where all possible airflow pathways were defined.

Given this frame of thought, a mathematical algorithm was developed to represent this network in terms of a mathematical network structure namely $N = < P, Q >$, where P and Q represents a structure for nodes and paths, respectively. A P vector contains the labeling of each of the packages that conform the pallet footprint ($P = p_i, \forall\, p_i \in \{1, \dots, k\}$. Where k is the total amount of packages contained in the pallet footprint. Subsequently, the structure for all airflow pathways was defined by Q, which is a subset of P ($Q \subseteq P \times P$). This subset is defined as the path between an initial node p_i and an ending node p_e. Thus, an airflow pathway $q_i : p_i \Rightarrow p_e$ is contained in $Q_i =< p_i , p_e >$ (Tarjan 1971). Finally, the labelled network corresponding to the pallet footprint is shown in Figure 5.17, for the standard kiwifruit MBP pallet footprint.

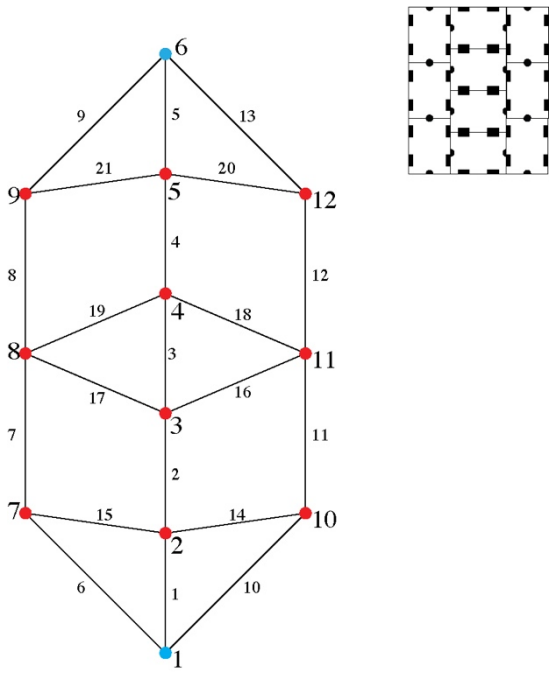

Figure 5.17. *Airflow network for a Modular Bulk Pack pallet footprint. Nodes are labelled in bold.*

Figure 5.16c contains a total of 12 nodes, 10 loops, and at least one path – from all possible airflow pathways between the two fixed nodes – which are represented from Equation 5.8 to Equation 5.11, respectively, and labelled after the diagram in Figure 5.17. The node equations corresponding to the fixed nodes (labelled 1 and 6 and denoted in blue) were not considered. Thus, a node matrix was defined as $A_{node} = a_{ij}$, where $i \in \{1, \dots, n\} \wedge j \in \{1, \dots, m\}$. n being the total number of unknown nodes and m being the total amount of airflow pathways in the network. This matrix was therefore written as:

$$a_{ij} = \begin{cases} 1, & \text{the airflow pathway } j \text{ enters the node } i \\ -1, & \text{the airflow pathway } j \text{ exits the node } i \\ 0, & \text{otherwise} \end{cases} \quad 5.54$$

Subsequently, the process of identifying the network loops was developed. Firstly, the spanning tree of the network $N = < P, Q >$, defined as $T(N)$, is a subgraph of N that contains all nodes of P with the minimum number of edges of Q (Figure 5.18a), and consequently, all edges of N that are not part of the spanning tree are shown in Figure 18b. Thus, $T = < P, Q_T >$, where Q_T is a subset of Q, that represents the airflow pathways structure that are contained in the spanning tree ($q_i{}^T : p_i \Rightarrow p_e$). Subsequently, a connectivity matrix that indicates the adjacency of each nodes interconnected by at least one airflow pathway was defined as $A(Q_T) = a_{ij}$, where $i \wedge j \in \{1, \dots, k\}$, and:

$$a_{ij} = \begin{cases} 1, & \text{the node } i \text{ is adjacent to node } j \\ 0, & \text{otherwise} \end{cases} \quad 5.55$$

a.) Spanning tree of N, $T(N) = < P , Q_T >$ b.) Non-Spanning tree edges of N

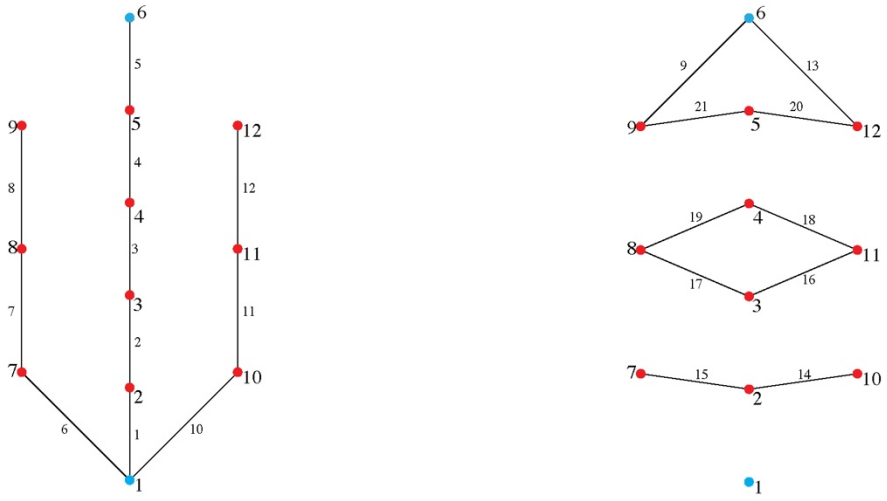

Figure 5.18. *a.) Spanning tree of the network N. b.) All pathways that are not part of the spanning tree. Nodes were labelled in bold.*

The power vector of the matrix $A(Q_T)$ (Equation 5.56) was defined as the sum of each column of the connectivity matrix, and it determines the number of adjacent nodes for each node within the network.

$$\mathrm{P} = [p_i] = \sum_{j=1}^{k} a_{ij} \qquad 5.56$$

The total amount of loops (c) in a network is given by the relationship $c = m - n + 1$, where m represents the total amount of airflow pathways and n the total amount of unknown nodes of the network (denoted as red in the network sketch of Figure 5.17). The information obtained from all the identified loops within the network were represented in a loop matrix $A_{loop} = a_{ij}$, where $i \epsilon \{1, \dots, c\} \wedge j \epsilon \{1, \dots, m\}$. c represents the total number of loops considered in the network, and m represents the total number of nodes (Kirby et al. 2016). Subsequently, prior to computing the amount of loops in the network, a catenation of the edges conforming the spanning tree plus one edge outside the spanning tree served as the main concept behind the loop identification, by an iterative algorithm. In this routine, all

edges connecting a node with only one adjacent node were deleted from the loop cycle ($p_i = 1$). Thus, each of the nodes within the loop had at least 2 adjacent nodes ($p_i \geq 2$). This algorithm was constructed based on the framework provided by the MATLAB Graph Theory Toolbox (Iglin, 2021). Consequently, all loops were constructed anti-clockwise, and the elements of A_{loop} were defined as:

$$a_{ij} = \begin{cases} 1, & \text{pathway } j \text{ is part of the loop } i \text{ in the anti} - \text{clockwise direction} \\ -1, & \text{pathway } j \text{ is part of the loop } i \text{ in the clockwise direction} \\ 0, & \text{otherwise} \end{cases} \quad 5.57$$

Figure 5.19 shows the total of identified nodes in our network, where these were oriented in the anti-clockwise direction. In addition, at least one path equation must be considered (Figure 5.20), as to the total amount of airflow pathways m must be equal to the total number of equations. Thus, by the using the relationship stated in Equation 5.11, a path equation was developed. Finally, $A_{path} = a_j$, where $j \epsilon \{1, \dots, m\}$, and:

$$a_j = \begin{cases} 1, & \text{the airflow pathway } j \text{ is part of the path between two fixes nodes} \\ 0, & \text{otherwise} \end{cases} \quad 5.58$$

By following these procedures, all pertinent equations of a given network were computed in a programming environment. Thus, the next pertinent step is to implement an algorithm that solves this system of equations, by using an iterative method based on the matrices of nodes, loops, and path (A_{node}, A_{loop} and A_{path}, respectively).

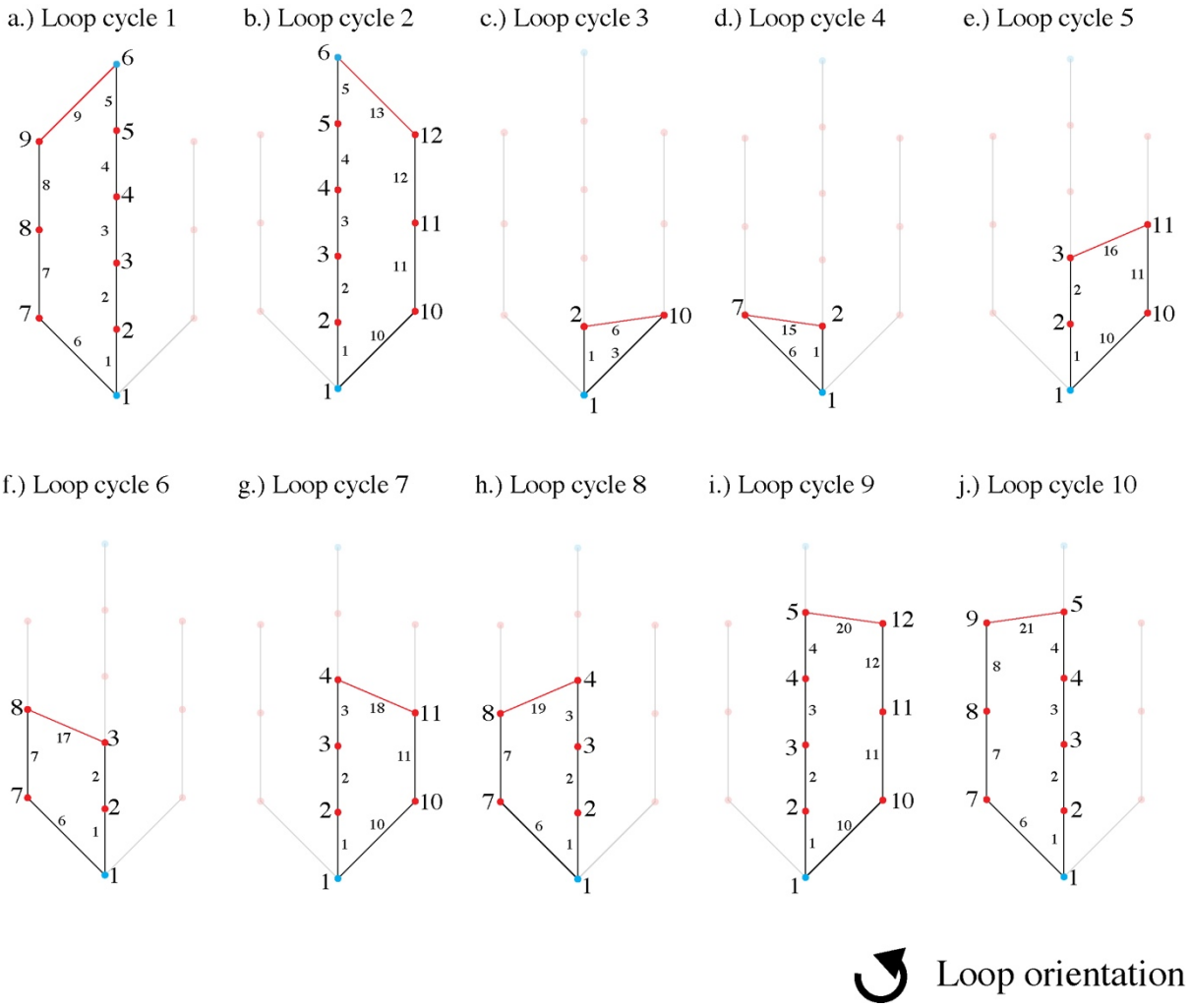

Figure 5.19. *Identified loop cycles in a pallet footprint. The edges marked in red correspond to the added edges that were not part of the spanning tree. Labelling of paths are assigned according to each identified loop.*

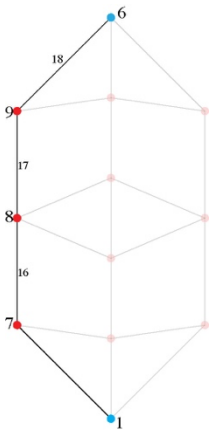

Figure 5.20. *Diagram of a path within a network between two fixed nodes of known pressure.*

5.4.1. Solving algorithm

Once all set of equations were identified and transformed into a matrix notation, all the non-linear equations had to be solved iteratively – with the purpose being to develop an efficient iterative routine that meets the criteria of being fast, robust and flexible. Various algorithms allow the solving of a set of n non-linear equations with m unknown values. In hydraulic systems, hardy-cross method for pipe network prediction has been widely used (Cross 1936). Alternatively, Smale (2004) used the Newton-Raphson method to solve non-linear equations for the estimation of airflow in shipping systems. However, a previous investigation by Ellis (1996) explored a new method for solving such system of equations: the 'so-called' linearized method for solving resistance network problems. This approach initializes the solving algorithm by giving an initial estimate of the airflow rates namely $\dot{Q}^{(n)}$ (n being the iteration number), and subsequently, the non-linear loop equations (Equation 5.10) were transformed to linear equations by:

$$\Delta P = R \cdot \dot{Q}^2 = R \cdot \left|\dot{Q}^n\right| \cdot \dot{Q}^{n-1} \qquad 5.59$$

Where,

ΔP: Pressure drop between two adjacent nodes (Pa)

R: Resistance between two adjacent notes (-)

$\dot{Q}^n$: Estimate of the airflow rate at the iteration n (m^3/s).

$\dot{Q}^{n-1}$: Estimate of the airflow rate at previous iteration n (m^3/s).

Likewise, each subsequent iteration $n+1$ was defined by the mean between the previous and the present iteration:

$$\dot{Q}^{n+1} = \frac{\dot{Q}^{n} + \dot{Q}^{n-1}}{2} \tag{5.60}$$

This approach gives the model robustness, avoiding oscillations around the solution (Wood and Charles 1972). Additionally, a change between iterations was the constraint used to achieve the desired model convergence. The rate of change associated to each successive iterations was described by:

$$\Delta\dot{Q} = \frac{\left|\dot{Q}^{n} - \dot{Q}^{n-1}\right|}{\dot{Q}^{n-1}} \tag{5.61}$$

Once all the airflow pathways within the network $\dot{Q}_i$ ($\forall\, i \,\epsilon\, \{1, \ldots, m\}$) reached the desired convergence criteria, the model reached a solution for the entire system, thus providing a prediction of the airflow distribution within a given pallet footprint. For this case, an arbitrary convergence criteria of at $1{\cdot}10^{-9}$ was chosen.

5.5. Resistance calculations and model performance

The total open area (TOA) of each face of the package, and its consequent effective TOA on partially obstructed ventholes were calculated for an MBP pallet footprint using the geometrical model described in section 5.3. Subsequently, the resistances for each airflow pathways between packages of the pallet footprint were calculated and are described in Table 5.2. Firstly, All loss coefficients (k) were calculated according to Equations 5.1-5.3, for all venthole size and locations (Figure 5.21a). As expected, an obstructed venthole will have a minor effective TOA, and consequently, a larger k value. These packages are located in the network as airflow pathways 14-21 (Figure 5.21b). Lastly, using the network information into the network solver, all path, loop, and node equations were solved until a convergence between all iterations were met.

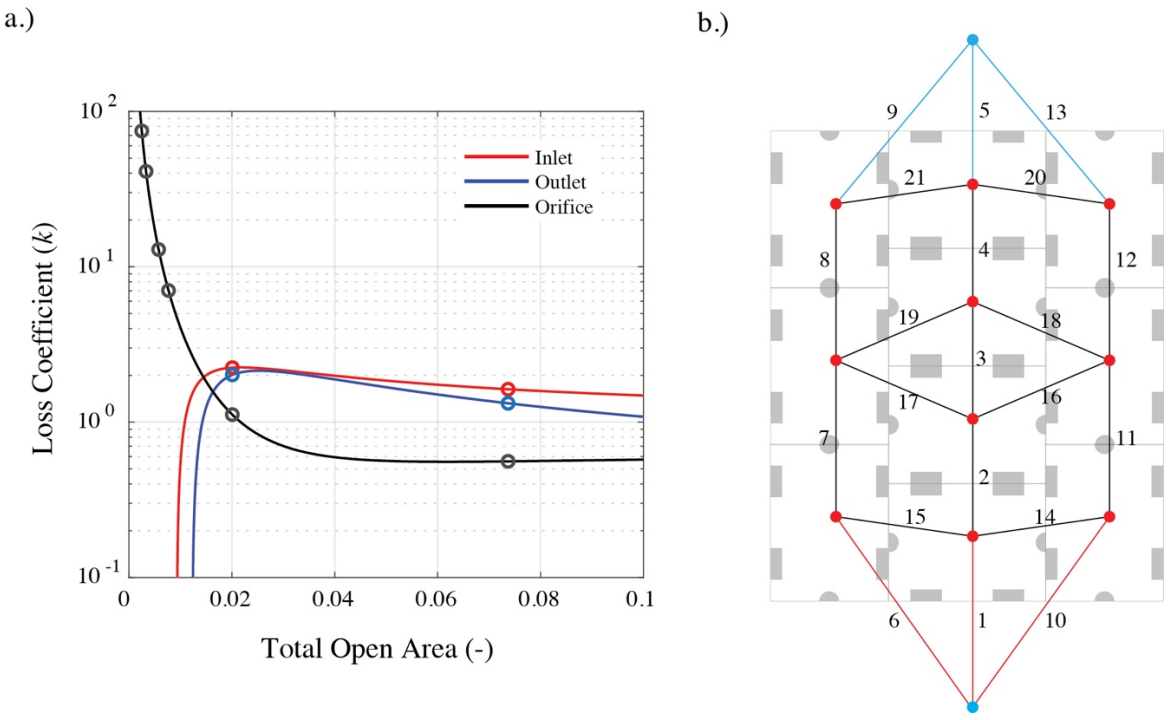

Figure 5.21. *a.) Calculated loss coefficient (k) for all vents areas in a standard MBP pallet footprint, b.) Network of pathways for a standard MBP pallet footprint. Airflow pathways for the inlet, orifice and outlet of the pallet are denoted in red, black and blue, respectively.*

Table 5.2. *Calculated airflow resistances (Equation 5.7) for all airflow pathways labelled in Figure 5.21.*

Venthole location	Package panel	Venthole area (m^2)	TOA (%)	Loss coefficient, k (-)	Airflow resistance, R (-)	Airflow pathway
Inlet	Frontface	$56 \cdot 10^{-4}$	7.18	1.64	$3.15 \cdot 10^{4}$	1
	Endface	$12.3 \cdot 10^{-4}$	2.11	2.24	$8.83 \cdot 10^{5}$	6, 10
Orifice	Frontface	$56 \cdot 10^{-4}$	7.18	0.55	$1.07 \cdot 10^{4}$	2, 3, 4
	Endface	$12.3 \cdot 10^{-4}$	2.11	1.04	$4.14 \cdot 10^{5}$	7, 8, 11, 12
	Overlapped	$2.17 \cdot 10^{-4}$	0.28	59.63	$7.64 \cdot 10^{8}$	14, 15
	Overlapped	$4.77 \cdot 10^{-4}$	0.61	11.43	$3.03 \cdot 10^{7}$	16, 17
	Overlapped	$4.77 \cdot 10^{-4}$	0.61	11.43	$3.03 \cdot 10^{7}$	18, 19
	Overlapped	$2.17 \cdot 10^{-4}$	0.28	59.63	$7.64 \cdot 10^{8}$	20, 21
Outlet	Frontface	$56 \cdot 10^{-4}$	7.18	1.34	$2.58 \cdot 10^{4}$	5
	Endface	$12.3 \cdot 10^{-4}$	2.11	2.07	$8.19 \cdot 10^{5}$	9, 13

Subsequent to the model simulation, the volumetric flowrate through the pallet layer was calculated as the total airflow that passes through all paths between fixed nodes using the relationship in equation 5.6. Typically, the cost function in optimising precooling operations is to enhance the amount of refrigerated air that passes through the pallet at constant mechanical effort – by means of imposed pressure drop. Thus, the volumetric airflow rate that passes through a pallet layer at a given fan speed was calculated as:

$$\dot{Q}_{Pallet} = \sqrt{\frac{\Delta P_{Pallet}}{\sum_{i}^{p_1} R_i}} + \sqrt{\frac{\Delta P_{Pallet}}{\sum_{j}^{p_2} R_j}} + \sqrt{\frac{\Delta P_{Pallet}}{\sum_{k}^{p_3} R_k}} \qquad 5.62$$

Where the amount of airflow through two fixed nodes are accounted for as the sum of the airflow through the pathways p_1, p_2 and p_3. Thereof, airflow pathways from 6 to 9, from 1 to 5 and from 10 to 13 were considered in p_1, p_2 and p_3, respectively.

A single routine for a standard MBP pallet footprint was developed entirely using MATLAB. Thereof, the model could successfully predicted the airflow distribution by means of a given package design in approximately 8.8 seconds. As part of the routine, the geometric model took 3.4 seconds to predict the effective venthole areas within the pallet, while the network solver took 5.4 seconds. The step of calculating the resistances was found to be < 1 second. As the code of the model includes a series of plotting functions and iterative for loops, the process can still be optimised to achieve lesser time. However, as a first approximation, the obtained solving time gives a reasonable result in terms of computational efficiency, which is one of the aims of this project, to develop a fast airflow modelling approach to predict airflow distribution in palletised produce.

5.6. Sensitivity analysis and numerical convergence

5.6.1. Model Verification

Using the network information of section 5.5 for an MBP pallet footprint, the airflow distribution was simulated using the formulated modelling routine. Thereof, a total pallet pressure drop of 130 Pa was set, thus matching with the empirical MBP data measured and evaluated in Chapter 3, at the highest fan speed (1200 rpm). Averaged values of pressure drop through the pallet and pressure at each package considered all the studied packaging configurations. Firstly, the model successfully reproduced the pressure drop curve when compared to the empirical measured data, thus predicting the total airflow that passes through the pallet layer within the range of the measured data Figure 5.22a. Additionally,

the model aimed to reproduce the pressure distribution within the pallet layer for all packages, where a maximum difference of 15.1 % was observed at the pallet inlet into package 5/8 (Figure 5.22b). However, this difference lie within the margins of uncertainty respect to the measured data.

As the resistances of the model were obtained using the same pallet footprint and partial data from the Modular Bulk Package pallet footprint (MBP), this data comparison is considered a verification of the model, and not a validation (Grace and Taghipour, 2004). For the model to be validated, it shall be tested against data generated from a different package design or pallet footprint, which is presented in the subsequent chapter on model validation.

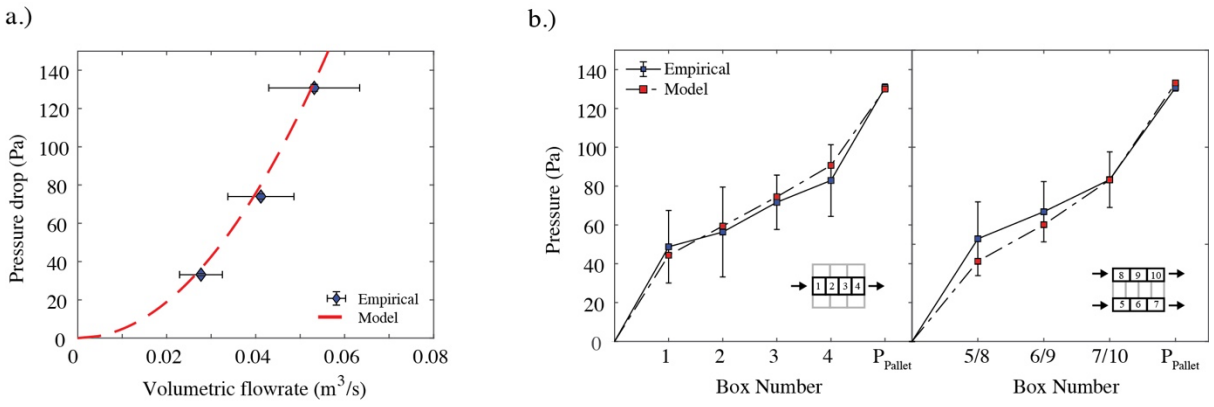

Figure 5.22. *Comparison between predicted and empirical data for a standard kiwifruit Modular Bulk Package (MBP) pallet footprint, where a.) Pressure drop curve of the pallet layer, and b.) Pressure distribution within packages (Pa).*

5.6.2. Effect of changes in air temperature on model performance

When stablishing the boundary conditions and simulation set up of the airflow model, it is imperative to refer to the temperature change of the air and its effect on the model prediction. Due to the model framework, the main thermophysical variable that required consideration in the algorithm is the air density. As the model assumes a turbulent airflow regime, the effect of the viscous forces was neglected. Overall, the changes in the thermophysical properties of the air are greatly influenced by the ambient temperature (Tsilingiris, 2008). Thereof, a standard precooling operation of palletised kiwifruit occurs at ≈ 0°C (O'Sullivan, 2016). Figure 5.23 shows the model results for air at 0 and 20 °C. Overall, the differences in the inlet volumetric flowrate of 3.34 % was found at 100 Pa as a comparison point (Figure 5.23a), while the difference in pressure distribution were only 0.8 % (Figure 5.23b). Consequently, a relative small effect of the change in temperature on the model sensitivity was observed. This effect is desirable when designing experimental monitoring of airflow in a palletised stack of packages, as conducting experiments at ambient temperature would not have a considerable effect.

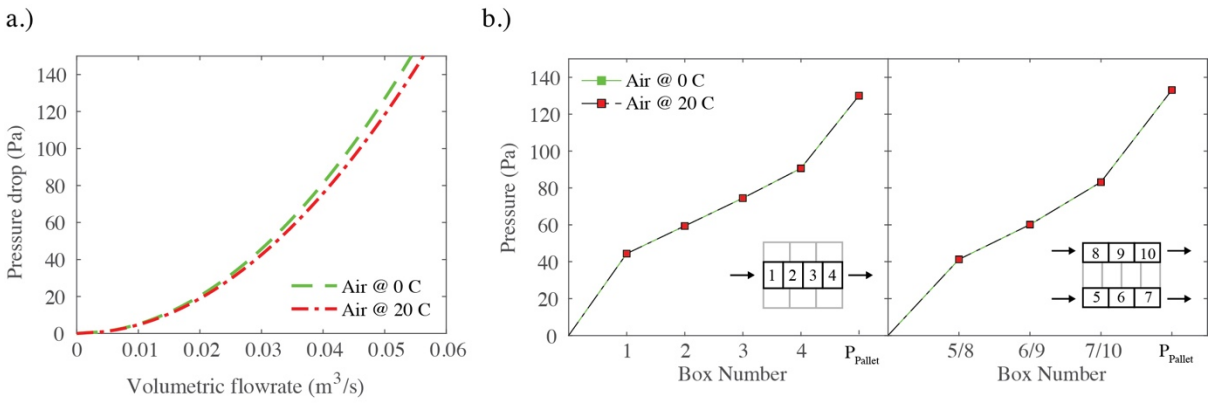

Figure 5.23. *a.) Predicted pressure curve and b.) Pressure distribution of an MBP footprint with air temperatures at 0 and 20 ℃.*

5.6.3. Changes in package design

Changing the package design by means of venthole dimensions has an influence in their resulting total open area (TOA), and consequently on the airflow distribution within the pallet. To account for this using the developed airflow model, two different operational changes were made by doubling the venthole TOA at the end and front face of the standard MBP package, as indicated in Figure 5.24b and Figure 5.24c, respectively. Additionally, the model simulated the airflow distribution of all the studied package designs at pressure drop through the pallet layer of 100 Pa, making this the comparison point.

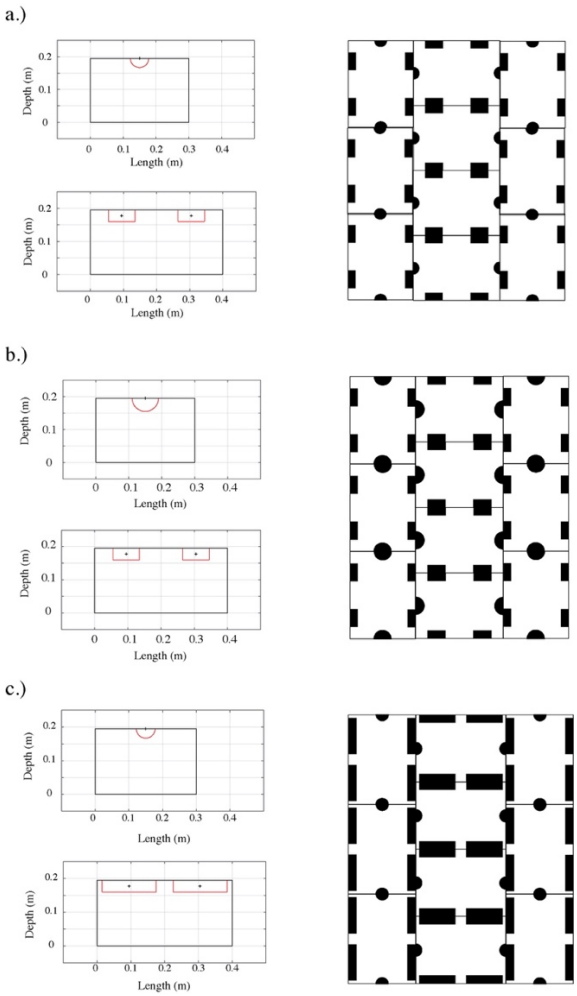

Figure 5.24. *Diagram of vent panels and pallet footprint for: a.) Status quo Modular Bulk Package (MBP), b.) MBP with doubled Total Open Area at the endface panel, and c.) MBP with doubled TOA at the frontface of the package.*

The airflow rate through the pallet layer at 100 Pa increased 45.2 % compared to the standard MBP package design when doubling the TOA of the frontface of the package, whilst doubling the TOA of the endface of the package increased the airflow rate by 25.9 % (Figure 5.25a). As expected, the increasing of the TOA resulted in a lower airflow resistance, thus allowing more airflow through the pallet at the same operational pressure drop, thus potentially enhancing the precooling process without incurring in an increase of fan power. Additionally, overall minor differences in pressure of 10.5 and 16.7 % were found at the packages close to the outlet in the central and side columns of the pallet layer, respectively within all studied cases (Figure 5.25b). Theoretically, as the pressure drop through the pallet remained constant, the pressure at each package also reminded relatively constant. In contrast, differences in pressure at the back of the pallet were found to be due to the minor changes in loss coefficient for TOA higher than the studied ventholes, as shown in the curves in Figure 5.21a.

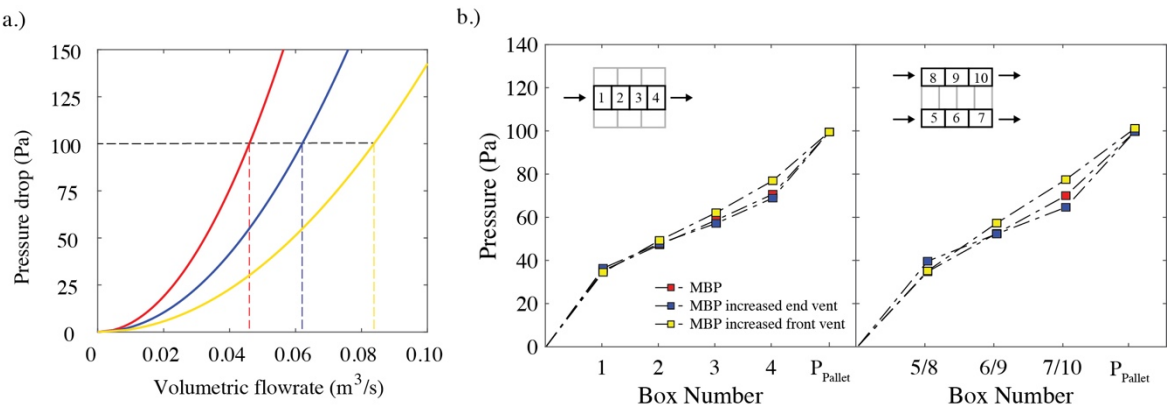

Figure 5.25.*Predicted airflow and pressure distribution of different vent design for an MBP footprint.*

Similarly, Figure 5.26 shows the percentage of airflow distribution within the pallet layer, in comparison with the total volumetric flowrate through the pallet layer, for all the simulated package designs. By increasing the end vent size (Figure 5.26b), around 22.8 % of the total airflow enters through the end face of the packages, in comparison with a standard MBP package, with 12.4 % (Figure 5.26a). Additionally, air flowrate entering the frontface of the package decreased from 75.6 to 55.2 % of the total airflow rate by increasing the end vent size. Alternatively, by increasing the front vent size (Figure

5.26c), about 87.5 % of the total airflow entered through the front face of the packages, in comparison with a standard MBP package, with 75.6 % (Figure 5.26a). Additionally, air flowrate entering the endface of the package decreased from 12.4 to 6.2 % of the total airflow rate. Overall, it was shown that by increasing the venthole size, the amount of airflow that goes through the pallet layer increased considerably at a constant pressure drop through the pallet layer.

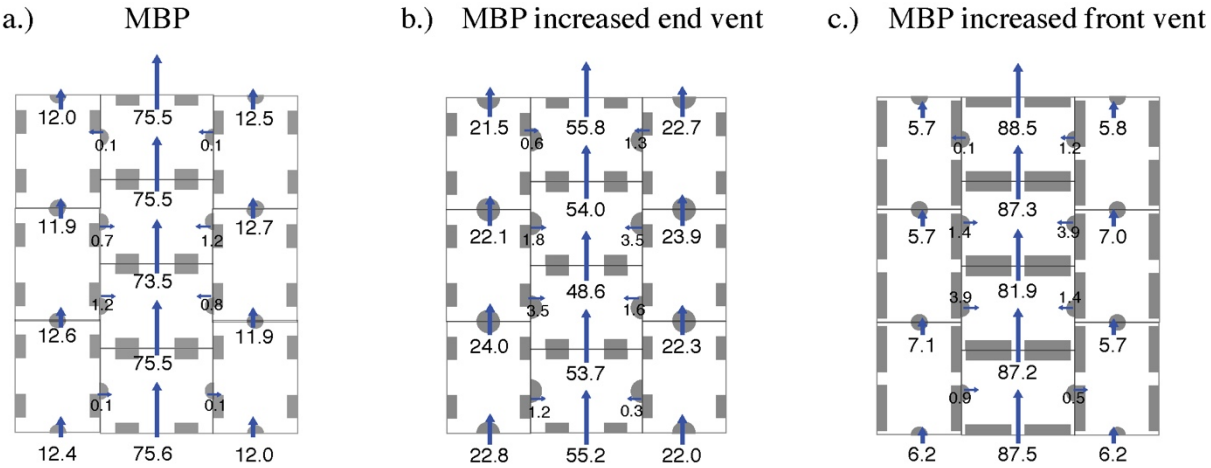

Figure 5.26. *Airflow distribution (% respect to the total volumetric flowrate through the pallet layer) for three different vent design.*

5.7. Conclusions

A mathematical model to predict airflow distribution in palletised kiwifruit packages was developed and verified against an empirical pallet-scale data of MBP. This model was constructed of three major steps, where the package design parameters (venthole size, number, location and package dimensions) and pallet footprint were considered. Firstly, a geometrical model that construct a pallet footprint and calculates the effective venthole areas within the pallet was mathematically described by transforming the package dimensions to spatial coordinates. Secondly, the obtained effective venthole areas for each package were transformed in resistance values, by using the relationships obtained in Chapter 4, and subsequently, a set of nodes, loops, and path equations were obtained by an algorithm that takes as an input the network nodes and pathways within the pallet footprint. Thirdly, an iterative algorithm that solves the set of equations obtained from the airflow network was constructed, based on a linearized method. This model was capable to predict the airflow distribution of a given system within 10 seconds, which serves as a potential tool as a part of a wider optimization routine that can predict cooling efficiency during precooling operations.

Subsequently, a model verification was conducted against empirical data of a status quo MBP footprint, showing no apparent significant differences between empirical and measured data of pressure drop and volumetric flowrate. Additionally, a maximum difference of 15.1% in pressure was observed at the inlet of the side column (box 5/8). However, those differences were found not to be significant in comparison to the variability of the measured data. A model sensitivity was performed to assess the relative effect of temperature on the air density, showing a difference of 3.34 and 0.8 % on the output variables of volumetric flowrate and pressure distribution, respectively. Lastly, comparisons of two alternative MBP vent designs were simulated. At pressure drop through the pallet layer of 100 Pa, an increase of the volumetric flowrate through the pallet layer of 25.9 and 45.2 % was achieved by doubling the size at the end and front face of the package, respectively. Additionally, pressure differences at the back of the

pallet footprint of 10.5 and 16.7 % were found for the central and side columns of the pallet, respectively.

Subsequent to the development of a modelling framework to predict airflow distribution in palletised systems, a validation process must be accounted for, assessing the applicability of the model on a wide range of package designs and pallet footprint. Thereof, the model shall be contrasted to the collected data in Chapter 4. More specifically, to obtain airflow predictions in cases when the pallet footprint and orientation varies, and consequently, new set of equations within the airflow network must be solved.

6. Airflow model validation

6.1. Introduction

A simplified resistance airflow model to predict airflow distribution in a palletised system was develop and verified in Chapter 5. Despite the good performance of the model against empirical data, the model still must be tested against other package design constraints, thus assessing the model capability to be applied to diverse scenarios.

Previously, the experimental airflow distribution in palletised systems was investigated in Chapter 4. There, diverse packaging design variables were investigated. Among them, a column of individual tray (IT) design and an alternative package design, called Alternative Modular Loose (AML) were tested. Additionally, a standard modular loose design (ML) and a change of orientation on the standard Modular Bulk Pack design (MBP) were also tested, where the airflow entered the 1.2 m face instead. Subsequently, semi-empirical relationships to calculate loss coefficient of a venthole, and therefore, its resistance, were also developed for ventholes at the inlet, outlet, and internal ventholes within the pallet layer.

Finally, the applicability of the resistance network model was assessed by:

- Use of the resistance airflow model to predict the airflow performance of four different pallet footprints to evaluate package design of IT, AML, ML and pallet orientation on MBP designs.
- Compare predicted values of pressure and volumetric flowrate of the studied scenarios with empirical data obtained from Chapter 4.

6.2. Validation System description

The airflow characteristics of palletised systems were characterized extensively in Chapter 4. More specifically, the effect of package design and pallet footprint on the relative airflow resistances were investigated. Consequently, these same variables were explored by the airflow model. Figure 6.1 shows the package designs and pallet footprint of the considered systems. The IT package design has dimensions of 0.5 × 0.3 × 6.5 m and 9.2 % TOA on the frontface of the package. However, there are no ventholes on the endface of the package design, thus only one column of boxes were considered for the model validation. The AML has dimensions of 0.5 × 0.3 × 0.12 m and 10 and 3.4 % TOA in the front and endface, respectively. The ML design has dimensions of 0.4 × 0.3 × 0.12 m and 11.6 and 3.4 % TOA for the front and endface, respectively. Finally, the MBP has dimensions of 0.4 (m) × 0.3 (m) × 0.195 (m) and TOA of 7.2 and 2.7 % in the front and endface, respectively. All pallet footprint and airflow directions are shown in Figure 6.1.

Empirical measurements of pressure during forced-draft operation were conducted using a precooling simulator connected to a centrifugal variable speed control fan (AP0502AA5/16, Fantech, Wellington, NZ), developed by O'Sullivan (2016). Additionally, one differential pressure sensor (P992-1B-A, Sensata-Kavlico, MA, USA) was placed at the center of each package, plus one pressure sensor (SSCSNBN002NDAA5, Honeywell, Morris Plains, USA) outside of the pallet layer as indicated as P_2 in Figure 6.2. Volumetric flowrate through the pallet layer was monitored with a hot wire anemometer (9545 Velocicalc Air velocity meter, TSI, USA) according to the method outlined in section 4.2.3. Values of pressure and volumetric flowrate were averaged over the experimental period, at three fan speeds (600, 900 and 1200 rpm). Averaged values of measured pressure drop through the pallet (ΔP_{Pallet}) were used as inputs of the model.

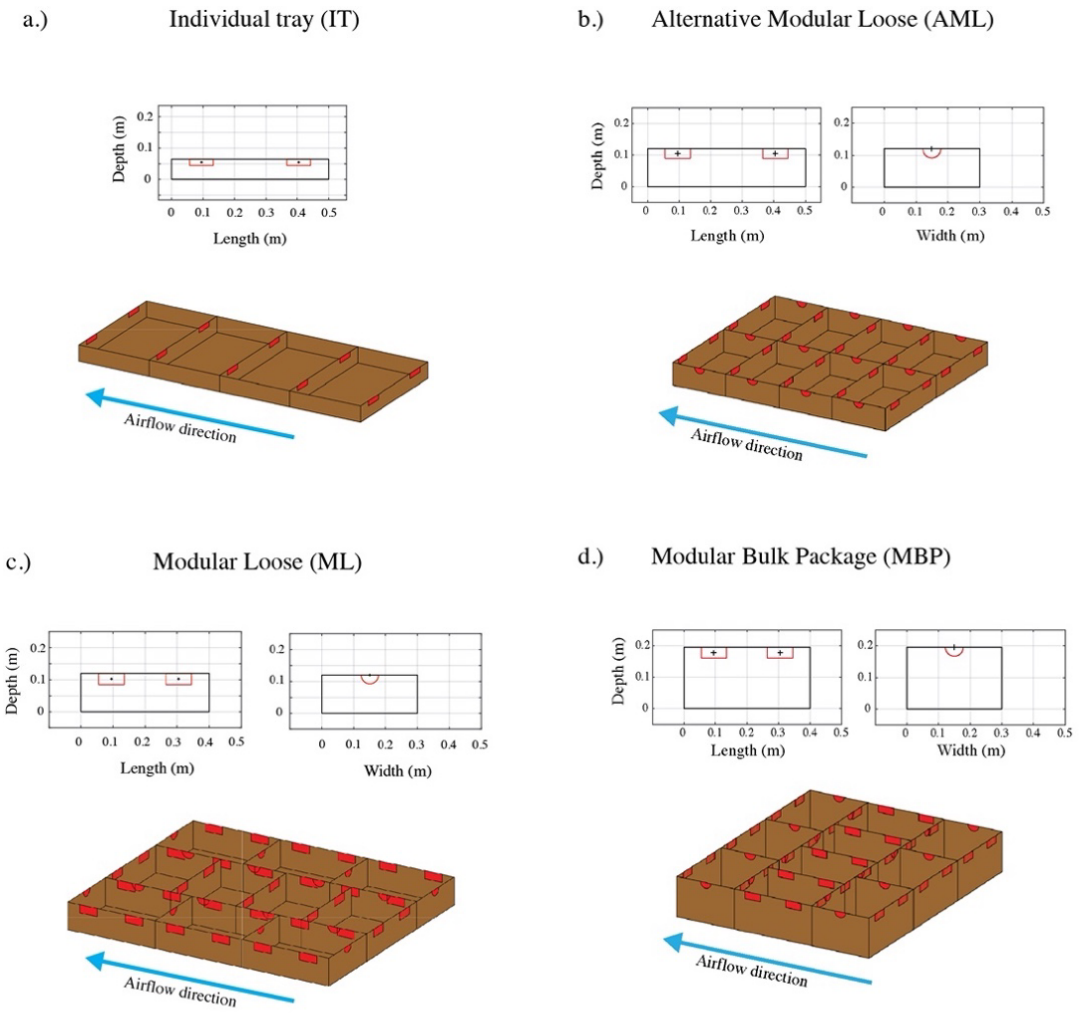

Figure 6.1. *Package design and pallet footprint of: a.) Alternative Modular Loose (AML) and b.) Modular Bulk Package (MBP) with airflow entering the 1.2 m face.*

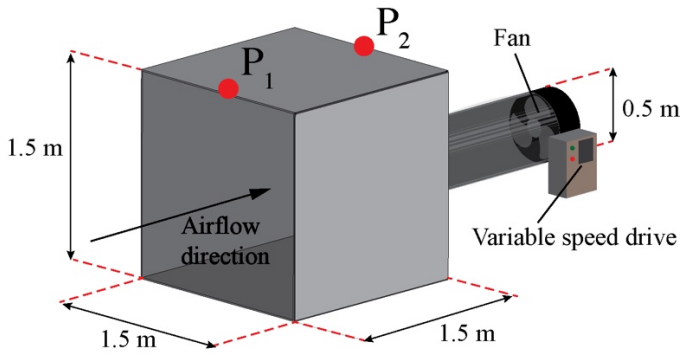

Figure 6.2: *Diagram of the forced-draft cooler simulator developed by O'Sullivan (2016).*

6.3. Network model settings

Semi-empirical relationships to estimate venthole resistances were developed in Chapter 4, and subsequently, a modelling framework to predict airflow distribution in palletised systems was developed in Chapter 5. The model tested two design parameters that influence airflow distribution in a stack: package design and pallet footprint. Firstly, the model predicted the airflow distribution for all pallet footprints in Figure 6.1. Averaged ambient conditions of 19 °C and 80 % RH were considered for this simulation, and thus, a relative air density of 1.292 kg/m^3. Subsequently, the airflow resistances were calculated according to equations 5.1, 5.2 and 5.3. Each of the pallet footprints were transformed into arrays of pathways and nodes, conforming two networks of the form $N = < P, Q >$, where P and Q represents a structure for nodes and paths, respectively (see section 5.4). The resulting diagram of the networks for all the studied pallet footprints are shown in Figure 6.3.

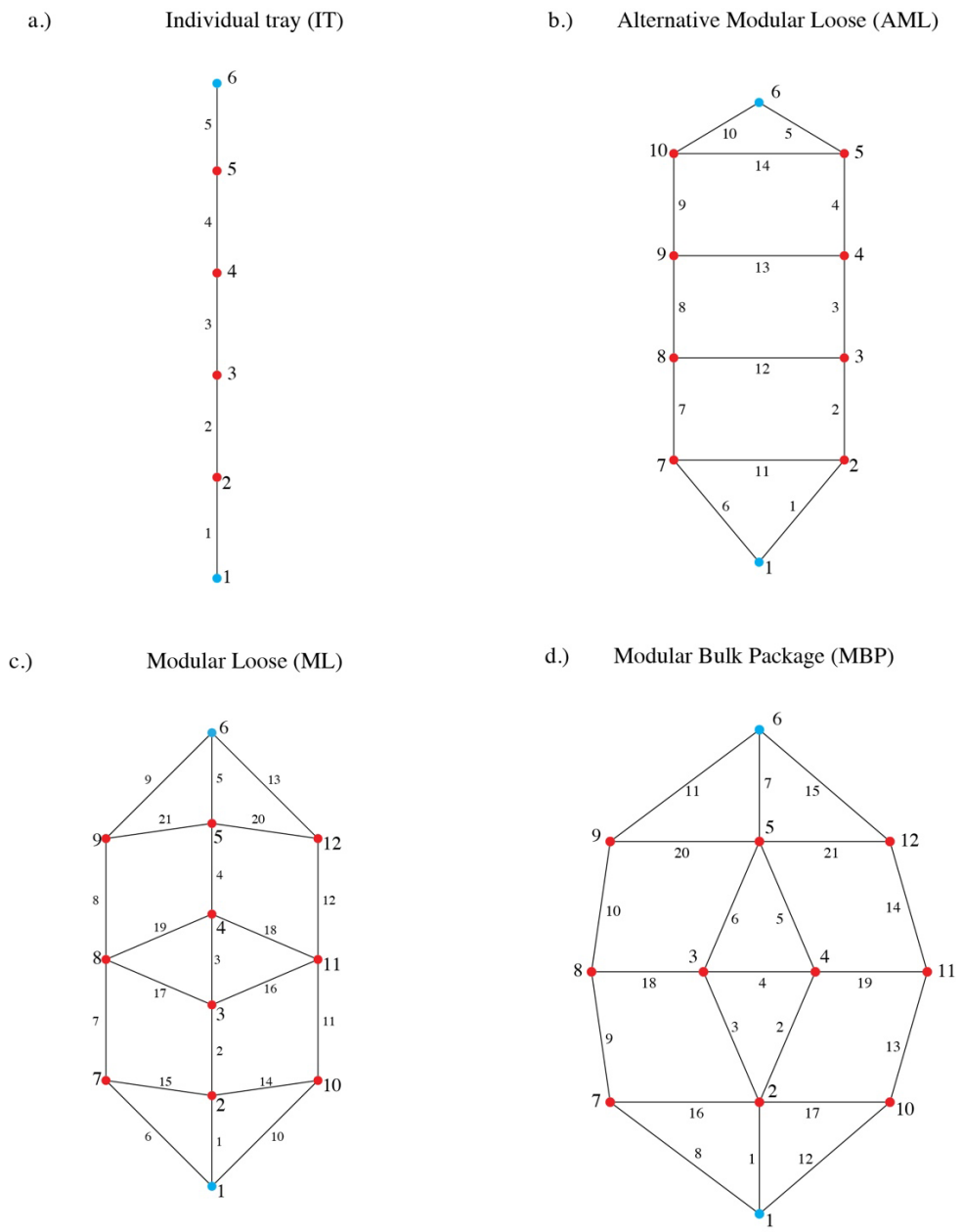

Figure 6.3: *Network structure for: a.) Alternative Modular Loose and b.) Modular Bulk Package (MBP) with airflow entering the 1.2 m face.*

A mass balance at each package given by the detected red nodes resulted in 4, 8 and 10 node equations for the IT, AML; and ML/MBP pallet footprints, respectively. A total of 5 loop equations were solved for the pallet footprint of 8 packages of AML design (Figure 6.4). Additionally, a total of 10 loop equations were solved for the ML and MBP package designs. As the is no ventholes on the endface of the IT design, no airflow exchange between columns of packages was considered, and thus, no loop

equations were solved. Finally, one path equation was solved for each pallet footprint (blue nodes in Figure 6.3), thus completing the mathematical constraint of the model, where the amount of equations must be equal to the amount of unknown airflow pathways (Ellis 1996).

Simulations at 600, 900 and 1200 rpm were performed for each pallet footprint, given by the measured ΔP_{Pallet} as input for the model. Thus, by matching a single pressure drop value, the pressure distribution in each package within the pallet layer was subsequently predicted. The minimum convergence criteria given by the sum of error between subsequent iterations for the model solver was set at $1 \cdot 10^{-13}$, at which value stop the iteration process.

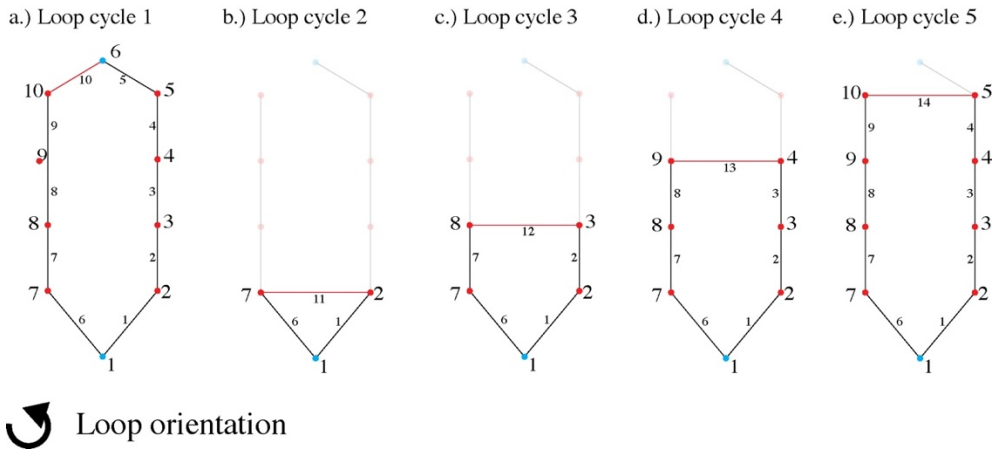

Figure 6.4: *Identified loops between airflow pathways for a pallet of Alternative Modular Loose (AML) design.*

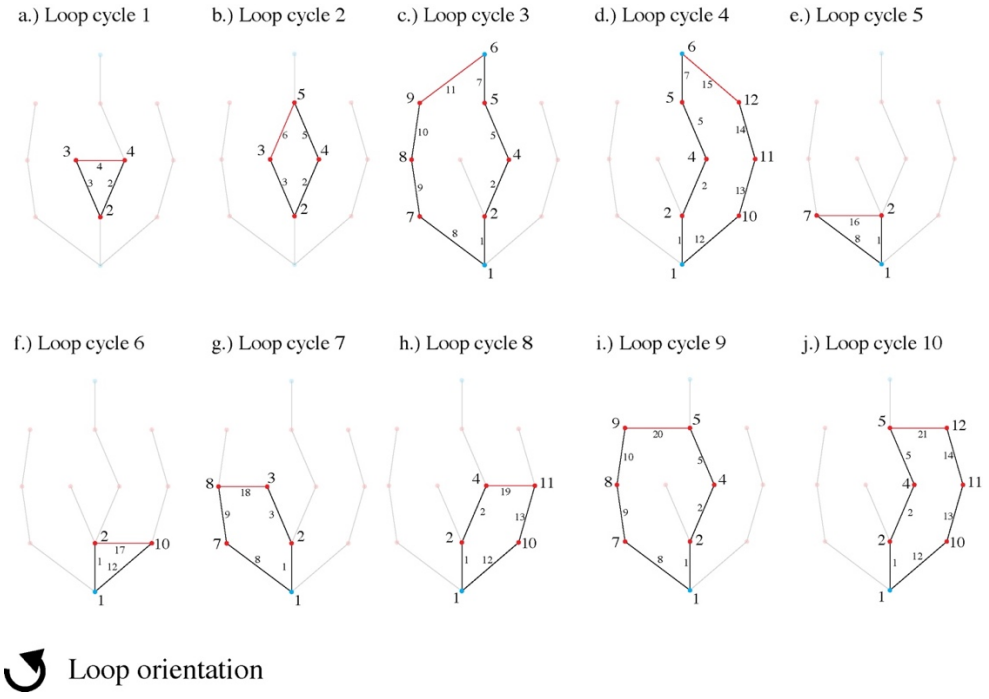

Figure 6.5: *Identified loops between airflow pathways for a pallet of Modular Bulk Package (MBP) with airflow entering the 1.2 m face.*

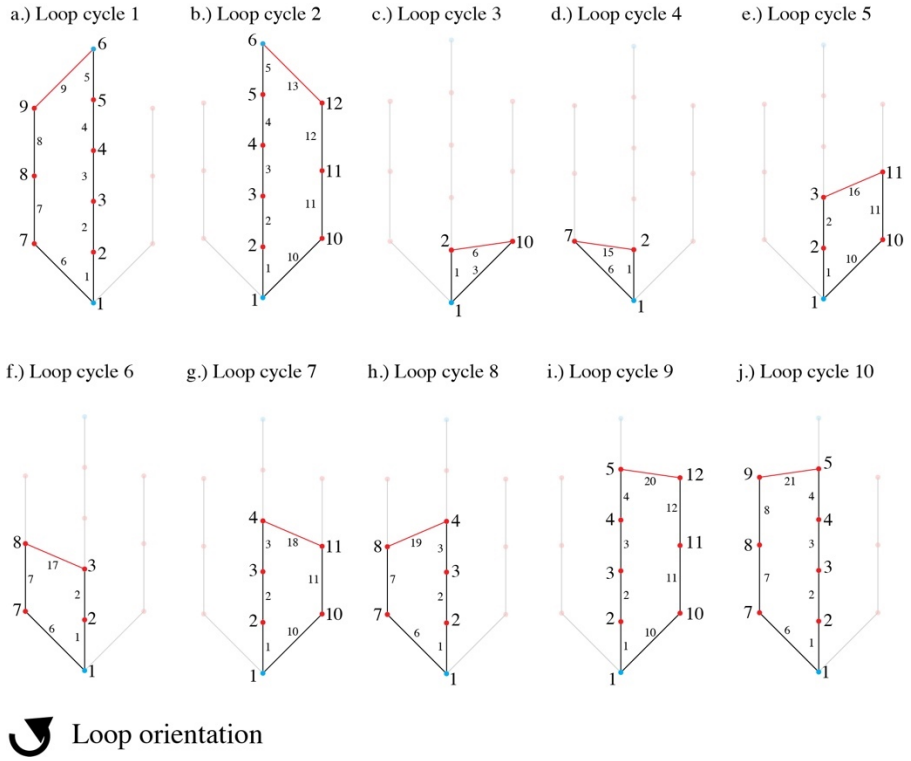

Figure 6.6. *Identified loop between airflow pathways for a pallet of Modular Loose (ML) design.*

6.4. Data analysis

Assuming that some packages within the pallet footprint are identical in terms of design and position, they shall receive the same amount of airflow. Therefore, a symmetry line was considered for the AML, ML and MBP pallet footprints Figure 6.7. As a result, empirically obtained values of variables such as pressure at each package (P) and pressure drop through each venthole (ΔP) were averaged for each symmetric package.

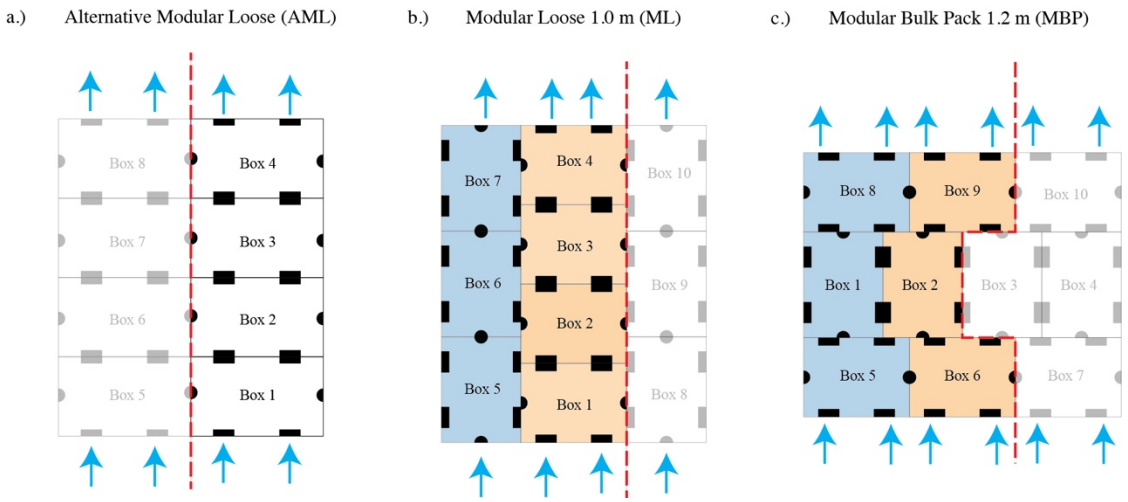

Figure 6.7: *Line of symmetry for: a.) Alternative Modular Loose and b.) Modular Bulk Package (MBP) with airflow entering the 1.2 m face.*

The estimated prediction error was defined as the percentage of difference between measured and predicted data with respect to the experimental variable of interest. This error was estimated by the following relationship:

$$Error\ (\%) = \frac{\left|X_{exp} - X_{model}\right|}{X_{exp}} \cdot 100 \qquad 6.1$$

Where X makes reference to a specific variable of analysis. In this case, this value was adopted to the variables of pressure in each package (P), pressure drop at venthole (ΔP), and volumetric flowrate ($\dot{Q}_{pallet}$). Additionally, the root mean squared error (RMSE) of the predicted pressure at each package with respect to the collected data was calculated for each column of the pallet layer:

$$RMSE = \sqrt{\frac{\sum(Error_P)^2}{N}} \tag{6.2}$$

Where $Error_P$ is the error in pressure at each package, as calculated by equation 6.1 (%) and N the number of packages of each column within the pallet footprint. Similarly, the root mean squared error with respect to the predicted and measured pressure drop through each venthole was calculated. Finally, the volumetric flowrate through the pallet layer at all studied fan speeds was estimated as follows:

$$RMSE = \sqrt{\frac{\sum\left(Error_{\dot{Q}}\right)^2}{N}} \tag{6.3}$$

Where $Error_{\dot{Q}}$ is the error volumetric flowrate through the pallet layer at all studied fan speeds N, as calculated by equation 6.1.

6.5. Validation results and discussions

The simulation results on pressure curve, as well as the pressure distribution and pressure drop in each package within the column of boxes are shown in Figure 6.8, for the IT design. Poor agreement between simulated and empirical results were found when predicting the amount of airflow through a pallet layer at a given by pressure drop (Figure 6.8a), where relative error in volumetric flowrate of 20.6, 28.4 and 32.46 % were found at 600, 900 and 1200 rpm, respectively. Additionally, the RMSE of pressure at all packages ranged from 25.5 to 30 % (Table 6.1). Maximum RMSE of 40 % – averaged over all fan speeds – was found in P_2, while minimum RMSE of 22% was found in predicted pressure at P_4 (Figure 6.8b). Consequently, large error was found in pressure drop through the venthole between boxes. Differences between predicted and measured pressure drop through ventholes were found larger than 100% at the middle of the column – venthole between P_2 and P_3 – and at the outlet of the column (Figure 6.8c). Additionally, RMSE of 140, 182 and 230 % were found at 600, 900 and 1200 rpm, respectively (Table 6.2). The lack of precision of the model was found to be due to inaccurate prediction of the airflow resistances within the system. As the model considered only one relationship to account for resistance at venthole between packages, the calculated values are only a function of the TOA. However, different rates of pressure drop were observed between packages within the column of boxes, where larger pressure drop is observed closer to the column inlet, while decreasing towards the outlet of the pallet layer. Additionally, the same power fan was applied to a single column of boxes, which constitutes only half pallet of IT design, in comparison to the other studied systems where a whole pallet footprint was considered. These differences in the geometry of the studied pallet system can thus influence the observed airflow resistances, in detriment of an accurate prediction, where equations 5.1-5.3 are no longer suitable.

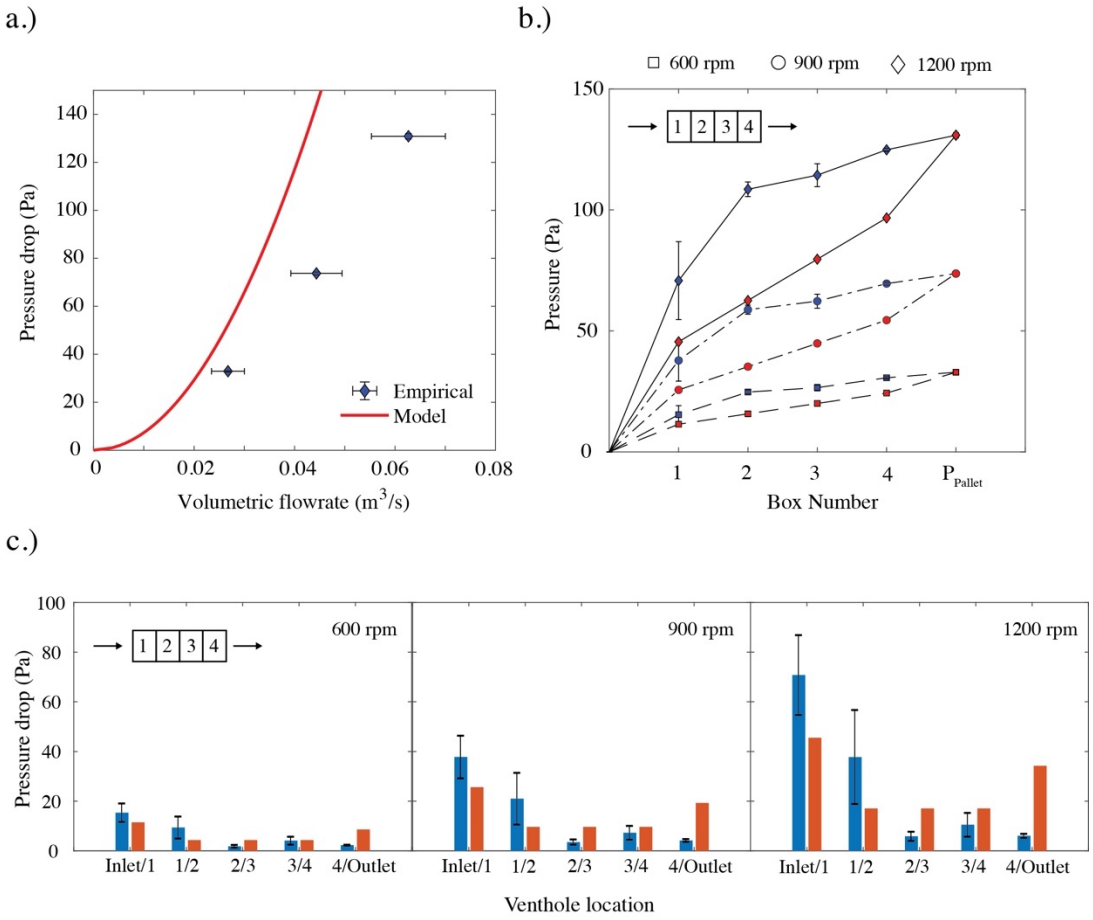

Figure 6.8. *Model validation results at all studied fan speeds for a pallet footprint of IT design, where a.) Predicted pressure curve through the pallet layer, b.) Predicted pressure at each package (Pa) and c.) Pressure drop between all ventholes within the pallet footprint (Pa).*

On the other hand, the model successfully predicted the apparent pressure distribution and volumetric flowrate through an AML pallet footprint, for all fan speeds (Figure 6.9a). Relative error of predicted volumetric flowrate with respect to the empirical measurements of 2.53, 4.64 and 5.57 % were found at 600, 900 and 1200 rpm, respectively. Additionally, averaged pressure RMSE of 8.21 % was found for all packages at all studied fan speeds (Table 6.1). Maximum relative error of 14.8 % was found at P_1, while minimum RMSE value of 3 % was found at P_3 (Figure 6.9b). Consequently, according to Table 6.2, the largest error on pressure drop through the ventholes was found at the outlet of the pallet layer, where averaged relative error of 26% was found over all studied fan speeds, whilst 15 % error was found at the inlet of the pallet layer (Figure 6.9c). The relative minimum error of the model is given

by the use of equations based on empirical data that included the AML, ML and MBP designs. Moreover, the model was designed to predict network distribution in pallet footprints with standard dimensions of 1.0 x 1.2 m, unlike the case of the IT package. Similarly to the IT design, having a single relationship for the internal venthole resistance increased its uncertainty, for not considering the effect of the upstream components in the loss coefficient, thus underestimating the turbulent dissipation within the back of the pallet. Schmandt and Herwig (2011) stated that the resistance associated to the entropy field generation can be segmented in turbulent dissipation rates at the upstream, at the component, and at the downstream of the component – in this case, a venthole. Based on this hypothesis, the turbulent dissipation rate towards the outlet was greatly affected by the turbulence generated by the upstream ventholes. Similarly, Smale (2004) stated that a decrease of kinetic energy towards the interior of the pallet due to poor resistance estimation can result in a poor prediction of the temperature change over time. With respect to the state of the art pallet footprint (see section 5.5.1), the model effectively predicted the airflow distribution in a pallet layer with two symmetrical columns along the airflow direction, providing the kinetic driving force to optimize forced-draft cooling for these pallet arrangements.

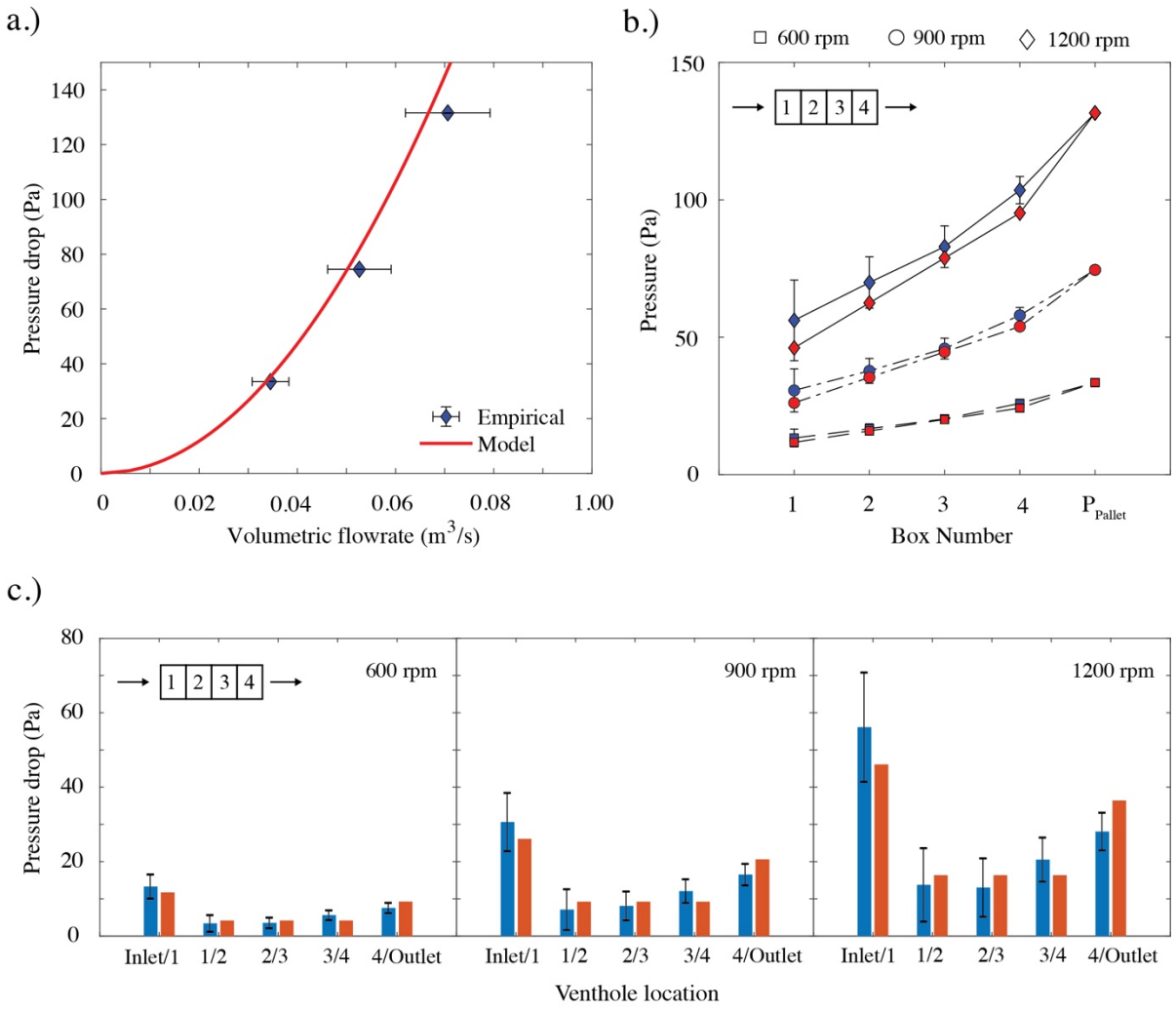

Figure 6.9: *Model validation results at all studied fan speeds for a pallet footprint of AML design, where a.) Predicted pressure curve through the pallet layer, b.) Predicted pressure at each package (Pa) and c.) Pressure drop between all ventholes within the pallet footprint (Pa).*

Table 6.1. *Relative error (%) of each package within the pallet layer for all pressure drop across a pallet layer of AML.*

		Package number				
		P_1	P_2	P_3	P_4	RMSE (%)
Individual tray (IT)	Error ΔP_1 (%)	25.60	36.43	24.60	20.66	24.55
	Error ΔP_2(%)	32.19	40.06	28.02	21.71	27.92
	Error ΔP_3(%)	35.70	42.35	30.37	22.55	30.00
Alternative Modular Loose (AML)	Error ΔP_1 (%)	11.87	5.01	1.10	6.56	6.48
	Error ΔP_2(%)	14.78	6.35	2.73	7.06	7.95
	Error ΔP_3(%)	17.83	10.63	4.96	8.04	10.20

Table 6.2 *Relative error (%) at each venthole and for the total volumetric flowrate within the pallet layer, for all total pressure drop for a pallet layer of AML.*

		Venthole location					
		Inlet/1	1/2	2/3	3/4	4/Outlet	RMSE (%)
Individual tray (IT)	Error ΔP_1	25.60	54.21	137.25	4.94	275.24	140.15
	Error ΔP_2	32.19	54.22	173.56	32.35	361.51	182.12
	Error ΔP_3	35.70	54.81	192.50	62.75	468.59	230.15
Alternative Modular Loose (AML)	Error ΔP_1	11.87	21.73	17.32	26.18	22.75	20.57
	Error ΔP_2	14.78	29.84	14.09	23.47	24.75	22.26
	Error ΔP_3	17.83	18.72	25.43	20.46	29.72	22.88

Similarly to the AML design, the model predicted the airflow distribution through a pallet layer of ML design. Differences in volumetric flowrate through the pallet layer of 1.17, 1.39 and 1.09 % were observed at 600, 900 and 1200 rpm, respectively. Similarly, RMSE of pressure in the packages of 4.14 and 7.57 % were found at the centre and lateral columns of packages, respectively. While maximum error between predicted and measured pressure of 9.1 % was found at P_6, minimum error of 0.5 % was found at package P_3. Consequently, maximum error at the venthole of 23.9 % was found at the venthole between P_2 and P_3, whilst error of 2.9 % was found between the packages $P_{5/8}$ and $P_{6/7}$. Lastly, averaged RMSE over all fan speeds of 11.8 and 12.37 % were found in central and lateral column of packages respectively.

Table 6.3. *Relative error (%) between measured and predicted pressure at each package through a pallet layer of ML design, for all the studied fan speeds..*

	Centre column					Lateral column			
	P_1	P_2	P_3	P_4	RMSE	P_5/ P_8	P_6/ P_9	P_7/ P_{10}	RMSE
Error 600 rpm (%)	4.78	4.80	0.20	2.21	4.23	3.69	8.11	5.98	6.20
Error 900 rpm (%)	5.54	5.51	0.57	1.14	3.96	7.34	9.24	7.04	7.93
Error 1200 rpm (%)	5.65	6.23	0.59	0.73	4.23	7.32	9.94	8.26	8.58

Table 6.4. *Relative error (%) at each venthole between measured and predicted pressure drop through each venthole through a pallet layer of ML design, for all the studied fan speed.*

	Venthole	Error 600 rpm (%)	Error 900 rpm (%)	Error 1200 rpm (%)
Centre column	Inlet/ P_1	4.78	5.54	5.65
	P_1/P_2	4.86	5.42	7.63
	P_2/P_3	21.34	23.00	27.55
	P_3/P_4	9.58	3.51	1.31
	P_4/Outlet	6.05	3.54	2.35
	RMSE	11.23	11.08	13.09
Lateral column	Inlet/ $P_{5/8}$	3.70	7.34	7.32
	$P_{5/8}/P_{5/8}$	19.43	14.59	17.13
	$P_{5/8}/P_{5/8}$	4.67	3.96	0.04
	$P_{5/8}$/Outlet	12.37	16.05	19.86
	RMSE	11.89	11.62	13.61

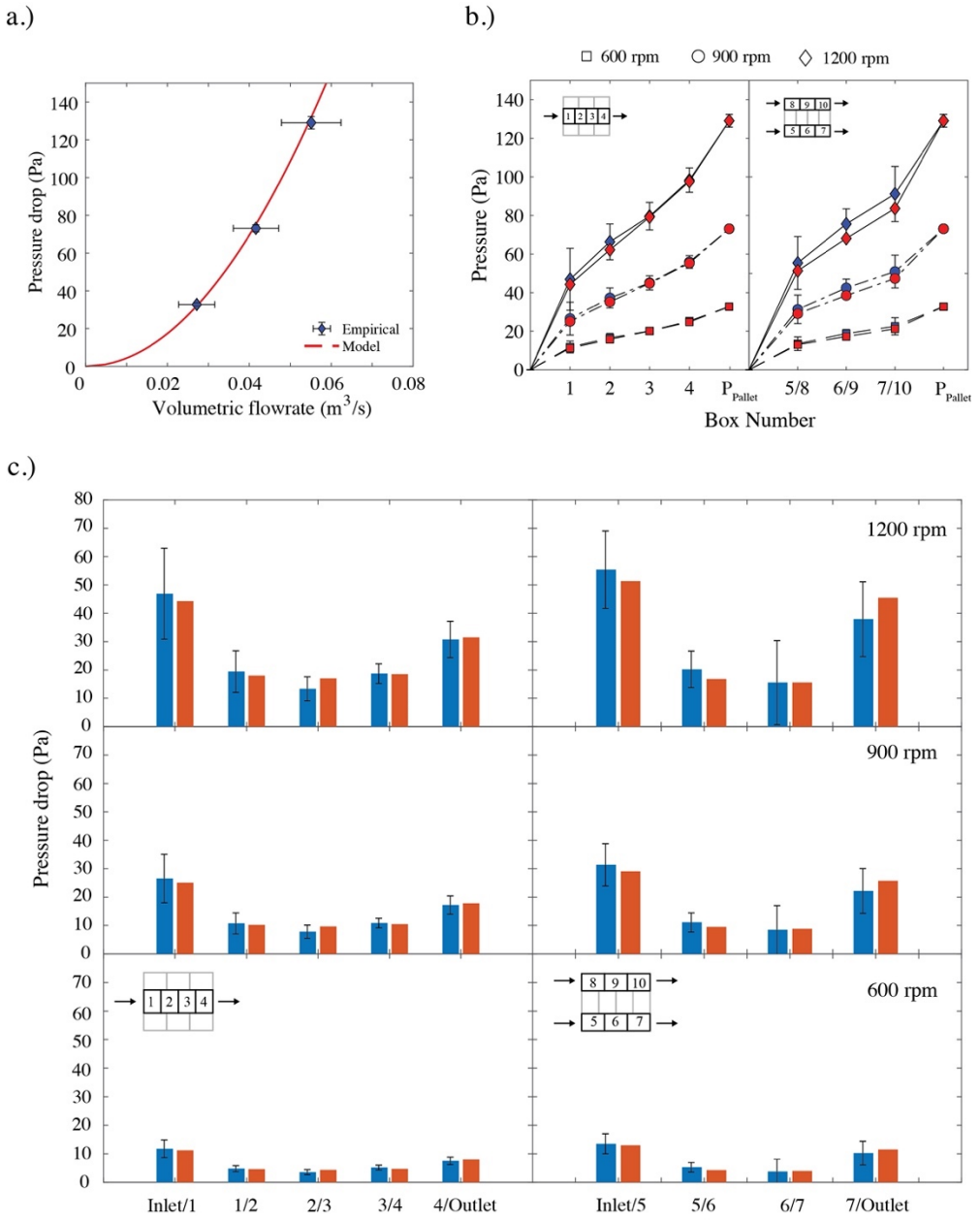

Figure 6.10. *Validation results for a pallet layer of ML design, where a.) Predicted pressure curve through the pallet layer, b.) Predicted pressure at each package (Pa) and c.) Pressure drop between all ventholes within the pallet footprint (Pa).*

Large errors were found when predicting the airflow distribution of a pallet layer of MBP design, when airflow enters through the 1.2 m face. Error in volumetric flowrate of 24.8, 27.7 and 29.2 % were found at 600, 900 and 1200 rpm, respectively (Figure 6.11a). Additionally, average RMSE at all fan speeds of 67.9 and 67.8 were found at the centre and lateral columns, respectively (Table 6.5 Relative error of each package within the pallet layer for all studied fan speeds across a pallet layer of MBP.). Largest error (> 99 %) were observed in the first packages of each column, while minimum error was observed at the end of the pallet layer (< 2 %). Similarly, RMSE of pressure drop at al ventholes resulted larger than 100% for all columns and fan speeds (Table 6.6). While largest error were observed at the ventholes between $P_{2/3}$ and P_6 and between P_1 and P_5, minimum error were found at the ventholes between P_9 and $P_{2/3}$ and P_8 and P_1. In all cases, minimum and maximum error in both columns were observed at the same location respect to the airflow direction.

Largest differences were observed at the inlet of the pallet layer and at the obstructed ventholes between packages (Figure 6.11b). Thereof, the pressure drop through the inlet venthole was almost null, while at the obstructed venthole area the error reached its maximum observed error for all studied fan speeds (Figure 6.11c). Despite this lack of fitting of the model with respect to the empirical values, the pressure at the back of the pallet somewhat converged towards the input pressure drop through the pallet layer (Figure 6.11b). The error at this location went down to at least 2 %, for both columns along the airflow direction. This phenomenon might not entirely have a physical meaning, however, it indicates that the model converged according to its own mathematical constraints. Finally, the overall lack of prediction can be narrowed to the poor estimation of the systems resistances when ventholes were partially obstructed along the airflow direction.

Table 6.5 *Relative error of each package within the pallet layer for all studied fan speeds across a pallet layer of MBP.*

	Centre column				Lateral column			
	P_9	P_2/P_3	P_6	RMSE	P_8	P_1	P_5	RMSE
Error 600 rpm (%)	99.37	62.73	0.3	67.90	99.90	62.02	1.12	67.89
Error 900 rpm (%)	99.38	62.54	0.84	67.86	99.91	61.89	1.61	67.86
Error 1200 rpm (%)	99.39	62.41	1.31	67.82	99.91	61.71	1.76	67.80

Table 6.6 *Relative error (%) at each venthole between measured and predicted pressure drop through each venthole through a pallet layer of MBP design, for all the studied fan speed.*

	Venthole	Error 600 rpm (%)	Error 900 rpm (%)	Error 1200 rpm (%)
Centre column	Inlet/ P_9	99.37	99.39	99.40
	$P_9/P_{2/3}$	53.00	53.00	52.58
	$P_{2/3}/P_6$	136.89	138.27	138.61
	P_6/Outlet	95.94	96.44	96.43
	RMSE	100.87	101.37	101.44
Lateral column	Inlet/ P_8	99.90	99.91	99.91
	P_8/P_1	51.77	51.24	50.83
	P_1/P_5	132.60	134.46	133.14
	P_5/Outlet	99.48	99.54	99.53
	RMSE	100.18	100.74	100.25

Any unplanned venthole obstruction (i.e. by fruit or plastic packaging) along the airflow direction will have an effect on the effective TOA, influencing the airflow field, and consequently, the resistance of each venthole within the pallet layer. In the case of the AML and ML pallet footprints (Figure 6.9Figure 6.10), the TOA of the ventholes along the airflow direction remained constant, thus given a relative more uniform airflow field. In contrast. by modifying the internal pallet configuration, and consequently the airflow field, the amount of entropy generation at each venthole changes, thus affecting their resistance. To account for these challenges, Smale (2004) used a case-sensitive pallet scale resistance values based on the Ramsin equation. However, this approach does not try to interpret the resistances within the palletised systems.

One way to address the problem of accurately predicting airflow resistances for any system is by numerically investigating the resulting airflow field through a palletised arrangement: the so-called Second Law Analysis (Bejan 2013; Herwig and Schmandt 2014; Schmandt and Herwig 2011). Using this approach, the problem of entropy generation is predicted as a consequence of loss of exergy within the system. However, such analyses are computationally expensive – which would require the use of a CFD model for obtaining the airflow field – thus deviating of the overall goal of this project: to develop a simplified airflow model that enables rapid optimisation. However, this research identified the need for further analysis and understanding of flow phenomenon that exist around ventholes and resulting flow fields.

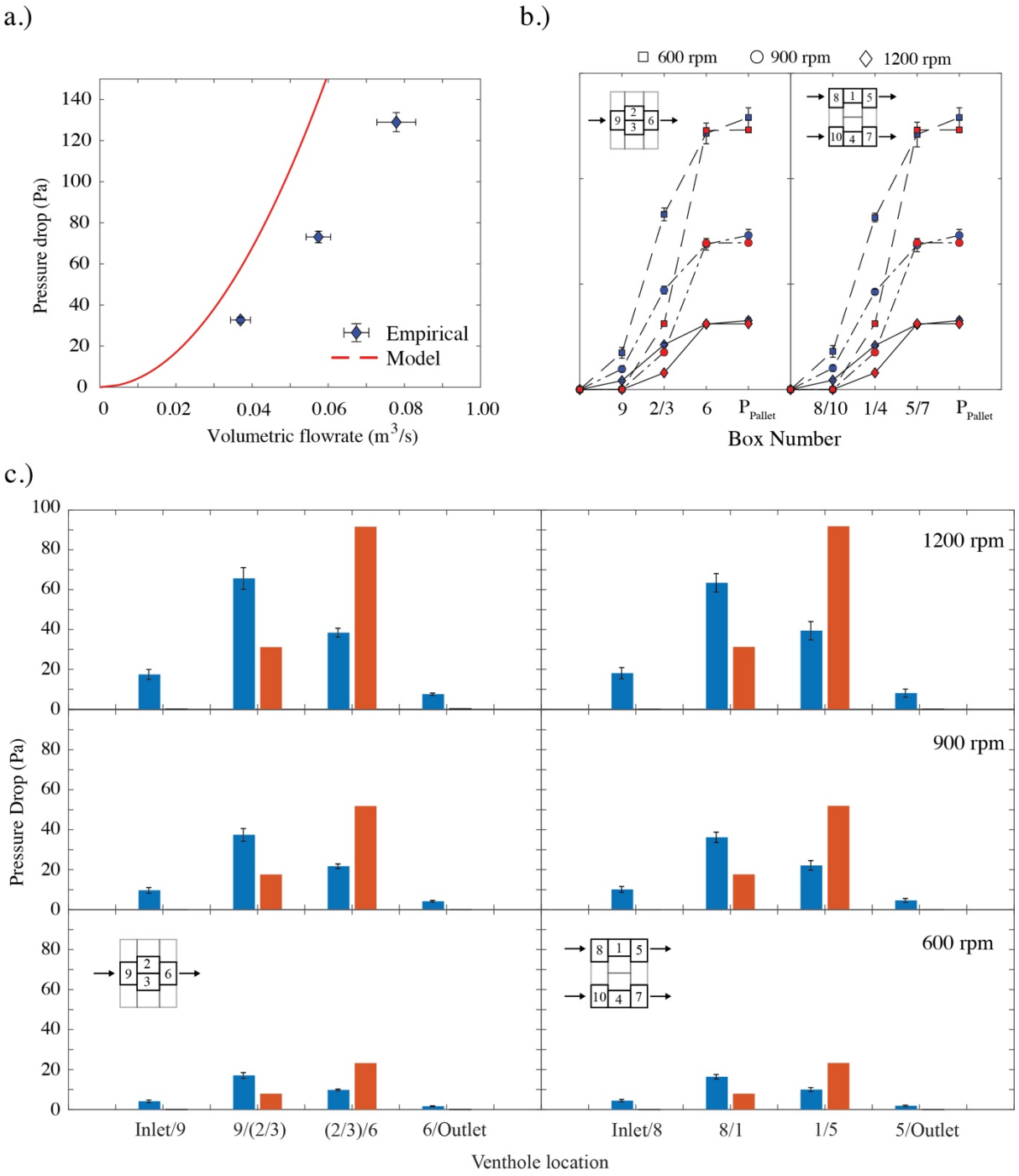

Figure 6.11: *Model validation for the Modular Bulk Package (MBP) package design with airflow entering the 1.2 m face. a.) Pressure at each package (Pa), b.) pressure drop between packages (Pa) and c.) Volumetric flowrate through the pallet layer.*

6.6. Conclusions

A resistance network airflow model was validated against experimental data, assessing the accuracy of the model. Thus, airflow through a pallet footprint of four different package designs were studied. More specifically, the pressure distribution, pressure drop at all ventholes and volumetric flowrate through the pallet layer were analysed.

The model successfully predicted the airflow performance of a pallet layer of AML and ML design, for all fan speeds. Averaged errors in volumetric flowrate of 4.24 and 1.21 % were found over all fan speeds for the AML and ML pallet footprints, respectively. Additionally, RMSE of pressure drop through all ventholes of 21.9 and 12.11 % were found. The major source of error was found to occur due to the uncertainty given by the high level of turbulence, as a result of the ventholes at the upstream of the last ventholes. Additionally, the model assigned a single loss coefficient to all ventholes between packages. On the other hand, the model failed to predict the airflow distribution through a pallet layer of IT design, and a pallet footprint of MBP when airflow enters through the 1.2 m face. Averaged error in volumetric flowrate of 27.15 and 27.23 % were found for the IT and MBP designs, respectively. RMSE through the column of boxes of IT design of 184.14 % was found, whilst RMSE values of 101.2 and 100.4 % were found for the MBP for the centre and lateral columns of boxes, respectively.

The model was assessed to predict the airflow performance only for a pallet layer with constant internal TOA along the airflow direction. A poor estimation was obtained when one or more ventholes along the airflow direction were obstructed. The solver convergence showed analytical robustness to provide a solution using the stablished convergence criteria. Finally, a more dedicated study on the entropy generation within a palletised system is suggested as an approach to obtain a more realistic estimation of the multiple resistances involved along airflow pathways.

7. Conclusions and recommendations

7.1. Conclusions

The major aim of this research was to provide a mathematical framework for the prediction of airflow distribution inside pallet of polylined produce. Thereof, different venthole design features (vent size, location and number) were investigated. Subsequently, the project aimed to find correlation between vent design parameters and airflow resistances. Finally, a resistance network modelling approach was developed and validated to predict airflow distribution in palletised kiwifruit.

Initially, exploratory experiments were conducted regarding the airflow characteristic of forced draft cooling as a function of package design, prior to construction of a model. Firstly, the design characteristics of an orifice plate were studied, concluding that the impact of parameters such as location and number of vents are of little importance to the airflow resistance in comparison to the orifice size, determined by its Total Open Area (TOA). As the TOA increased, the loss coefficient of the plate decreased notably for all studied vent sizes. Additionally, as expected, the effect of having more than one orifice plate in a duct, resembling a package-like system influenced the resistance of all orifices within the system. That is, the total network through which the air flows must be considered, orifices in isolation perform differently to the individual orifices in a sequence of orifices. Additionally, the accuracy of literature based analytical relationships to calculate the loss coefficient of an orifice in a duct were assessed against empirically measured data, providing a tool to calculate airflow resistances based on the orifice size. Differences of 5 % were found between the studied relationships to account for the loss coefficient. Moreover, the selected function contained less variables that account for flow regime characteristics, for a subsequent integration into the model.

Subsequent experiments investigated the pressure distribution in a model system representing a pallet layer for several different kiwifruit package designs and pallet footprints. The internal packaging elements within a pallet layer were found to influence the airflow that passes through the pallet layer for all the studied package designs. Additionally, about 50% of the total pressure drop was found at the inlet of the pallet layer for all the studied scenarios. Differences of 52 % were found on volumetric flowrate through the pallet layer when changing the orientation towards the 1.2 m facing the airflow, where the TOA increased at the face of the pallet. Subsequently, empirically obtained values of loss coefficient were fitted using literature based relationships given by the TOA of each venthole within the pallet. RMSE of 0.50, 0.25 and 0.09 were found for the fitted equations at the inlet, venthole between two packages and at the outlet, respectively.

Thereafter, a geometrical procedure that generates Cartesian coordinates of all venthole within a palletised system and a geometrical algorithm that calculates effective venthole area of two obstructed ventholes were developed. Additionally, a topological analysis that visualises a resistance network and subsequently the nodes and loops equations was also developed for a given pallet footprint. Finally, a network solver based on an iterative linearized method was developed, solving the system of equations for a given footprint in about 10 seconds.

Finally, the model was verified against a status quo pallet footprint of Modular Bulk Package (MBP) design, where maximum error between measured and predicted pressure at the package of 15 % was found. Subsequently, the model was validated against four different pallet footprints: an IT, ML, AML and MBP footprint with the 1.2 m facing the airflow. Good agreement was found between the model and experimental data for the ML and AML designs. At 600, 900 and 1200 rpm, differences in volumetric flowrate of 2.24 and 1.21 % were found. Additionally, pressure drop distribution in all venthole was predicted with RMSE of 21.9 and 12.1 % for the AML and ML designs, respectively.

However, poor performance of the model was found when predicting the airflow distribution for the pallet footprints of IT and MBP designs. Average differences in volumetric flowrate of 27.5 and 27.2 % were found. Additionally, RMSE of pressure drop through the ventholes of 184.1 and 100.6 % were found for the IT and MBP footprints, respectively. Deficient performance of the model was influenced majorly pallet dimensions and poor loss coefficient estimation due to venthole obstructions along the airflow direction.

7.2. Challenges and experimental considerations

A series of exploratory wind tunnel experiments (Chapter 3) were performed to assess the accuracy of the sensing instruments: more specifically regarding to the pressure sensors and anemometry inside a duct, thus assessing the effect of vent design and its consequent airflow resistances. Subsequently, pressure and velocity through palletised systems were measured in a forced-draft cooling simulator. However, such trials were time consuming considering number of monitored variables and repetitions for each package design and pallet configurations, along with experimental set up of all sensing systems. Therefore, a limited number of scenarios where tested during this investigation. Additionally, there was only one hot wire anemometer to estimate the volumetric flowrate through the pallet layer by means of a local measurement at each vent facing the incoming airflow. It would have been advantageous to instead use an in-pallet anemometry method, such as gas tracing methods (Smale 2004; Smale, Moureh, and Cortella 2006; Pham et al. 2021) or local wireless anemometry (Geyer et al. 2018).

As kiwifruit is usually a polylined produce, it was straight forward to use an averaged value of superficial velocity within a package, (i.e. by assuming that air passes through the head space above the polyliner without significant movement into the polylined package) as recommended by Olatunji (2018). However, the system changes dramatically for a package without polyliner. Thereof, air can

take a circuitous route between the fruit. In this instance, the internal geometry inside the package must be considered as a semi-porous matrix, as the size of the fruit objects relative to the dimensions of the package is too big to allow a porous media to be taken, while at the same time the air flow route is too complex (and not easily known) to be considered as a pipe flow.

7.3. Recommendations

7.3.1. Further investigation of airflow resistances

Among the finding of this research, the resistance of a pallet footprint is majorly influenced by size of ventholes within the systems. Likewise, the loss coefficient of a given venthole is influenced by its size, given by its TOA ratio. Thereof, a scaled experimental set-up of a pallet layer can thus be investigated, where large sets of data for different package designs and pallet footprints can be investigated with somewhat ease of implementation. Additionally, variables such as volumetric flowrate and pressure within the system can be measured without incurring in time consuming experimental set-up. Additionally, additional measuring points such as point velocity at each venthole can aid more detailed information of airflow through vents (Geyer et al. 2018). Moreover, the use of more complex measuring methods such as particle image velocimetry, which in such scaled systems (i.e. scaled systems made of transparent material) might monitor 2D slices of the airflow field at the ventholes (Smale 2004; Smale, Moureh, and Cortella 2006; Pham et al. 2021).

Although the resistance airflow model proved to be a useful tool to rapidly predict the airflow distribution, the influence of diverse package arrangements into the airflow resistances associated to the package effective ventholes is still a black box. A new paradigm on the concept of airflow resistance introduced by Bejan (2013) and Herwig and Schmandt (2014) entangled the airflow resistances with

entropy generation of a given system: the so-called Second Law Analysis (SLA). Schmandt and Herwig (2011) and Kock and Herwig (2005) defined the loss coefficient of pipe components as the integration of the difference of the velocity field over the component, based on the Gouy-Stodola theorem (Pal 2017), relating the loss of mechanical work with the increase entropy of a system. Most importantly, this change of paradigm has a wide potential on changing the perspective of loses in flow motion, namely, from pipe flow to more complex system such as convective heat transfer process (Avellaneda et al. 2020). What was traditionally called loss coefficient and could be found in tabulated values, nowadays can be calculated through numerical simulations.

7.3.2. Potential applications of the airflow network model

As indicated in Chapter 6, the model successfully predicted the airflow distribution on pallet footprints with constant TOA along the airflow direction. Thereof, the model can be used to predict airflow distribution of similar palletised systems (i.e. without venthole obstructions and pallet dimensions of 1.0 x 1.2 m). The comparison of two tentative package designs with varying TOA can be accounted for using different pallet footprints. Volumetric airflow efficiency through the pallet layer can be assessed at constant fan speed for two or more package designs. Additionally, the effect of the venthole TOA for a given package design can be assessed using the airflow network model in relatively short computation time. Additionally, the needed fan power to pull a given amount of airflow through a pallet layer can be estimated by characterising the pallet resistance considering a standard ten layer pallet footprint, replicating industry conditions. Moreover, the package aerodynamic efficiency can be estimated in terms of a minimum calculated airflow resistance, Using the proposed relationships that account for loss coefficient of all ventholes.

7.3.3. Development of an integrated modelling routine for cooling applications

This project was conducted under the conception of decoupling the momentum and energy balances of a cooling scenario. As the fan speed remains constant during the cooling process, the momentum balance is considered to be steady-state. In contrast, an energy balance at fruit level during cooling is considered to be unsteady state, as the temperature of all fruit decreases over time, until reaching storage temperature, Previously, Olatunji (2018) developed a heat transfer model based on a zonal approach that considers averaged airflow at the headspace of the package as an input of the model. However, during convective cooling, the air temperature at each package can play a role in palletised systems, specially at the beginning of the cooling period, where airflow entering the pack of the pallet layer gets warmer airflow due to fast heat removal from the produce. Thereof, a pallet scale airflow heat balance is therefore needed to contemplate the use of a zonal approach coupled with an airflow model. Moreover, as air temperature changes over time, each package within the system shall be cooled at different rates, and the amount of zones to be solved increased as the number of packages also increases (considering 100 zones per package).

Additionally, the integration of the airflow network modelling approach can be extrapolated to other cooling scenarios, such as storage and transport, when resistances are accounted for appropriately. Thereof, aerodynamic efficiency during the cold chain can be thus estimated when airflow during precooling and subsequent transport (such as network model from Smale (2004)) are coupled. Ultimately, the use of an integrated modelling approach for momentum and energy during precooling scenarios can be used for subsequent optimisation routines to inform package design. Most importantly, a computationally efficient modelling approach can inform over a large amount of package designs (i.e. 100) without incurring in CFD modelling approaches.

References

Adam, Nicolas J., Giovanni De Cesare, Anton J. Schleiss, Sylvain Richard, and Cécile Muench-Alligné. 2016. 'Head loss coefficient through sharp-edged orifices', *IOP Conference Series: Earth and Environmental Science*, 49: 062009.

Ai, Z. T., and C. M. Mak. 2013. 'Pressure Losses across Multiple Fittings in Ventilation Ducts', *The Scientific World Journal*, 2013: 11.

Alvarez, G., and D. Flick. 1999. 'Analysis of heterogeneous cooling of agricultural products inside bins Part I: aerodynamic study', *Journal of food engineering*, 39: 227-37.

Alvarez, Graciela, Pierre-Emmanuel Bournet, and Denis Flick. 2003. 'Two-dimensional simulation of turbulent flow and transfer through stacked spheres', *Simulation bi dimensionnelle des écoulements et des transferts dans un empilement de sphères (French)*, 46: 2459-69.

Ambaw, A., Matia Mukama, and U. L. Opara. 2017. 'Analysis of the effects of package design on the rate and uniformity of cooling of stacked pomegranates: Numerical and experimental studies', *Computers and Electronics in Agriculture*, 136: 13-24.

ASHRAE handbook. 1985. (American Society of Heating, Refrigerating, and Air-Conditioning Engineers).

ASHRAE handbook. 1994. (American Society of Heating, Refrigerating, and Air-Conditioning Engineers).

Ateş, Sami. 2017. 'Hydraulic modelling of control devices in loop equations of water distribution networks', *Flow Measurement and Instrumentation*, 53: 243-60.

Avellaneda, J. M., F. Bataille, A. Toutant, and G. Flamant. 2020. 'Entropy generation minimization in a channel flow: Application to different advection-diffusion processes and boundary conditions', *Chemical Engineering Science*, 220: 115601.

Bejan, Adrian. 2013. *Entropy Generation Minimization : the Method of Thermodynamic Optimization of Finite-Size Systems and Finite-Time Processes* (CRC Press).

Berry, T. M., A. Ambaw, T. Defraeye, C. Coetzee, and Umezuruike Linus Opara. 2019. 'Moisture adsorption in palletised corrugated fibreboard cartons under shipping conditions: A CFD modelling approach', *Food and Bioproducts Processing*, 114: 43-59.

Bondy, John Adrian, and Uppaluri Siva Ramachandra Murty. 1976. *Graph theory with applications* (Macmillan London).

Boyette, Michael Doyle, L George Wilson, and Edmund Anthony Estes. 1989. 'Forced-air cooling', *AG-North Carolina Agricultural Extension Service, North Carolina State University (USA)*.

Brosnan, Tadhg, and Da-Wen Sun. 2001. 'Precooling techniques and applications for horticultural products — a review', *Techniques de préréfrigération et applications pour les produits horticoles passées en revue (French)*, 24: 154-70.

Carson, James K., and Andrew R. East. 2018. 'The cold chain in New Zealand – A review', *International Journal of Refrigeration*, 87: 185-92.

Chaomuang, Nattawut, Denis Flick, Alain Denis, and Onrawee Laguerre. 2020. 'Experimental and numerical characterization of airflow in a closed refrigerated display cabinet using PIV and CFD techniques', *International Journal of Refrigeration*, 111: 168-77.

Chow, Chuen-yen. 1979. *An introduction to computational fluid mechanics* (Wiley).

Cross, Hardy. 1936. "Analysis of flow in networks of conduits or conductors." In.: University of Illinois at Urbana Champaign, College of Engineering. Engineering Experiment Station.

de Castro, Larissa R, Clement Vigneault, and Luis AB Cortez. 2004. 'Container opening design for horticultural produce cooling efficiency', *Journal of Food Agriculture and Environment*, 2: 135-40.

de Castro, Larissa R., Clément Vigneault, and Luís A. B. Cortez. 2005. 'Cooling performance of horticultural produce in containers with peripheral openings', *Postharvest Biology and Technology*, 38: 254-61.

Defraeye, Thijs, Paul Cronjé, Tarl Berry, Umezuruike Linus Opara, Andrew East, Maarten Hertog, Pieter Verboven, and Bart Nicolai. 2015. 'Review: Towards integrated performance evaluation of future packaging for fresh produce in the cold chain', *Trends in Food Science & Technology*, 44: 201-25.

Defraeye, Thijs, Rutger Lambrecht, Mulugeta Admasu Delele, Alemayehu Ambaw Tsige, Umezuruike Linus Opara, Paul Cronjé, Pieter Verboven, and Bart Nicolai. 2014. 'Forced-convective cooling of citrus fruit: Cooling conditions and energy consumption in relation to package design', *Journal of food engineering*, 121: 118-27.

Defraeye, Thijs, Rutger Lambrecht, Alemayehu Ambaw Tsige, Mulugeta Admasu Delele, Umezuruike Linus Opara, Paul Cronjé, Pieter Verboven, and Bart Nicolai. 2013. 'Forced-convective cooling of citrus fruit: Package design', *Journal of food engineering*, 118: 8-18.

Dehghannya, Jalal, Michael Ngadi, and Clement Vigneault. 2010. 'Mathematical Modeling Procedures for Airflow, Heat and Mass Transfer During Forced Convection Cooling of Produce: A Review', *Food Engineering Reviews*, 2: 227-43.

Dehghannya, Jalal, Michael Ngadi, and Clement Vigneault. 2011. 'Mathematical modeling of airflow and heat transfer during forced convection cooling of produce considering various package vent areas', *Food Control*, 22: 1393-99.

Delele, M. A., E. Tijskens, Y. T. Atalay, Q. T. Ho, H. Ramon, B. M. Nicolai, and P. Verboven. 2008. 'Combined discrete element and CFD modelling of airflow through random stacking of horticultural products in vented boxes', *Journal of food engineering*, 89: 33-41.

Dincer, Ibrahim. 1995. 'Air flow precooling of individual grapes', *Journal of food engineering*, 26: 243-49.

East, A. R., L. Doleh, P. B. Jeffery, N. Tapia, S. G. Gwanpua, and A. F. Woolf. 2018. "What happens in a full-scale kiwifruit curing stack?" In, 525-32. International Society for Horticultural Science (ISHS), Leuven, Belgium.

East, A. R., and N. J. Smale. 2008. 'Combining a hybrid genetic algorithm and a heat transfer model to optimise an insulated box for use in the transport of perishables', *Vaccine*, 26: 1322-34.

East, Andrew, Peter Jeffery, and Richard Love. 2013. "Investigating asymmetrical packaging as a technique to reduce heterogeneity during pre-cooling of fresh produce [USB]." In *2nd IIR International Conference on Sustainability and the Cold Chain, Paris, France*.

Ellis, D. J. 1996. *Convergence of iterative solvers for the simulation of a water distribution pipe network / by D.J. Ellis, A.R. Simpson* (University of Adelaide, Dept. of Civil and Environmental Engineering: Adelaide).

Fahimnia, Behnam, Michael G. H. Bell, David A. Hensher, and Joseph Sarkis. 2015. *Green logistics and transportation : a sustainable supply chain perspective* (Springer).

Ferrua, M. J., and R. P. Singh. 2009a. 'Design guidelines for the forced-air cooling process of strawberries', *Recommandations pour la conception du processus de refroidissement par air forcé de fraises (English)*, 32: 1932-43.

Ferrua, M. J., and R. P. Singh. 2009b. 'Modeling the forced-air cooling process of fresh strawberry packages, Part I: Numerical model', *International Journal of Refrigeration*: 335.

Ferrua, M. J., and R. P. Singh. 2009c. 'Modeling the forced-air cooling process of fresh strawberry packages, Part II: Experimental validation of the flow model', *Modélisation du processus de refroidissement par air forcé des fraises fraîches emballées. Partie II : validation expérimentale du modèle de l'écoulement (French)*, 32: 349-58.

Ferrua, M. J., and R. P. Singh. 2009d. 'Modeling the forced-air cooling process of fresh strawberry packages, Part III: Experimental validation of the energy model', *Modélisation du processus de refroidissement par air forcé des fraises fraîches emballées. Partie III : validation expérimentale du modéle énergétique (French)*, 32: 359-68.

Gao, Qi, HongPing Wang, and GongXin Shen. 2013. 'Review on development of volumetric particle image velocimetry', *Chinese Science Bulletin*, 58: 4541-56.

Getahun, Samuel, Alemayehu Ambaw, Mulugeta Delele, Chris J. Meyer, and Umezuruike Linus Opara. 2017. 'Analysis of airflow and heat transfer inside fruit packed refrigerated shipping container: Part II – Evaluation of apple packaging design and vertical flow resistance', *Journal of food engineering*, 203: 83-94.

Geyer, Martin, Ulrike Praeger, Ingo Truppel, Holger Scaar, Daniel A. Neuwald, Reiner Jedermann, and Klaus Gottschalk. 2018. 'Measuring Device for Air Speed in Macroporous Media and Its Application Inside Apple Storage Bins', *Sensors*, 18: 576.

Grace, John R., and Fariborz Taghipour. 2004. 'Verification and validation of CFD models and dynamic similarity for fluidized beds', *Powder Technology*, 139: 99-110.

Gruyters, W., T. Van De Looverbosch, Z. Wang, S. Janssen, P. Verboven, T. Defraeye, and B. M. Nicolaï. 2020. 'Revealing shape variability and cultivar effects on cooling of packaged fruit by combining CT-imaging with explicit CFD modelling', *Postharvest Biology and Technology*, 162: 111098.

Gruyters, W., P. Verboven, E. Diels, S. Rogge, B. Smeets, H. Ramon, T. Defraeye, and B. M. Nicolaï. 2018. 'Modelling Cooling of Packaged Fruit Using 3D Shape Models', *Food and Bioprocess Technology*.

Han, Jia-Wei, Chun-Jiang Zhao, Jian-Ping Qian, Luis Ruiz-Garcia, and Xiang Zhang. 2018. 'Numerical modeling of forced-air cooling of palletized apple: Integral evaluation of cooling efficiency', *International Journal of Refrigeration*, 89: 131-41.

Han, Jia-Wei, Chun-Jiang Zhao, Xin-Ting Yang, Jian-Ping Qian, and Bei-Lei Fan. 2015. 'Computational modeling of airflow and heat transfer in a vented box during cooling: Optimal package design', *Applied Thermal Engineering*, 91: 883-93.

Han, Jia-Wei, Wen-Ying Zhu, and Zeng-Tao Ji. 2019. 'Comparison of veracity and application of different CFD turbulence models for refrigerated transport', *Artificial Intelligence in Agriculture*, 3: 11-17.

Herwig, Heinz, and Bastian Schmandt. 2014. "How to Determine Losses in a Flow Field: A Paradigm Shift towards the Second Law Analysis." In, 2959-89.

Idelchik, I. E., and M. O. Steinberg. 1994. *Handbook of hydraulic resistance* (CRC Press: Boca Raton, FL).

Idelchik, I.E. 1987. "Handbook of hydraulic resistance." In.: American Society of Mechanical Engineers.

Kirby, Edward C., Roger B. Mallion, Paul Pollak, and Pawel J. Skrzynski. 2016. 'What Kirchhoff Actually did Concerning Spanning Trees in Electrical Networks and its Relationship to Modern Graph-Theoretical Work', *CROATICA CHEMICA ACTA*, 89.

Kock, Fabian, and Heinz Herwig. 2005. 'Entropy production calculation for turbulent shear flows and their implementation in cfd codes', *International Journal of Heat and Fluid Flow*, 26: 672-80.

Kondjoyan, Alain. 2006. 'A review on surface heat and mass transfer coefficients during air chilling and storage of food products', *International Journal of Refrigeration*, 29: 863-75.

Martinez-Hermosilla, Gonzalo A., Celia Kueh, Karl Dahm, and John E. Bronlund. 2018. 'Combined modelling methodology for optimisation of box design based on hybrid genetic algorithm', *Packaging Technology and Science*, 31: 709-22.

McIlroy, Malcolm S. 1950. 'Direct-Reading Electric Analyzer for Pipeline Networks', *Journal (American Water Works Association)*, 42: 347-66.

Merai, M., D. Flick, L. Guillier, S. Duret, and O. Laguerre. 2018. 'Experimental characterization of airflow inside a refrigerated trailer loaded with carcasses', *International Journal of Refrigeration*, 88: 337-46.

Mercier, Samuel, Jeffrey K. Brecht, and Ismail Uysal. 2019. 'Commercial forced-air precooling of strawberries: A temperature distribution and correlation study', *Journal of food engineering*, 242: 47-54.

Montgomery, Douglas C. 2017. *Design and analysis of experiments* (John Wiley & Sons, Inc.).

Mukama, Matia, Alemayehu Ambaw, Tarl Michael Berry, and Umezuruike Linus Opara. 2017. 'Energy usage of forced air precooling of pomegranate fruit inside ventilated cartons', *Journal of food engineering*, 215: 126-33.

Mukama, Matia, Alemayehu Ambaw, Tarl Michael Berry, and Umezuruike Linus Opara. 2019. 'Analysing the dynamics of quality loss during precooling and ambient storage of pomegranate fruit', *Journal of food engineering*, 245: 166-73.

Mukama, Matia, Alemayehu Ambaw, and Umezuruike Linus Opara. 2020. 'A virtual prototyping approach for redesigning the vent-holes of packaging for handling pomegranate fruit – A short communication', *Journal of food engineering*, 270: 109762.

Ngcobo, Mduduzi E. K., Mulugeta A. Delele, Umezuruike Linus Opara, and Chris J. Meyer. 2013. 'Performance of multi-packaging for table grapes based on airflow, cooling rates and fruit quality', *Journal of food engineering*, 116: 613-21.

Ngcobo, Mduduzi E. K., Mulugeta A. Delele, Umezuruike Linus Opara, Cobus J. Zietsman, and Chris J. Meyer. 2012. 'Resistance to airflow and cooling patterns through multi-scale packaging of table grapes', *International Journal of Refrigeration*, 35: 445-52.

Nourgaliev, R. R., T. N. Dinh, T. G. Theofanous, and D. Joseph. 2003. 'The lattice Boltzmann equation method: theoretical interpretation, numerics and implications', *International Journal of Multiphase Flow*, 29: 117-69.

O'Sullivan, Justin. 2016. *Significant factors affecting the forced-air cooling process of polylined horticultural produce : a thesis presented in partial fulfilment of the requirements for the degree of Doctor of Philosophy in Food Technology at Massey University, Palmerston North, New Zealand*.

O'Sullivan, Justin, Maria J. Ferrua, Richard Love, Pieter Verboven, Bart Nicolai, and Andrew East. 2016. 'Modelling the forced-air cooling mechanisms and performance of polylined horticultural produce', *Postharvest Biology and Technology*: 23.

O'Sullivan, Justin, Maria Ferrua, Richard Love, Pieter Verboven, Bart Nicolaï, and Andrew East. 2014. 'Airflow measurement techniques for the improvement of forced-air cooling, refrigeration and drying operations', *Journal of food engineering*, 143: 90-101.

O'Sullivan, Justin L., Maria J. Ferrua, Richard Love, Pieter Verboven, Bart Nicolaï, and Andrew East. 2017. 'Forced-air cooling of polylined horticultural produce: Optimal cooling conditions and package design', *Postharvest Biology and Technology*, 126: 67-75.

Olatunji, J. R., R. J. Love, Y. M. Shim, and A. R. East. 2020. 'An automated random stacking tool for packaged horticultural produce', *Journal of food engineering*: 110037.

Olatunji, J. R., R. J. Love, Y. M. Shim, M. J. Ferrua, and A. R. East. 2017. 'Quantifying and visualising variation in batch operations: A new heterogeneity index', *Journal of food engineering*, 196: 81-93.

Olatunji, Jamal Rimkeit. 2018. *An integrated modelling approach to inform package design for optimal cooling of horticultural produce : a thesis presented in partial fulfilment of the requirements for the degree of Doctor of Philosophy in Food Technology at Massey University, Palmerston North, New Zealand*.

Pal, Rajinder. 2017. 'Demystification of the Gouy-Stodola theorem of thermodynamics for closed systems', *International Journal of Mechanical Engineering Education*, 45: 142-53.

Park, J. 2015. "Numerical Simulation of Turbulent Flow Over Staggered Tubes Using Multi-Relaxation Time Lattice Boltzmann Method." In *Proceedings of the 2015 International Conference on Electrical, Automation and Mechanical Engineering*, 201-04. Atlantis Press.

Pathare, Pankaj B., Umezuruike Linus Opara, Clément Vigneault, Mulugeta A. Delele, and Fahad Al-Julanda Al-Said. 2012. 'Design of Packaging Vents for Cooling Fresh Horticultural Produce', *Food and Bioprocess Technology*, 5: 2031-45.

Pham, Anh Thu, Jean Moureh, Mourad Belaidi, and Denis Flick. 2021. 'CFD modelling of a pallet of heat-generating product applied to a cheese product', *International Journal of Refrigeration*, 128: 163-76.

Rennels, Donald C, and Hobart M Hudson. 2012. *Pipe Flow: A Practical and Comprehensive Guide* (John Wiley & Sons).

Rogge, Seppe, Thijs Defraeye, Els Herremans, Pieter Verboven, and Bart M. Nicolaï. 2015. 'A 3D contour based geometrical model generator for complex-shaped horticultural products', *Journal of food engineering*, 157: 24-32.

Schmandt, Bastian, and Heinz Herwig. 2011. 'Loss Coefficients in Laminar Flows: Essential for the Design of Micro Flow Systems', *PAMM*, 11: 27-30.

Shim, YM, JR Olatunji, J Zhao, RJ Love, MJ Ferrua, and AR East. 2016. "Industry survey on the pressure drop across palletised horticultural produce during precooling." In *4th IIR International Conference on Sustainability and the Cold Chain, Auckland, New Zealand*.

Smale, N. J., J. Moureh, and G. Cortella. 2006. 'Review Article: A review of numerical models of airflow in refrigerated food applications', *Revue des modèles numériques de l'écoulement d'air dans la réfrigération des produits alimentaires (French)*, 29: 911-30.

Smale, Nicholas John. 2004. *Mathematical modelling of airflow in shipping systems : model development and testing : a thesis presented in partial fulfilment of the requirements for the degree of Doctor of Philosophy in Food Technology at Massey University, Palmerston North, New Zealand* (2004).

Tanner, D. J., A. C. Cleland, and L. U. Opara. 2002. 'A generalised mathematical modelling methodology for the design of horticultural food packages exposed to refrigerated conditions Part 2. Heat transfer modelling and testing', *Modélisation mathématique des emballages de produits alimentaires réfrigérés. Partie 2. Modélisation du transfert de chaleur et essais (French)*, 25: 43-53.

Tanner, D. J., A. C. Cleland, L. U. Opara, and T. R. Robertson. 2002. 'A generalised mathematical modelling methodology for design of horticultural food packages exposed to refrigerated conditions: part 1, formulation', *Modélisation mathématique des emballages de produits alimentaires réfrigérés. Partie 1. Formulation (French)*, 25: 33-42.

Tanner, David James. 1998. *Mathematical modelling for design of horticultural packaging : a thesis presented in partial fulfilment of the requirements for the degree of Doctor of Philosophy in Food Engineering at Massey University*.

Tarjan, R. 1971. "Depth-first search and linear graph algorithms." In *12th Annual Symposium on Switching and Automata Theory (swat 1971)*, 114-21.

Thompson, A. K. 2014. 'Precooling.' in, *Fruit and Vegetables* (John Wiley & Sons, Ltd).

Thompson, James F, F Gordon Mitchell, and Tom R Rumsay. 2008. *Commercial cooling of fruits, vegetables, and flowers* (UCANR Publications).

Tsilingiris, P. T. 2008. 'Thermophysical and transport properties of humid air at temperature range between 0 and 100 °C', *Energy Conversion and Management*, 49: 1098-110.

V. Chau, K., J. J. Gaffney, C. D. Baird, G. A. Church, and Ii. 1985. 'Resistance to Air Flow of Oranges in Bulk and in Cartons', *Transactions of the ASAE*, 28: 2083-88.

van der Sman, R. G. M. 2017. 'Flow through a filter plate backed by a packed bed of spheres', *Chemical Engineering Science*, 158: 154-63.

van der Sman, R. G. M., M. H. Ernst, and A. C. Berkenbosch. 2000. 'Lattice Boltzmann scheme for cooling of packed cut flowers', *International Journal of Heat and Mass Transfer*, 43: 577-87.

Van der Sman, RGM. 2002. 'Prediction of airflow through a vented box by the Darcy–Forchheimer equation', *Journal of food engineering*, 55: 49-57.

Verboven, P., M. L. Hoang, M. Baelmans, and B. M. Nicolaï. 2004. 'Airflow through Beds of Apples and Chicory Roots', *Biosystems Engineering*, 88: 117-25.

Verboven, P., M. L. Hoang, and B. M. Nicolaï. 2003. "MODELLING TURBULENT AIR FLOW IN COOL ROOMS FOR HORTICULTURAL PRODUCTS." In, 435-41. International Society for Horticultural Science (ISHS), Leuven, Belgium.

Verboven, Pieter, D. Flick, B. M. Nicolaï, and G. Alvarez. 2006. 'Modelling transport phenomena in refrigerated food bulks, packages and stacks: basics and advances', *International Journal of Refrigeration*, 29: 985-97.

Vigneault, C., and B. Goyette. 2002. 'Design of plastic container opening to optimize forced–air precooling of fruits and vegetables', *Applied Engineering in Agriculture*, 18: 73.

Vigneault, C., N. R. Markarian, A. da Silva, and B. Goyette. 2004. 'Pressure drop during forced-air ventilation of various horticultural produce in containers with different opening configurations', *Transactions of the ASAE*, 47: 807-14.

Vigneault, Clément, Bernard Goyette, and Larissa R. de Castro. 2006. 'Maximum slat width for cooling efficiency of horticultural produce in wooden crates', *Postharvest Biology and Technology*, 40: 308-13.

Whitaker, Stephen. 1996. 'The Forchheimer equation: A theoretical development', *Transport in Porous Media*, 25: 27-61.

Wood, Don J, and Carl OA Charles. 1972. 'Hydraulic network analysis using linear theory', *Journal of the Hydraulics division*, 98: 1157-70.

Wu, Wentao, Paul Cronjé, Bart Nicolai, Pieter Verboven, Umezuruike Linus Opara, and Thijs Defraeye. 2018. 'Virtual cold chain method to model the postharvest temperature history and quality evolution of fresh fruit – A case study for citrus fruit packed in a single carton', *Computers and Electronics in Agriculture*, 144: 199-208.

Wu, Wentao, Philippe Häller, Paul Cronjé, and Thijs Defraeye. 2018. 'Full-scale experiments in forced-air precoolers for citrus fruit: Impact of packaging design and fruit size on cooling rate and heterogeneity', *Biosystems Engineering*, 169: 115-25.

Yasduda, Takahiro, Tomohisa Hashimoto, Hisato Minagawa, Koji Morinishi, and Nobuyuki Satofuka. 2013. 'Efficient Simulation for Incompressible Turbulent Flow Using Lattice Boltzmann Model', *Procedia Engineering*, 61: 173-78.

Zhao, Chun-Jiang, Jia-Wei Han, Xin-Ting Yang, Jian-Ping Qian, and Bei-Lei Fan. 2016. 'A review of computational fluid dynamics for forced-air cooling process', *Applied Energy*, 168: 314-31.

Zhao, Junyu Matthew. 2017. *Development of a mathematical model for 'Hayward' kiwifruit softening in the supply chain : a thesis presented in partial fulfilment of the requirements for the degree of Doctor of Philosophy in Food Technology at Massey University, New Zealand*.

Zou, Qisu, and Xiaoyi He. 1997. 'On pressure and velocity boundary conditions for the lattice Boltzmann BGK model', *Physics of Fluids*, 9: 1591-98.